Commissioned by the Swiss Confederation

Experimental and numerical track system evaluation:

Methodology for finding optimal components

Final Report

31st October 2023

Authors:

Dr. Bart Van Damme, Dr. Prof. Joël Cugnoni, Raphaël Nardin, Vincent Crausaz

Mandant	Confédération suisse ; Offices fédéraux de l'environnement (OFEV) et des transports (OFT), CH-3003 Berne. L'OFEV et l'OFT sont des offices du Département fédéral de l'environnement, des transports, de l'énergie et de la communication (DETEC)
Mandataire	Haute Ecole d'Ingénierie et de gestion du canton de Vaud, Institut COMATEC
Auteur/Autrice :	Prof. Joel Cugnoni
Accompagnement OFEV / OFT :	Franz Kuster, Fredy Fischer Robert Attinger, Christoph Dürig
N.B. :	Le présent rapport a été réalisé sur mandat des offices fédéraux de l'environnement (OFEV) et des transports (OFT). Le mandataire est seul responsable de son contenu.

Summary of the project and key results

Project goals

In the recent years, many new components have been developed to decrease noise radiation, mitigate ground vibrations and reduce track maintenance costs by protecting the ballast. Today, railway infrastructure managers are facing the challenge to evaluate and select the best components available for its future railway implementations and renewal.

However, due to the large number of combinations and the amount of time and work required to evaluate each potential solution, there is a critical need to be able to evaluate and preselect components more efficiently, using simpler lab scale measurements to characterize the components combined with numerical models to estimate multiple track performance criteria.

Based on the work undertaken previously in the Novel Rail Pad project, the goal of this project was

i) to develop a combined experimental & numerical evaluation method to provide a prognosis of different track component combinations in terms of their performance for noise, vibrations and ballast protection and

ii) use these prediction tools to explore the design space of component properties to identify the best combination of components to match a given performance target and thus allow railway infrastructure managers to formulate detailed system specifications in their procurements.

Project structure, deliverables and main findings

The project was structured in four main work packages each corresponding to specific deliverables which are listed below with the corresponding section of the present report for reference:

WP1: Method for the measurement of dynamic stiffness and damping of rail pads ; *Lead:* EMPA

Deliverables:

D1.1 Repeatable measurement setup of the dynamic stiffness and frequency-dependent damping (§ 1.4)

D1.2 Database of stiffness and damping for existing rail pads used on the Swiss network (§ 1.51.4)

Summary / Main findings:

The newly developed measurement for the vertical and lateral stiffness and damping of rail pads shows good agreement with data from numerical models. It yields more realistic results in a shorter amount of time than with DMA analysis and numerical models as used previously. A catalogue of properties for 7 rail pads is now available. An example of the comparison of the pad properties obtained with this method compared to the predictions taken from the Novel Railpad project is shown in Figure 1 below:

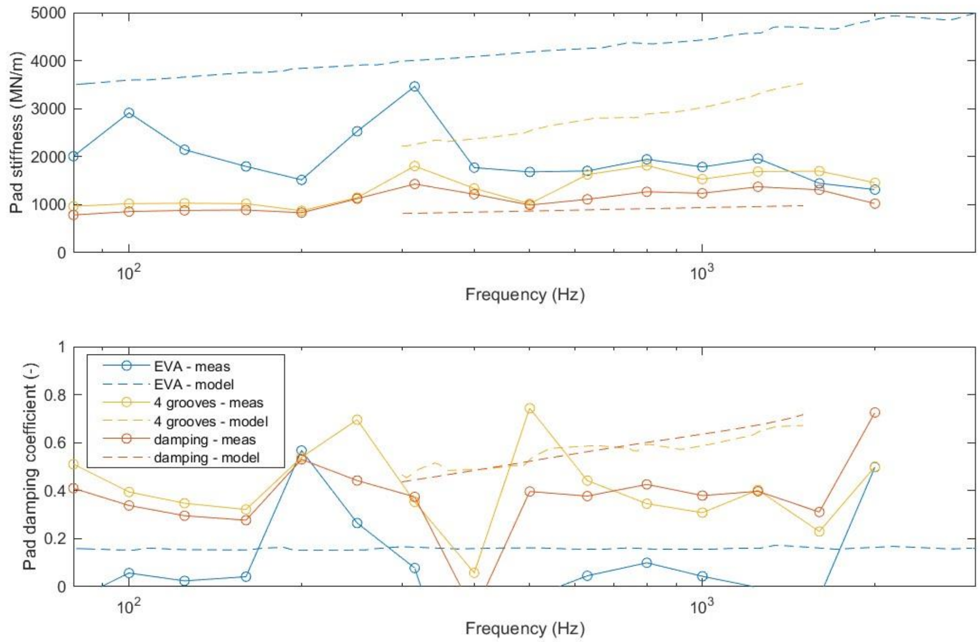

Figure 1: Vertical stiffness and damping ratio of three types of pads, and comparison with models from the Railpad Project.

WP2: Simulation methods for the prognosis of rail track performance indicators; *Lead:* HEIG-VD

Deliverables:

D2.1: Model comparison and validation based on experimental track data (§ 1.7)

D2.2: Updated modelling toolchain with the added possibility to change the sleeper and clamping systems (§ 1.8)

D2.3: Manual, software & user interface for mixed numerical – experimental sleeper identification and implementation of new sleepers in the modelling toolchain. (§ 1.9)

Summary / Main findings:

The open source "Rail track modelling toolbox" has been further validated against experimental data and extended to implement new options for track design and component changes (sleeper type, material and spacing, clamping system properties). A new numerical identification method has been developed to determine the effective properties of from modal analysis data of sleepers. The developed software tools are published in open-source on GitHub: https://github.com/jcugnoni-heig/RailTrackModellingToolbox/tree/track_evaluation

WP3: Experimental evaluation of selected combination of rail track components; *Lead:* HEIG-VD

Deliverables:

D3.1: Experimental modal analysis procedure to characterize sleepers & modal data for the selected sleepers (§ 1.10)

D3.2: FRF and noise radiation spectra measured on the three-sleeper cell setup for different system configurations. Relative influence of the different components on the performance indicators of the system (§ 2.2)

D3.3: Ranking of the different systems and evaluation of the dominant component properties affecting the system's vibration and noise radiation performance (§ 1.12).

Summary / Main findings:

The experimental parametric study on the three-sleeper setup of HEIG-VD led to an overall ranking and normalized performance rating (1 = best, 0 = worst) of different track component combinations which are summarized in Table 1 below:

Table 1 – Overall ranking of the systems with their associated overall rating, from three-sleeper cell measurement results.

Rating 0.0 … 1.0 *best→*; Rank 10 … 1 *best→*

OVERALL			45° curves		6° straight lines		ACOUSTICS		VIBRATION					
									SLEEPER + RAIL		SLEEPER		RAIL	
Rank	Rating	SYSTEM	Rank	Rating	Rank	Rating	Rank	Rating	Rank	Rating	Rank	Rating	Rank	Rating
1	0.97	B91 USP 60E2 W14 SemperSilent	1	0.96	1	0.97	1	1.00	1	0.93	1	0.94	1	0.92
2	0.93	B91 60E2 W14 SemperSilent	2	0.93	2	0.93	2	0.96	2	0.89	2	0.91	2	0.87
3	0.65	B91 USP 60E2 W14 SBB hard pad	3	0.61	3	0.70	3	0.55	3	0.76	3	0.91	4	0.61
4	0.57	B91 60E2 W14 SBB hard pad	6	0.47	5	0.66	5	0.46	4	0.67	7	0.76	5	0.59
5	0.55	B91 USP 60E2 W14 soft pad	7	0.46	6	0.63	4	0.49	6	0.60	4	0.82	9	0.37
6	0.51	B91 60E2 W14 soft pad	9	0.35	4	0.68	6	0.44	7	0.59	6	0.78	8	0.40
7	0.50	B91 54E2 W14 SBB hard pad	4	0.50	8	0.49	7	0.37	5	0.62	8	0.69	7	0.56
8	0.38	B91 54E2 W14 soft pad	10	0.22	7	0.54	8	0.30	9	0.46	5	0.79	10	0.13
9	0.32	Rp-IV 54E2 SKL12 SBB hard pad	5	0.50	10	0.14	9	0.27	10	0.36	10	0.17	6	0.56
10	0.31	Rp-IV 54E2 Kpo3 NONE	8	0.42	9	0.20	10	0.13	8	0.48	9	0.21	3	0.75

The main observations from the three sleeper cell measurements are:

1. The dominant parameter for the noise reduction is the use of a high damping pad, which also provide the best performances in terms of reduced rail and sleeper vibrations both in 45° loading conditions (curves) and 6° (straight lines). The best combination overall to combine a high damping pad with USPs. In terms of economic / material efficiency, just changing to high damping pads seem more advantageous however.
2. The worst conditions in terms for noise are overall with soft pads, 54E2 rails or wooden sleepers.
3. The current SBB reference configuration of 60E2 rail with hard EVA pads and B91 sleepers without USPs is in the upper half of the combinations, but can be improved at least in terms of reducing ballast vibrations by adding USPs. However, switching to high damping pads seem more beneficial overall.

WP4: Numerical design space exploration to identify optimal component properties; *Lead:* HEIG-VD

Deliverables:

D4.1: Software for sensitivity analysis & analysis report detailing the effect of each component properties (§ 1.15)

D4.2: Software for scenario analysis & exploration of existing component combinations (§ 1.16)

D4.3: Software for parametric exploration and parametric study to identify the “sweet spots” (optima) (§1.17)

Summary / Main findings:

The software platform has been further developed to implement the possibility of running the simulations in batches, using parameter description files are input. The rail track modelling toolbox has been used to carried out sensitivity analysis of the track component properties on both acoustic and ballast protection performance indicators. Considering changes around the current SBB reference construction (hard EVA pad, 60E2 rail, B91 sleeper, no USP), the dominant parameters affecting noise radiation are: the sleeper spacing, the rail pad stiffness and damping, and to a lesser extent the ballast properties. USPs do not seem to affect noise radiation significantly but seem very effective at protecting the ballast.

The analysis of different combination of existing components gave overall similar conclusions as the experimental results on the three-sleeper cell: the combination of soft USPs with high damping pad give overall the best estimated performance in terms of both noise and ballast protection.

Multiple parametric studies have been carried out to scan the possible design space in order to identify the most optimal component properties based on the model predictions. The sleeper spacing was considered to costly and complicated to change for the achievable effect and thus the optimization focused on the rail pad and USP properties as shown below:

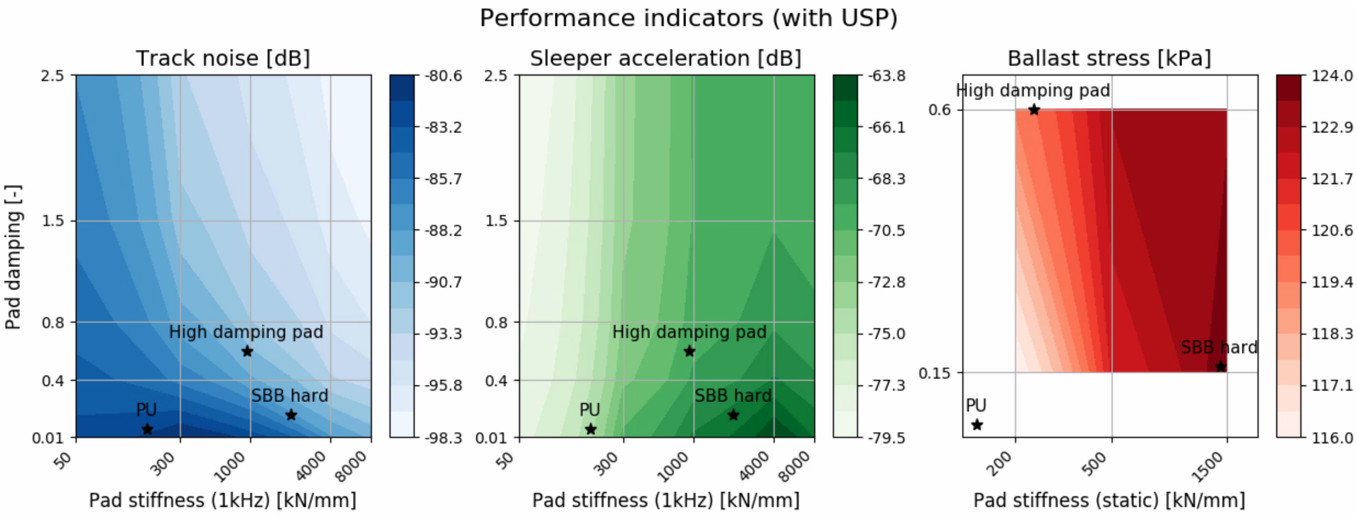

Figure 2 - Performance indicators (with USP)

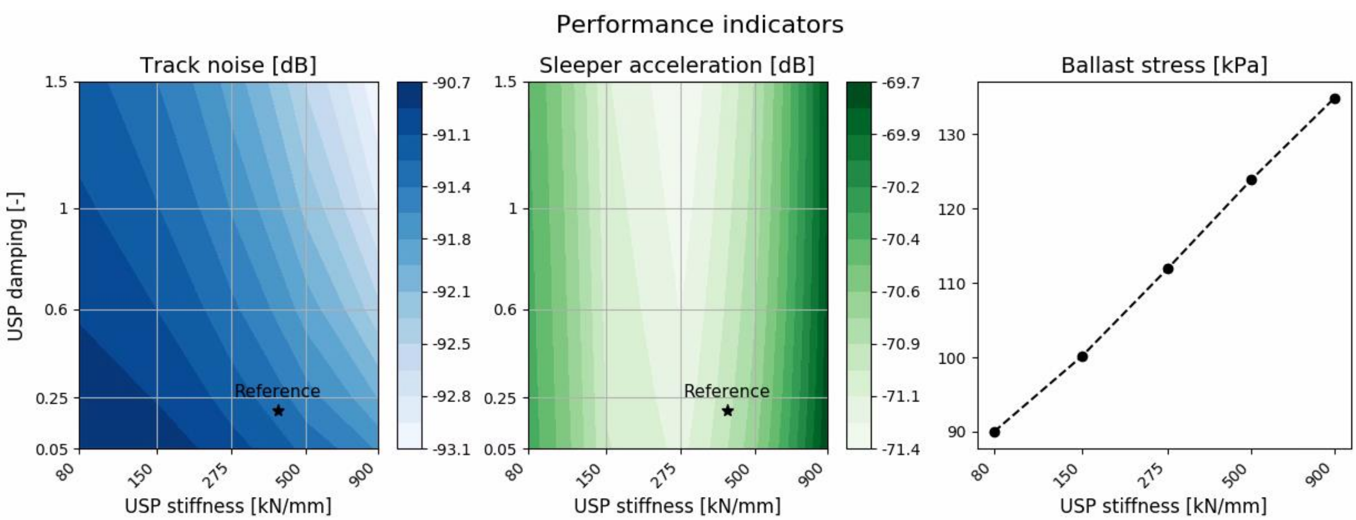

Figure 3 - Performance indicators vs. USP properties

As a final result, the following sweet spot for the component properties of the track have been identified as using 60E2 rails with B91 sleepers with a rail pad of medium stiffness (~1000 kN/mm at 1Khz, ~300 kN/mm static stiffness) and high damping (as high as possible, at least tan δ ~= 0.5) combined with soft USPs (around 200-300kN/mm). Based on the present models, such combination could provide both a significant noise reduction and a marked improvement in ballast protection compared to current track construction.

Introduction

1.1 Context

This report describes the work that was performed by HEIG-VD (School of Engineering and management Vaud) and in Yverdon-les-Bains and Empa in Dübendorf during the project "*Experimental and numerical track system evaluation: Methodology for finding optimal components*", financed by the Swiss Federal Office for the Environment (FOEN) (Bundesamt für Umwelt (BAFU)), in partnership with the Swiss federal railways (SBB). The goal of the project was to develop a mixed numerical – experimental methodology to analyze several components of rail tracks superstructure, and identify the best combinations to reduce track noise in priority and improve ballast protection.

1.2 Methodology

The three-sleeper-long experimental bench test in Heig-VD was used to perform vibration and acoustic measurements. Different combinations of sleepers, Under Sleeper Pads (USP), clamping systems, rail pads and rail profiles were tested to understand the influence of the components properties on noise and vibrations. Based on the observations, rankings were established to determine the most influent components and the best solutions.

Alongside these experiments, numerical simulations were performed for the same purposes. To make the simulations as accurate as possible, a bench test was set up in Empa to measure the in-situ dynamic stiffness and damping of rail pads. These were used in the modelling toolchain. Moreover, materials properties of sleepers were numerically identified based on modal measurements carried out in Heig-VD.

Simulations were carried out for the same purposes as measurements. In addition to comparing components combinations, they allowed performing parametric studies to better understand the influence of specific parameters on performance indicators. Most simulations were performed using three numerical models. The semi-analytical model, developed in Empa, allows computing Track Decay Rates (TDR) and Sound Pressure Levels (SPL) quickly. The multi-sleeper model is a harmonic model developed in Heig-VD and was used to analyze vibrations in sleepers and radiated noise at specific points along the track. Finally, the impulse model is a quasi-static FE model, which computes the stress distribution in the ballast during a pass-by.

Finally, it is important to keep in mind that there is an infinity of ways to define performance indicators. The way they were defined here aims at highlighting certain physical characteristics. The absolute results may vary depending on how indicators are defined, so the goal of simulations is to understand trends and differences between systems, and not to necessarily make accurate predictions of sound pressure levels, for instance. All models have their limitations, and they could not completely replace field measurements.

WP1: Method for the measurement of dynamic stiffness and damping of rail pads

1.3 Introduction

The majority of the Empa-contribution in this project was to develop a test for the dynamic stiffness of rail pads, so that pads can be objectively compared, and input data for the models can be generated. This is especially important for novel pads containing visco-elastic and/or rubbery components, since their equivalent stiffness is highly frequency-dependent.

There is no standardized test available for the frequency-dependent assessment of elastic properties of pads. The test should not be confused with static and dynamic tests according to EN 13146-9:2020, which only yields stiffness and damping up to 20 Hz. We aim to measure the stiffness and damping in the acoustically relevant frequency range above 200 Hz.

1.4 Task 1.1: Development of a dynamic stiffness and damping measurement setup

The development of a reliable and repeatable test bench involved several approaches with important difficulties. We refer to the intermediate reports for these intermediate steps.

The proposed test uses a concrete (B91) sleeper part as a support, and a steel mass with a foot similar to a steel rail (60e1, 150mm wide). The mass is clamped on the sleeper using two Skl14 clamps, which ensures the pad installation under realistic conditions.

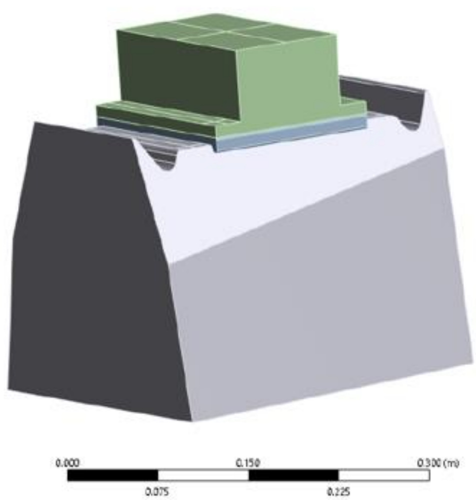

Figure 4: Experimental setup for the dynamic stiffness and damping measurement. Left: schematic drawing, right: laboratory setup.

The top mass is excited by an instrumented hammer (PCB 086C01) with a vinyl tip, from the top (to measure vertical stiffness and damping), and from the side (to measure lateral stiffness and damping). The motion of the steel mass and the sleeper are measured by two accelerometers .

The pad stiffness can be calculated from these measurements, assuming that the masses are rigid, and the springs are ideal, acting in one direction. The unknown stiffness of the foundation can be eliminated from the dynamic stiffness when both accelerations are known. The (complex) spring stiffness is then given by

$$k(\omega) = \omega^2 \frac{F + m a_m}{a_m - a_s}.$$

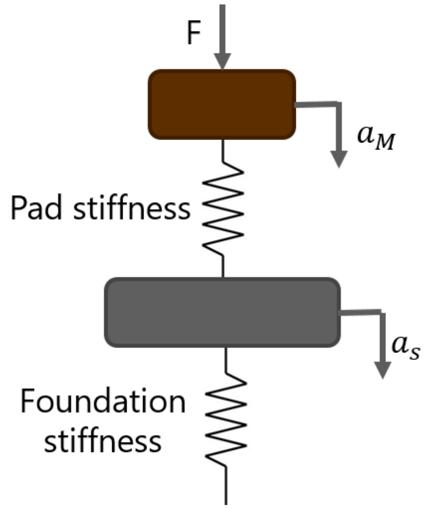

Figure 5: Schematic model of the experimental setup, showing the measured quantities for the calculation of the vertical stiffness.

The values F, a_m, and a_s are the (complex) Fourier transforms of the measured quantities. The resulting complex spring stiffness includes the frequency-dependent spring stiffness (the real part k_r) and damping contribution (the imaginary part k_i). The pad's damping coefficient is given by $c = k_i/k_r$.

The measured frequency range is limited by the stiffness of the pad. At higher frequencies, the pads do not behave as ideal springs but show higher deformation modes. At this point, the assumptions of the above formulas are no longer valid. We have found that this experimental setup yields reliable results up to 1000 Hz for soft pads (<200 kN/mm static stiffness) and up to 2500 Hz for hard pads (>800kN/mm). However, models show that the stiffness does not considerably change above 1000 Hz, so that the values can be assumed constant up to 5000 Hz.

1.5 Task 1.2: Measurement of a set of standard rail pads for validation of the test setup, and for implementation into the toolchain

A wide variety of pads was tested, on the one hand to validate model results from the Railpad Project, on the other hand to cover SBB's portfolio. The results of standardized measurements (as far as they are known), shown in the railpad project, are summarized in the table.

Table 2 - Measurements of the pads

		10 Hz		20 Hz	
pad	k (kN/mm)	k_r (kN/mm)	c (-)	k_r (kN/mm)	c (-)
EVA hard	1400	2110	0.09	2230	0.11
PU hard	350	480	0.09	640	0.11
Prototype 4 grooves	314	483	0.24	506	0.33
Prototype D grooves	341	555	0.17	595	0.23

The standardized measurements show various trends:

- The stiffness increases with frequency
- The damping can be roughly distinguished between low-damping pads (c < 0.15) and high-damping pads (c > 0.2).

- Pads with high damping show a rapid increase in stiffness from the static value to the dynamic values.

In what follows, we present the stiffness results for the pads listed above. In a first step, we validate the measurements by the model results of the Railpad Project. The models require detailed knowledge of the pads' material properties, which are difficult to measure for this type of materials. Small deviations in sample size, sample shape, or clamping conditions change the resulting elastic properties (typically the Young's modulus and loss modulus). Therefore, the modelled pad stiffness has a fairly large inherent error. We have detailed results for three pads: EVA hard, “High Damping Pad”, a single material high damping pad, and “4-grooves”, a two-material prototype pad consisting of EVA and PIB.

Doing the measurements, we find that the experiments rank the pads's stiffnesses in the correct order. High Damping Pad is the softest, EVA the hardest. The agreement between the model and measured stiffness for the High Damping Pad is remarkable. The prediction for EVA and 4-grooves pads is higher than the measurements. Already during the Railpad Project, it was clear that the material properties of EVA were too high to explain the pad's stiffness. These data were also used to model the 4-groove pad shell, so that the predicted stiffness turns out higher.

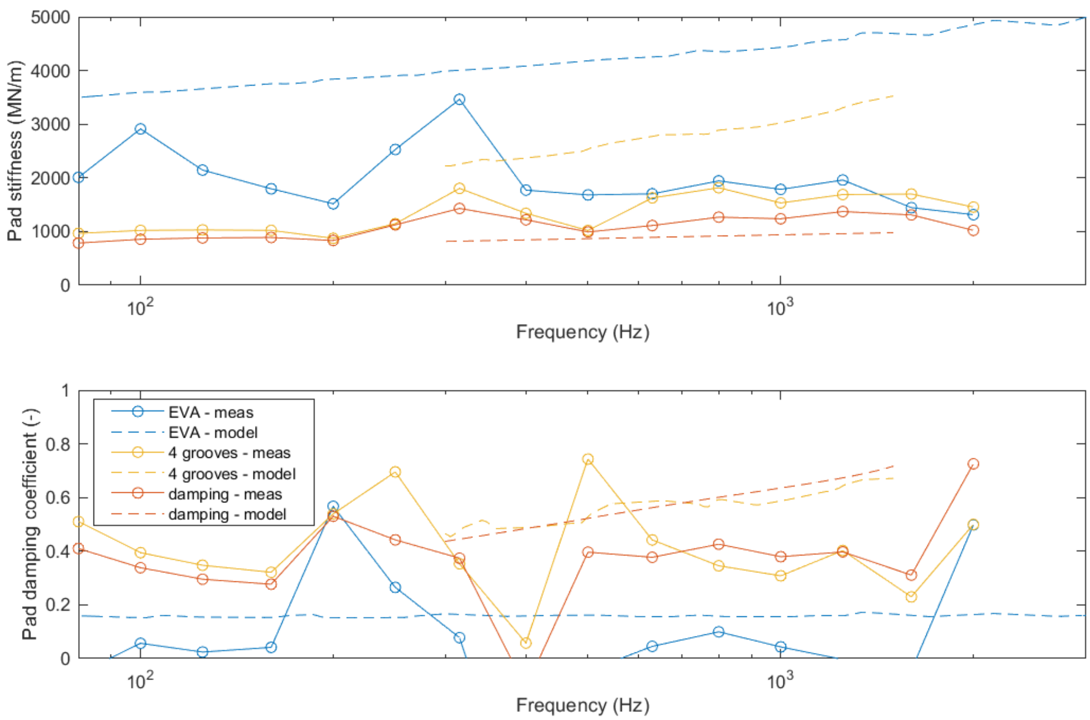

Figure 6: Vertical stiffness and damping ratio of three types of pads, and comparison with models from the Railpad Project.

The damping results show a similar trend. The EVA pads have a lower measured damping than the two other pads. However, due to the hardness of the pads, the measurements are very noisy which makes extracting the damping values extremely difficult. The predicted damping values of the two other pads are slightly higher than the measured ones.

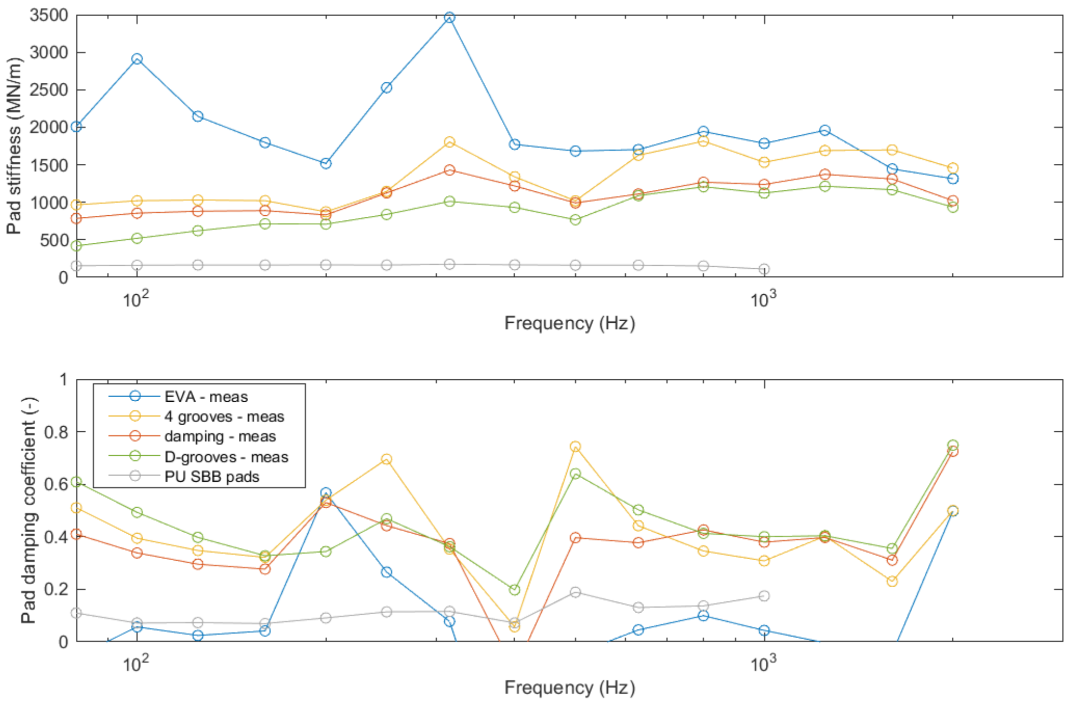

Figure 7: Comparison of the vertical stiffness and damping for a series of known pads.

Adding two additional known pads, the D-grooves prototypes and SBB polyurethane pads, confirms the validity of the measurements. PU pads have low damping and low stiffness, 10x below the vertical stiffness of EVA pads. The D-groove pads have a stiffness and damping comparable to the 4-groove pads, as was measurement in standardized stiffness tests. It can be seen that the D-groove pad stiffness increases more slowly with frequency. The low-frequency limit corresponds remarkably well with the dynamic standard measurements at 20 Hz. The low-frequency limit for 4-groove pads is higher in our tests than in the standardized test. It is possible that a higher precompression by the fastening system influences the overall stiffness.

The setup also allows to measure the lateral stiffness of the pad, although this is a complicated matter for different reasons. In models, we assume that the rail and sleeper are bonded to the top and bottom of the pad. In reality, the rail can slide (with friction) over the top of the pad. Moreover, friction between the clamps and the rail is changing the measured values much more than for the vertical motion. Models predict a lateral stiffness being an order of magnitude lower than the vertical stiffness, which is what our measurements should be able to reproduce.

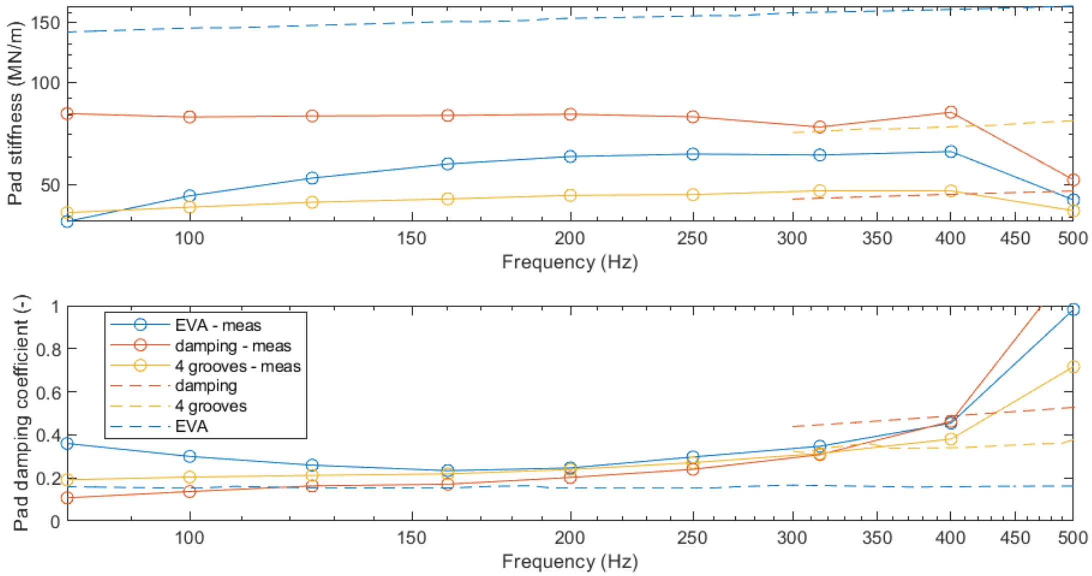

Figure 8: Lateral stiffness and damping ratio of three types of pads, and comparison with models from the Railpad Project.

The first results show the measurement results of the three modelled pads. It can be seen that the EVA and 4-grooves pads are once again considerably less stiff than in the models. This confirms that the material properties of EVA are probably overestimated in the models. The High damping Pad seem to be stiffer than predicted. This can be due to the complex interaction of the slits in the geometry and the sleeper. Surprisingly, the damping in the lateral direction is similar for all three pads. Once again, the imperfect contacts between the three parts might have an important contribution to the damping. Overall, the order of magnitude of the lateral stiffness and damping is well captured by the measurements. It clearly shows stiffness values that are 15-20 times lower than the vertical damping, as predicted in the Railpad Project.

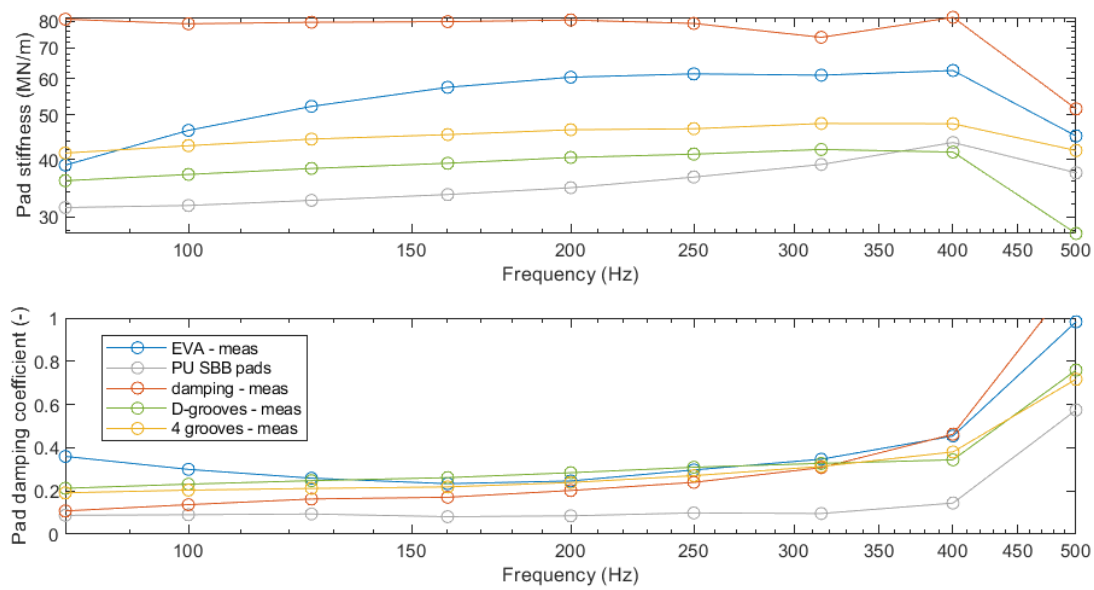

Figure 9: Comparison of the lateral stiffness and damping for a series of known pads.

The comparison of all known pads yields similar results. Once again, and surprisingly, the High Damping Pad show the highest lateral stiffness. However, the differences between the extremes (PU pads and hard pads are 3 times stiffer) are less pronounced than for the vertical stiffness (PU pads and hard pads are 10 times stiffer).

1.6 Overall conclusion

The newly developed measurement for the vertical and lateral stiffness and damping of rail pads shows good agreement with data from numerical models. Moreover, the measurement allows to take complex boundary conditions into account, and yields more realistic results than ideal numerical models. The lab measurement is a welcome addition to the tedious standardized measurements of static and dynamic stiffness, which require large test machines and is limited to 20 Hz as a maximum frequency. The lab measurement only takes a couple of minutes, yields vertical and lateral stiffness and damping, and is valid in the range between 80 and 1500 Hz (vertical) or 500 Hz (lateral). A catalogue of properties for 7 railpads is now available. The two deliverables are therefore achieved.

WP2: Simulation methods for the prognosis of rail track performance indicators

1.7 Task 2.1: Comparison of semi-analytical and dynamic sub structuring FE model of the track

The goal of this task is to validate the accuracy of the models. The multi-sleeper model is validated regarding acceleration Frequency Response Functions (FRF) at points along the rails, SPL differences between systems, and TDR. A 400-sleeper-long track is simulated with a frequency-independent unit force acting in the middle, such that it tends to reflect the behavior of an infinitely long track.

Firstly, one can compare the accelerance simulated to measurements at various sections along the track, as described in DIN EN 15461 [1] for TDR calculation. Figure 10 illustrates the 29 points where FRFs are observed. In the field experiments, an accelerometer is placed at position 0 and an instrumented hammer is used to hit the rail vertically and laterally at all positions. In the simulation, the rail is excited at position 0 and the resulting accelerations are observed at all positions, which is equivalent.

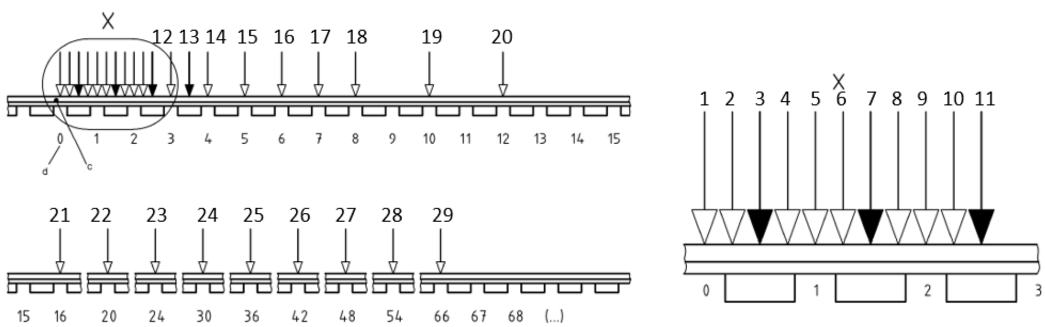

Figure 10 - Location of the 29 sections where FRFs are measured [1]

On Figure 11, the accelerance FRFs at three points are shown, comparing the multi-sleeper model numerical results to measurements between 200Hz and 2000Hz. Here, SBB hard rail pads and B91 concrete sleepers with USPs were used. Although a specific focus is addressed to the 300-1500Hz range, corresponding to rail-borne noise, it is interesting to extend it when looking at acceleration. The experimental and numerical curves are globally matching very well. There is however some discrepancies at low frequency for some cases below 300Hz but this does not represent an issue in the present project as the main results extracted from this model are related to the acceleration peaks at high frequencies that contribute to the noise radiation. The peak amplitudes are well captured as well as the general frequency distribution of the resonances, but a small frequency shift can be observed for some modes. Fortunately, it does not influence performance indicators, which are generally based on spectral integration. These small mismatch in resonance frequencies could be explained by the material properties assumed for the different components that may be slightly different from the exact physical values.

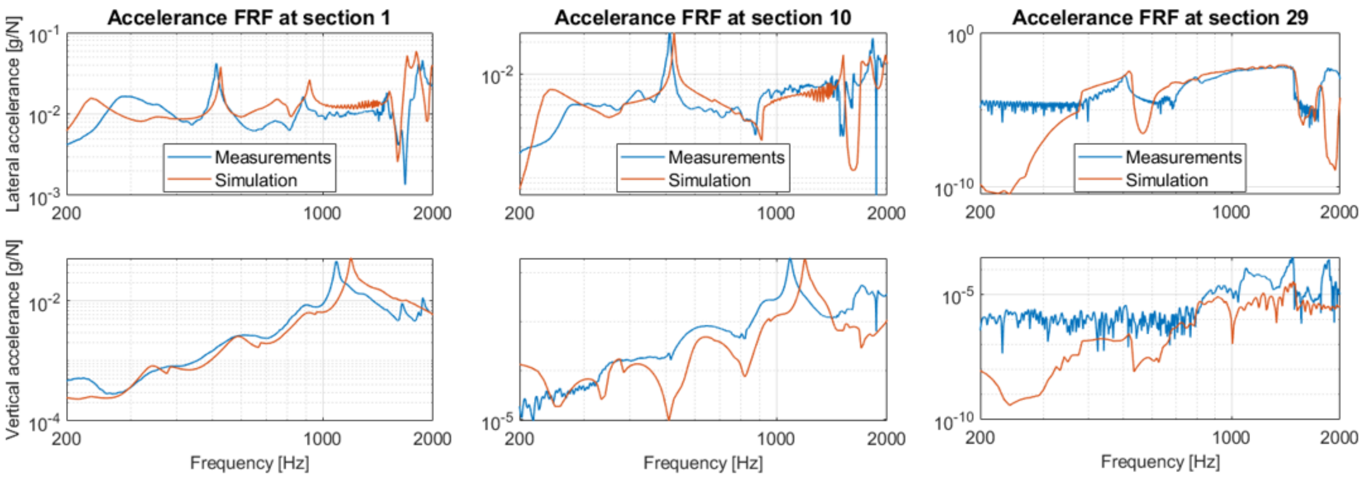

Figure 11 - Measured and simulated accelerance FRFs at three locations

For a more global overview of the accuracy of the model along the track, Figure 12 shows the mean accelerance from 200Hz to 2000Hz at each section mentioned above, for EVA pad (*i.e.* SBB hard pad) and for SemperSilent pad, respectively. The average values are well reproduced by the simulation. However, at a distance greater than 10 to 20m, the model prediction is underestimating the vibration levels in the vertical direction. This can be explained potentially by the relative difficulty in measuring accurate vibration data at long distances when using hard pads due to the noise floor of the sensors.

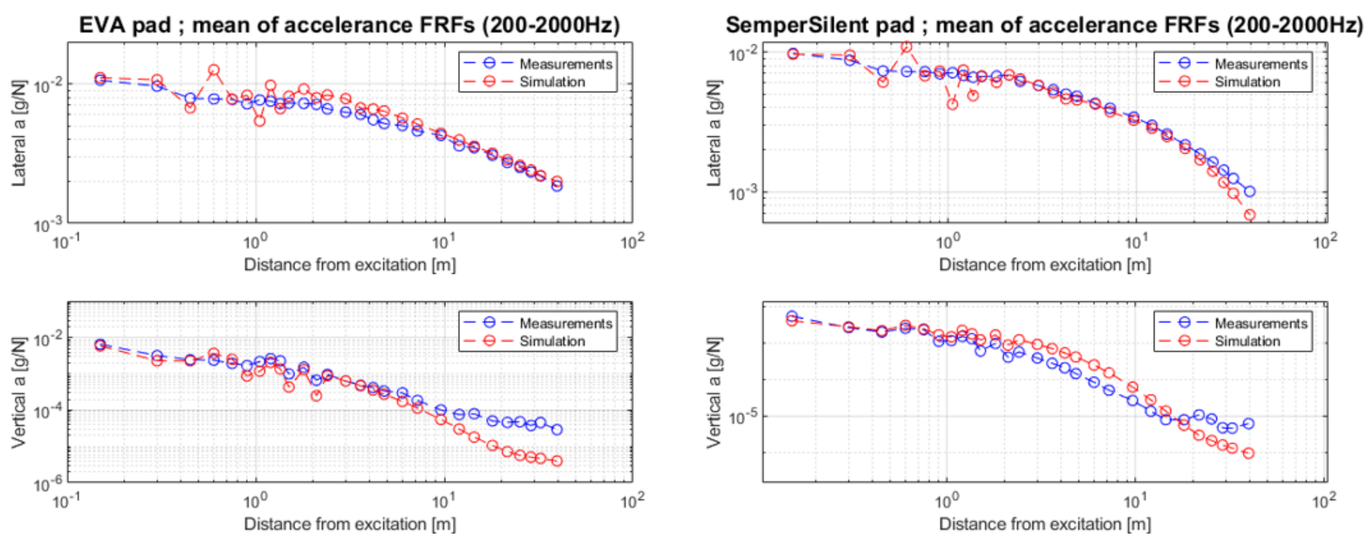

Figure 12 - Mean of the FRFs at all sections

These graphs brought the idea of computing the TDR with this model as well. Figure 13 compares the TDR in 3rd octave bands computed with the multi-sleeper model, the semi analytical model and the measurements for the SBB hard pad. The numerical results are very close to the measurements in the 300 to 1500Hz range. In particular, the multi-sleeper numerical model shows a very good agreement with the experimental data in the lateral direction.

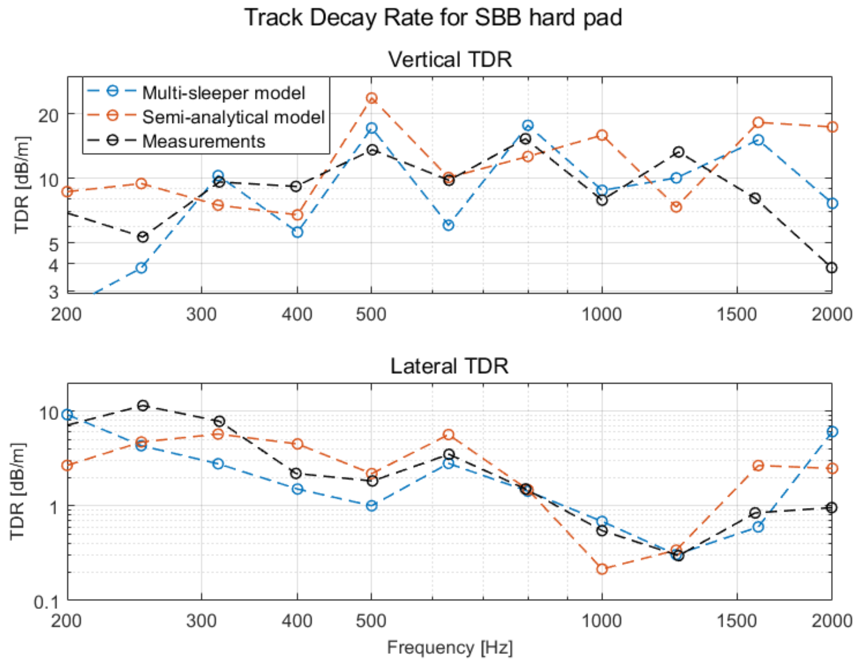

Figure 13 - TDR comparison for SBB hard pad

Finally, to validate the noise radiation assumptions of the multi-sleeper model, measurements that had been carried out in TUM (Münich) during the Novel Railpad project were reproduced numerically. The setup is an 18-sleeper-long test track, and the force and measurement points are as described in the Figure below.

Changing from the SBB hard pad to a high damping pad designed in the Railpad project, measurements predicted a noise reduction of 3dB, while the model predicts 2.2 dB. This difference, which is rather acceptable, can be due to

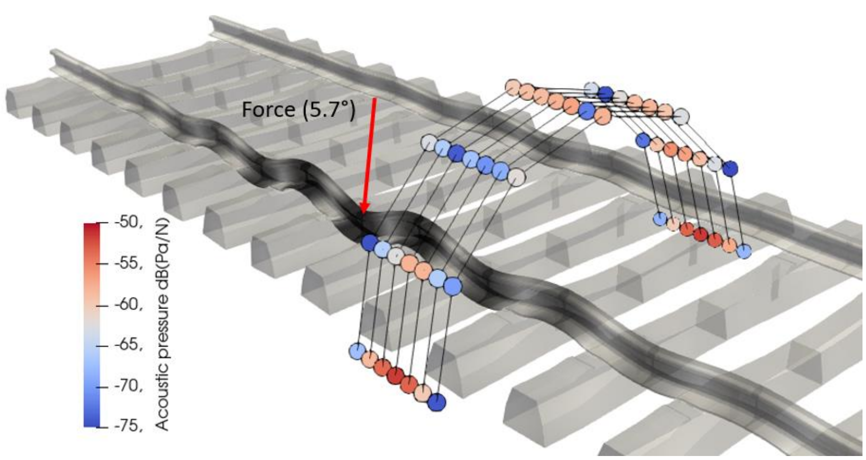

Figure 14 - Simulation of the acoustic measurements in TUM Münich

several factors: acoustic reflections which are not modeled in the simulation, imprecision of far-field to near-field scaling (measurements in near field, while simulations are in far field) and low coherence of the measurements at some frequencies due to some background noise. It is important to keep in mind that the models predictions are useful to compare systems, and it provides good indications about trends & rankings, but the absolute SPL values should not be considered with the current models as the acoustic modeling is not sufficiently detailed to capture the ground interactions, occlusions and reflections.

1.8 Task 2.2: Modular modelling of the sleeper & fastening systems in the simulation toolchain

Several improvements were implemented on the impulse model, used for ballast protection evaluation, and on the multi-sleeper model. Namely, the possibility to change the sleeper in a streamlined manner was implemented which was used for example to evaluate the RpIV wooden sleeper in the parametric studies in WP4. The user can simply browse the folders and select a sleeper mesh, which has been defined previously (Figure 15). Then, the elastic moduli in three directions, as well as Poisson's ratio, hysteretic damping coefficient and density are chosen. The rail geometry is now modular as well with several profiles already available (54E2 / 60E2).

Clamps are now explicitly modelled too. The mesh is defined as 3D spring elements (represented by lines in Figure 15) and the user can provide three stiffness and damping components. In the model, the clamps effect is to add stiffness and damping components in parallel to the rail pads. On a real track, they also pre-stress the rail pads, which tends to stiffen them due to their nearly incompressible nature. To model this effect, the preload of the clamping system must be taken into account in the rail pads properties definition (linearized properties around the preloaded state).

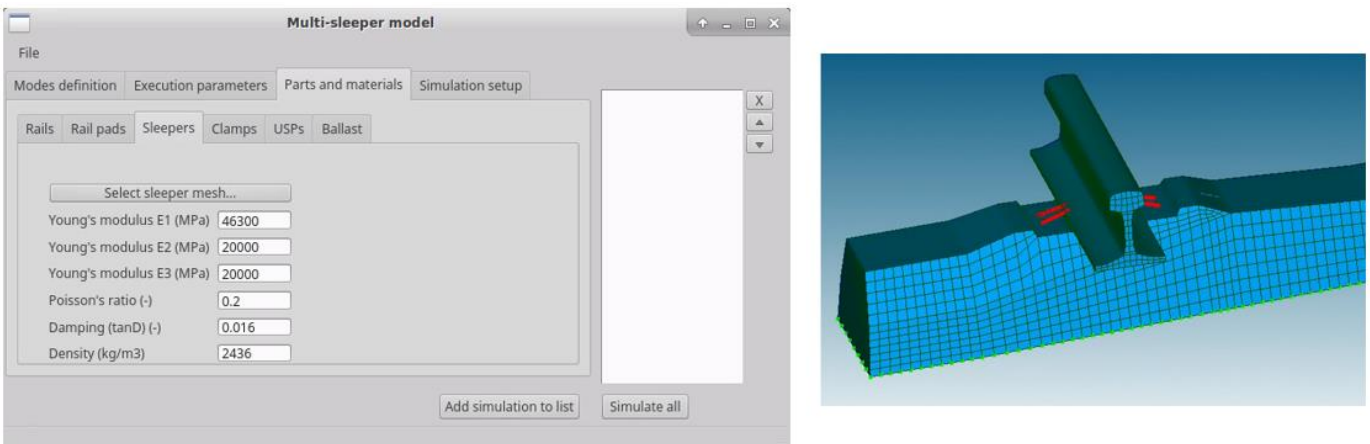

Figure 15 - Modularity of the multi-sleeper model and visualisation of the clamps

Finally, many other new functionalities were implemented to make the multi-sleeper model more modular:

- Sleeper spacing (in impulse model too): a simple variable can be changed to modify the sleeper spacing in the *Simulation setup* tab, set to 600mm by default.
- Sleeper vertical and horizontal stretch: an additional geometry transformation can be applied to change the overall shape of the sleepers. It is implemented in the model, but not part of the GUI yet. It was used in 1.17.1 as geometric parameter. Note that the pads properties are automatically adjusted to compensate their area increase in case of horizontal stretch, and leave their stiffness unchanged.
- Debug mode: when a simulation is over, the terminal remains opened to understand eventual issues more easily.
- Write MED files: unchecking this box allows generating results without the MED results database / visualization files, which are very large, and print only the FRF results text files.
- Macro-element modes selection: the simulations are still done in two steps. The first one computes the macro-element eigenmodes and stores them to be reused. The second and main one, much quicker, selects a subset of the pre-computed modes based on their effective unit mass. The user chooses the total effective unit mass from 0 (excluded; no modes) to 1 (included; all modes), and then chooses the number of rail and interface modes. The default values proposed ensure the convergence of simulations.

In the impulse model, improvements have been done to speed up simulations. Parallelization and time steps optimization are the main aspects that reduced simulation time from more than 20 hours to about 20 minutes. All those developments have been pushed on the Github repository of the project in the "track_evaluation" branch here: https://github.com/jcugnoni-heig/RailTrackModellingToolbox

1.9 Task 2.3: Mixed numerical-experimental identification method of sleeper

1.9.1 Method

The goal of this task is to use the experimental eigenmodes of the sleepers, described in Section 1.10, to identify their materials properties. The inputs are as described in Figure 16: a list of experimental eigen frequencies and their associated mode shapes, an initial guess of the nine orthotropic mechanical constants, and a mesh of the sleeper.

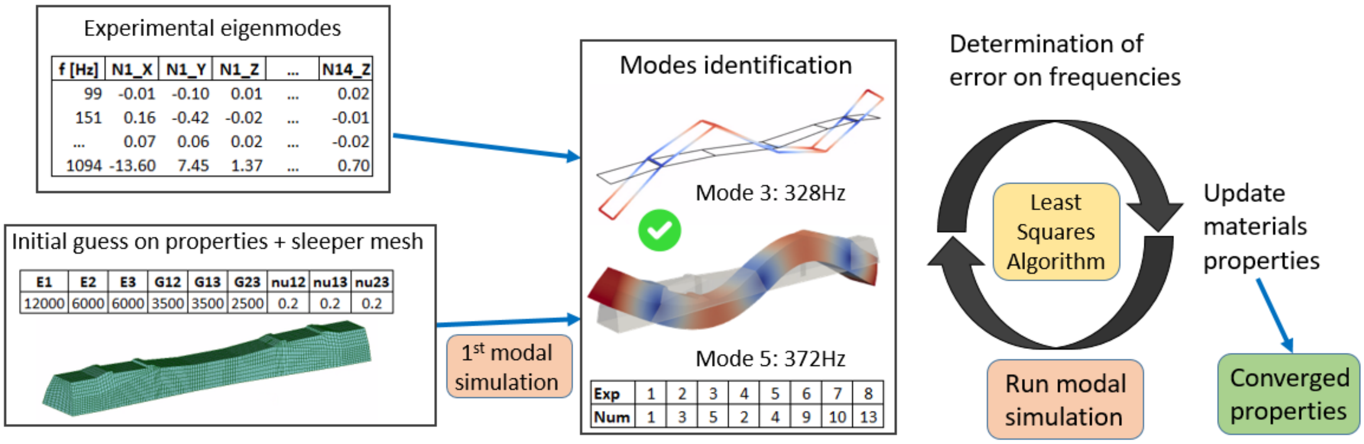

Figure 16 - Sleeper properties identification process

The model iteratively runs modal simulations and tries to associate each experimental mode to the numerical mode, whose shape corresponds best to the experimental mode shape. In practice, a MAC (Modal Assurance Criterion) matrix is defined with the scalar products between all experimental and numerical normalized mode shapes. An example of MAC matrix is shown in Figure 17: it corresponds to the first identification iteration with the RpIV wooden sleepers. Here, the initial properties were quite off the real ones and the modes orders were not the same experimentally and numerically. Despite that large mismatch in the initial guess the mode identification via the MAC matrix ensures that the optimization algorithm remains robust even when the order the modes changes. If the experimental and numerical mode shapes are identical and appear in the same order, the MAC matrix is filled with ones on the diagonal and zeros elsewhere.

		Numerical modes																
		1	**2**	**3**	**4**	**5**	**6**	**7**	**8**	**9**	**10**	**11**	**12**	**13**	**14**	**15**	**16**	**17**
Experimental modes	**1**	0.95	0.00	0.05	0.00	0.07	0.43	0.01	0.00	0.04	0.01	0.58	0.00	0.05	0.03	0.01	0.00	0.03
	2	0.19	0.00	0.03	0.05	0.83	0.14	0.00	0.00	0.01	0.05	0.10	0.01	0.15	0.01	0.00	0.00	0.06
	3	0.07	0.00	0.94	0.00	0.01	0.05	0.00	0.00	0.69	0.03	0.06	0.00	0.02	0.39	0.09	0.00	0.03
	4	0.02	0.00	0.09	0.00	0.03	0.05	0.00	0.02	0.07	0.80	0.00	0.00	0.07	0.05	0.01	0.01	0.02
	5	0.34	0.00	0.10	0.00	0.03	0.90	0.01	0.00	0.14	0.02	0.29	0.00	0.04	0.15	0.04	0.00	0.03
	6	0.09	0.00	0.07	0.03	0.32	0.12	0.00	0.00	0.05	0.04	0.08	0.01	0.80	0.03	0.01	0.00	0.02
	7	0.13	0.00	0.69	0.00	0.01	0.14	0.00	0.00	0.84	0.00	0.09	0.00	0.01	0.70	0.18	0.00	0.02
	8	0.15	0.00	0.01	0.00	0.03	0.08	0.00	0.02	0.06	0.02	0.18	0.00	0.03	0.07	0.02	0.01	0.72
	9	0.40	0.00	0.17	0.01	0.12	0.21	0.01	0.00	0.19	0.03	0.86	0.01	0.03	0.16	0.04	0.00	0.04
	10	0.15	0.00	0.03	0.00	0.05	0.17	0.00	0.00	0.63	0.04	0.07	0.00	0.15	0.86	0.25	0.00	0.08

Figure 17 - Initial MAC matrix obtained with the RpIV sleeper

Finally, a residues vector is defined as the relative error on each eigen frequency. A least square algorithm is used to accurately update the materials properties such that the errors are minimized, until convergence is achieved. The whole process may not be completely automated. Human intervention remains necessary to manually compare the mode shapes, especially when the MAC number is relatively low (poor accuracy of mode shapes). Also, some of the modes can sometimes not be identified, so they may be ignored and removed manually. Moreover, it is possible to choose which properties are fixed, and which are optimized. Depending on this, the algorithm can provide different results, and it remains the user's task to choose wisely how to carry out the optimization. However, the dominant properties affecting flexural modes are usually well identified; the Poisson parameters and transverse shear moduli are however more difficult to obtain and may need to be set manually based on literature data. Finally, the graph below shows an example of the convergence plot for three modes of the RpIV sleeper over the iterations of the optimization algorithm. The jumps seen in the graph corresponds to changes in mode pairing based on the MAC criterion. Despite these potential jumps, the optimization is robust and converges even when the initial values of the elastic properties are far from the actual ones-

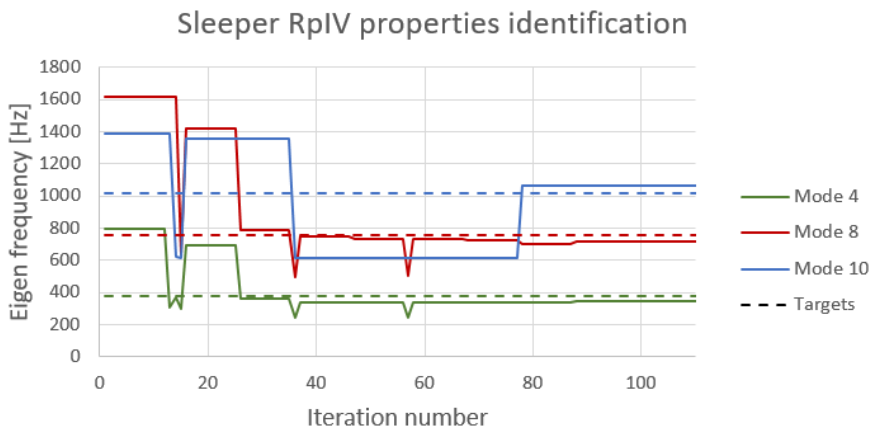

Figure 18 - Modal convergence during RpIV sleeper properties identification

1.9.2 Results

The results of property identification are presented in Table 3. In this case, all properties were selected for optimization and some of them, such as the transverse moduli E_T & E_N, shear coefficients G_TN end up with surprisingly low or high values. This is due to their small influence on the frequency of the measured modes which are mostly bending and torsion modes of a beam. Indeed, the main parameters affecting the frequencies of a beam in torsion / bending are the longitudinal modulus E_L, the shear moduli G_LN & G_LT and to some lesser extend the other parameters. The Poisson ratios are typically not very influential so they can either be left as is or set to the desired physical value. Note that the nomenclature for material orientation “NTL” = “XYZ” in the global coordinate system, such that X is the direction of the track, Y is the vertical direction, and Z is the lateral direction (*i.e.* the direction of the reinforcements for the concrete sleepers.

Also, one can argue that both reinforced concrete sleepers should have the same properties. The program provides different values because, firstly, the modes which could be identified were not exactly the same. Secondly, only 10 to 13 modes were used, so materials properties are optimized for that range (up to ~1600Hz). And thirdly, the results are quite sensitive to the initial guess, to the parameters bounds imposed, and to the tolerance with respect to these bounds.

Table 3 - Identified materials properties of sleepers

	E_L	E_T	E_N	NU_LT	NU_LN	NU_TN	G_LT	G_LN	G_TN
B91 / rail 60E2	46327	32888	37324	0.287	0.464	0.299	20730	18936	14774
B91 / rail 54E2	46432	14640	8652	0.227	0.101	0.217	15240	22405	6805
RpIV	14533	3280	5575	0.172	0.179	0.182	797	963	9026

The Table 4 shows the experimental modes considered, the frequencies obtained after optimization and the error for each mode. It is summarized in Figure 19 in terms of mean error and maximum error amongst the modes, for each sleeper. The errors obtained with concrete sleepers may be lower because some of their properties had been identified manually during the Railpad project, so the initial guess was already very good. Even for the RpIV sleeper, an average error of 4.3% and a maximum error of 13% (mode 2) are very acceptable in the end.

Table 4 - Sleepers modes used for properties identification

B91 / rail 60E2	Mode 1	Mode 2	Mode 3	Mode 4	Mode 5	Mode 6	Mode 7	Mode 8	Mode 9	Mode 10	Mode 11
Experimental [Hz]	113	125	341	363	386	658	724	738	1037	1084	1488
Optimized value [Hz]	112	124	342	363	394	659	712	758	1038	1065	1473
Error [%]	0.6	0.7	0.3	0.0	2.2	0.2	1.6	2.7	0.1	1.7	1.0

B91 / rail 54E2	Mode 1	Mode 2	Mode 3	Mode 4	Mode 5	Mode 6	Mode 7	Mode 8	Mode 9	Mode 10	Mode 11	Mode 12	Mode 13
Experimental [Hz]	110	120	328	348	370	630	710	748	994	1037	1400	1480	1539
Optimized value [Hz]	109	118	332	354	368	639	705	742	996	1045	1396	1458	1557
Error [%]	0.9	1.9	1.2	1.6	0.6	1.5	0.7	0.9	0.2	0.8	0.3	1.5	1.2

RpIV	Mode 1	Mode 2	Mode 3	Mode 4	Mode 5	Mode 6	Mode 7	Mode 8	Mode 9	Mode 10
Experimental [Hz]	100	150	248	376	430	558	659	756	867	1020
Optimized value [Hz]	99	170	250	346	439	530	643	717	853	1064
Error [%]	1.2	13.0	0.7	7.9	2.0	5.1	2.4	5.2	1.6	4.3

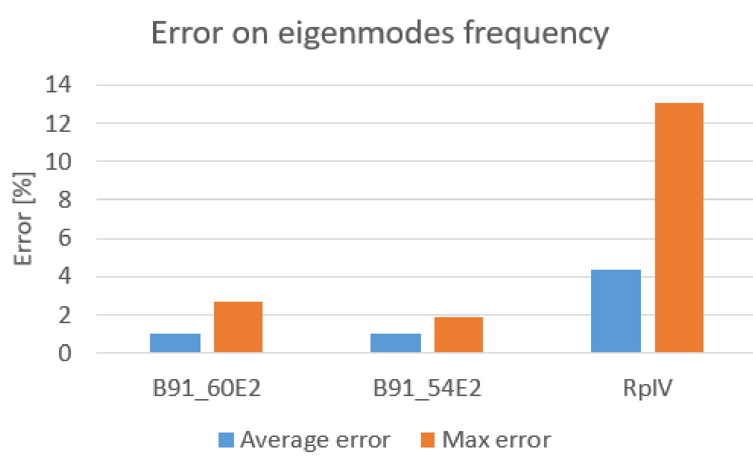

Figure 19 - Error on eigenmodes frequency

WP3: Experimental evaluation of selected combination of rail track components

1.10 Task 3.1: Modal analysis of selected sleepers and fasteners for property identification

1.10.1 Methods

The goal of the modal analysis is to identify the main resonance frequencies (eigenfrequencies) of the sleepers and their associated modal shapes (eigenmodes). It is done using an instrumented hammer and a tri-axial accelerometer.

To perform those measurements, the sleeper is suspended in the air to allow it to vibrate freely, and a mesh of nodes is defined (illustrated in Figure 20). The tri-axial accelerometer is placed on the reference node (in this case, node 1 according to Figure 20). All the nodes (1-14) are then successively hit with the instrumented hammer that records the impact force.

For each node, a Frequency Response Function (FRF) is computed. A FRF is the ratio of the acceleration spectrum measured by the accelerometer over the impact force spectrum measured by the hammer. Acceleration normalised by the force is called accelerance and is expressed in g/N. An example of FRF with the associated phase spectrum can be seen in Figure 21.

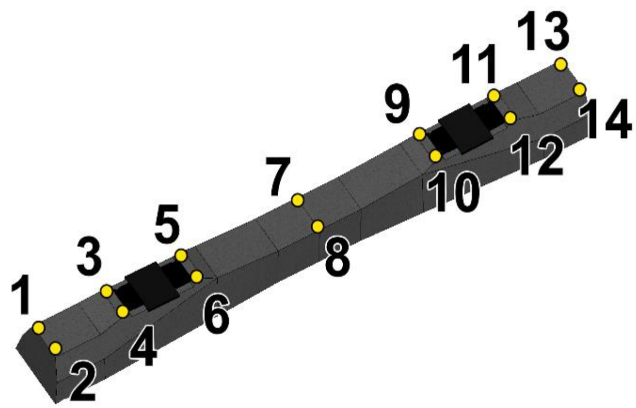

Figure 20 – Mesh used for the dynamic measurements of the sleeper, comprising of 14 nodes.

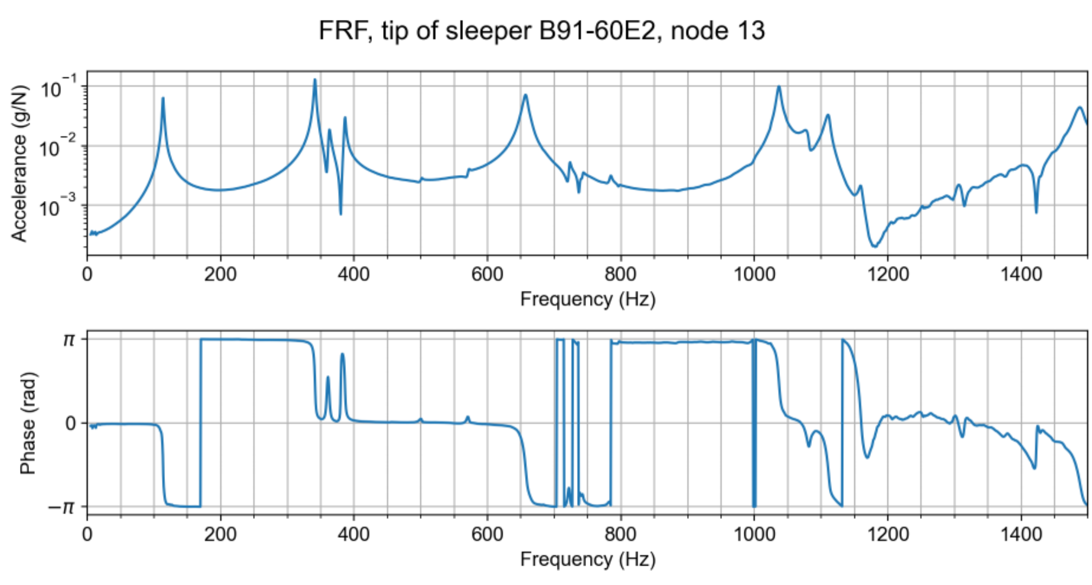

Figure 21 – Accelerance and phase FRF of the B91 60E2 sleeper on node 13, at the tip of the sleeper

These FRF are used for the identification the eigenmodes and eigenfrequencies of the sleepers. The final data consists in a list of eigenfrequencies and shapes that is then used for Task 3 of WP2, *Mixed numerical-experimental identification method of sleeper properties.*

1.10.2 Results

Three different kinds of sleepers have been tested:

- B91 60E2 (concrete)
- B91 54E2 (concrete)
- Rp-IV 54E2 (wood)

The list of the identified eigenfrequencies for each type of sleeper is shown in Table 5. The eigenfrequencies and the succession of shape types are very similar for the two concrete sleepers.

B91 60E2			B91 54E2			Rp-IV 54E2	
Mode frequency (Hz)	Mode shape		Mode frequency (Hz)	Mode shape		Mode frequency (Hz)	Mode shape
113	flexion		110	flexion		100	flexion
341	flexion		328	flexion		150	torsion
363	torsion		348	torsion		248	flexion
386	torsion		370	torsion		340	torsion
658	flexion		630	flexion		376	torsion
724	flexion		750	flexion		430	flexion
785	flexion		800	flexion		455	flexion
1037	flexion		994	flexion		501	torsion
1084	torsion		1037	torsion		558	torsion
1115	torsion		1110	torsion		659	flexion
1160	torsion		1070	torsion		684	flexion
1488	flexion		1400	flexion		731	torsion
1542	torsion		1480	torsion		756	torsion
						867	flexion
						894	torsion
						1020	flexion
						1150	flexion

Table 5 – Eigenfrequencies and their corresponding types.

1.11 Task 3.2: Three sleeper cell vibration and acoustic measurements for selected combination of components

1.11.1 Experimental setup

The experimental setup, depicted in Figure 23 and referred to as *the three-sleeper cell* or *unit-cell*, is a three-sleeper-long railway track segment laid on a ballast substitute made of 10cm-thick wooden beams. It is used to evaluate the vibrations and noise characteristics of various railway components. It also served as a reference for calibration and adjustment of the numeric models. Vibration is induced in the cell by an electromagnetic shaker attached to the tip of one of the rails, at either an angle of 45° or 5.7° (see Figure 23) and fed with white noise, in order to excite the whole frequency spectrum.

The 45° excitation orientation replicates the solicitations on the rail in a curve and allows studying the more global response of the setup, the horizontal and vertical planes being equally solicited. The 5.7° excitation scheme (also referred to as 6°), is closer to the excitation produced by a train pass-by in a straight line and allows studying a more realistic response of the setup.

The vibratory as well as the acoustic response of the unit-cell are measured for each selected combination of components. The measurement methods are briefly described below. Further technical information about those experimental measurements can be found in [2] [3] [4] [5].

It is important to keep in mind that this experimental bench is not a continuous track, and as such, may not be able to capture and show all the effects that apply to a continuous track such as track decay rate effects for example. On the contrary, it may also show effects that do not apply to a continuous track such as the effect of free ends of the rails. Also, although the wooden ballast substitute has a similar level of stiffness to real rock ballast, the sleeper-ballast contact cannot be accurately replicated, thus, effects that rely on that interaction, such as USP influence, may not be entirely captured. Nevertheless, this simple measurement setup was found to provide reliable comparison of noise and vibration levels for different types of pads (as found in the Novel Railpad project) and provides a simple and reproducible method to compare different systems & component choices in laboratory.

Figure 23 – The three-sleeper cell, with the automated gantry used for acoustic measurements, and the electromagnetic shaker set-up for a 45° excitation.

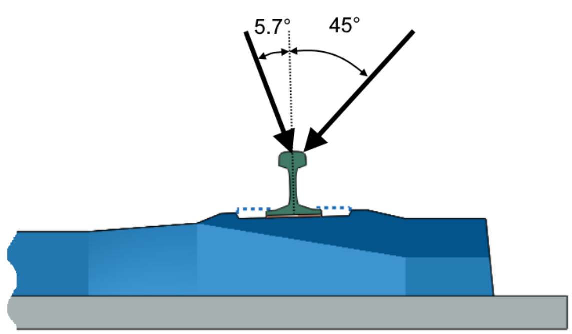

Figure 23 – The two excitation schemes, 5.7° & 45°.

1.11.2 Acoustic measurements

The acoustic measurements were carried out using a method called *acoustic intensimetry*. The main advantages of intensimetry are that it allows suppression of steady background noise and doesn't require an anechoic environment. It has been found to provide consistent and reliable results in the previous Novel Railpad project. A semi-automated gantry, visible in Figure 23, moves a pair of microphones along a virtual surface enclosing the three-sleeper cell. By performing multiple sound intensity measurements all around this surface, the total sound power (in W) emitted by the three-sleeper cell can be found. The spectrum of the sound power is then normalised by the squared spectrum of the exciting force. The resulting normalised power spectrum is a transfer function that represents the acoustic response of the unit-cell for an input force of 1 Newton.

The frequency range of interest is between 300 Hz and 1500 Hz. This is the range where rail vibrations are the main source of noise. Below 300 Hz, vibrations are mostly related to the sleepers and the ballast. By integrating the spectrum over the 300-1500Hz range, the radiated (normalised) acoustic power can be found. Other sub-ranges within this frequency range are also analysed in the same way to further investigate the difference in certain parts of the spectrum, like peaks, for example. Third-octave bands analysis is not used here as a **discrete spectrum bears more information, especially since the object of study is a harmonic response where the peaks and the modal aspect of the sound are of great interest.** A sample of a normalised power spectrum as well as the corresponding integrated normalised sound power levels are shown in Figure 24.

The L_W value of the 300-1500 Hz range is the numeric indicator used to compare different systems against each other, the lower the quieter and thus the better.

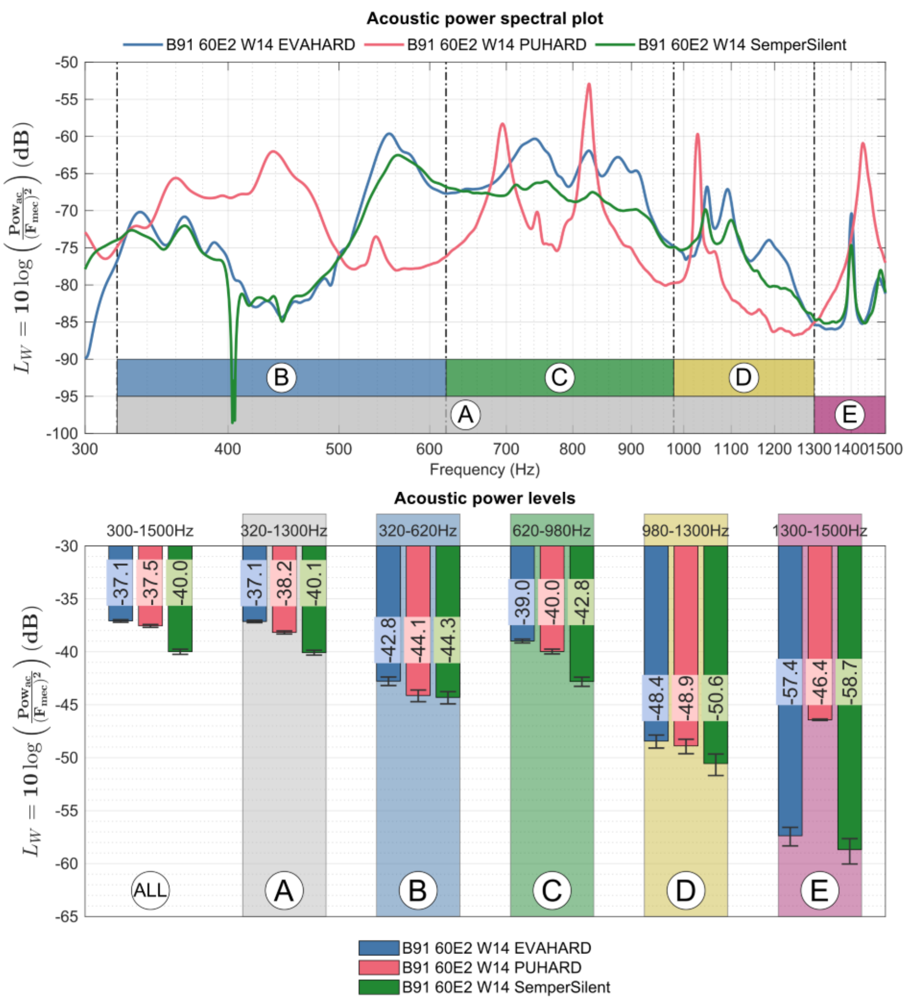

Figure 24 – Sample of acoustic measurement result. The top plot shows the normalised acoustic power plotted against the frequency. The bottom bar graph shows the power levels in decibels of the various ranges highlighted in the spectrum. Lower is better. In addition to the power levels in the bar graph, the modal behaviour of the different systems can be observed in the spectral plot.

1.11.3 Vibration measurements

The aim of vibratory measurements is to capture the dynamic behavior of the structure by measuring the acceleration of specific points. The concept is like the one of modal analysis described in Section 1.10. The three-sleeper cell is excited by an electromagnetic shaker to induce vibrations. The amplitude of these vibrations is measured with a tri-axial accelerometer at various nodes (show in Figure 25) on the cell while the force input by the shaker into the structure is also recorded. A FRF is obtained for each node by normalizing the acceleration spectrum measured by the accelerometer by the force spectrum of the shaker, which equals to accelerance. Throughout the present section, when the term ‘vibration’ is used, it refers to the accelerance values.

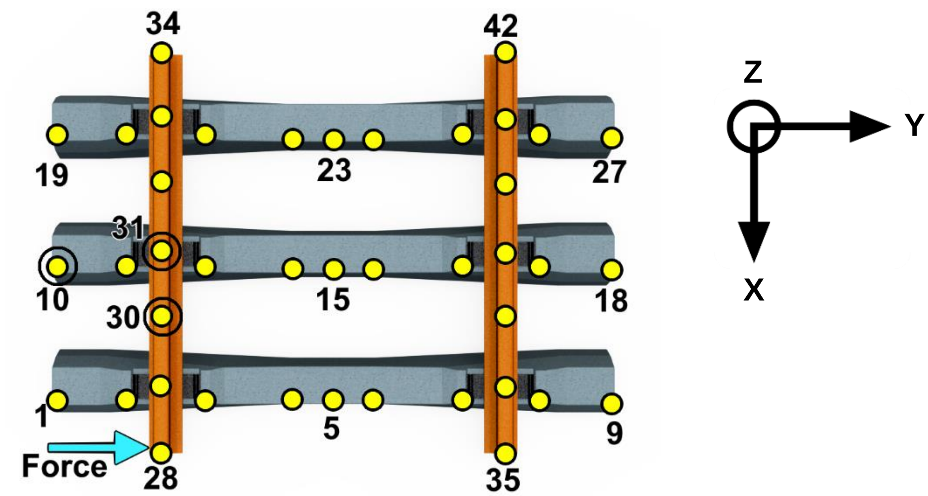

Figure 25 – The 42 nodes where the accelerance is measured. The three nodes of interest, 10, 31, and 31, are highlighted. The force is input in the vicinity of node 28, at either 45° inward or 6° outward (as illustrated in Figure 23). The axis system is displayed on the right. This axis convention is only valid in the present section

.

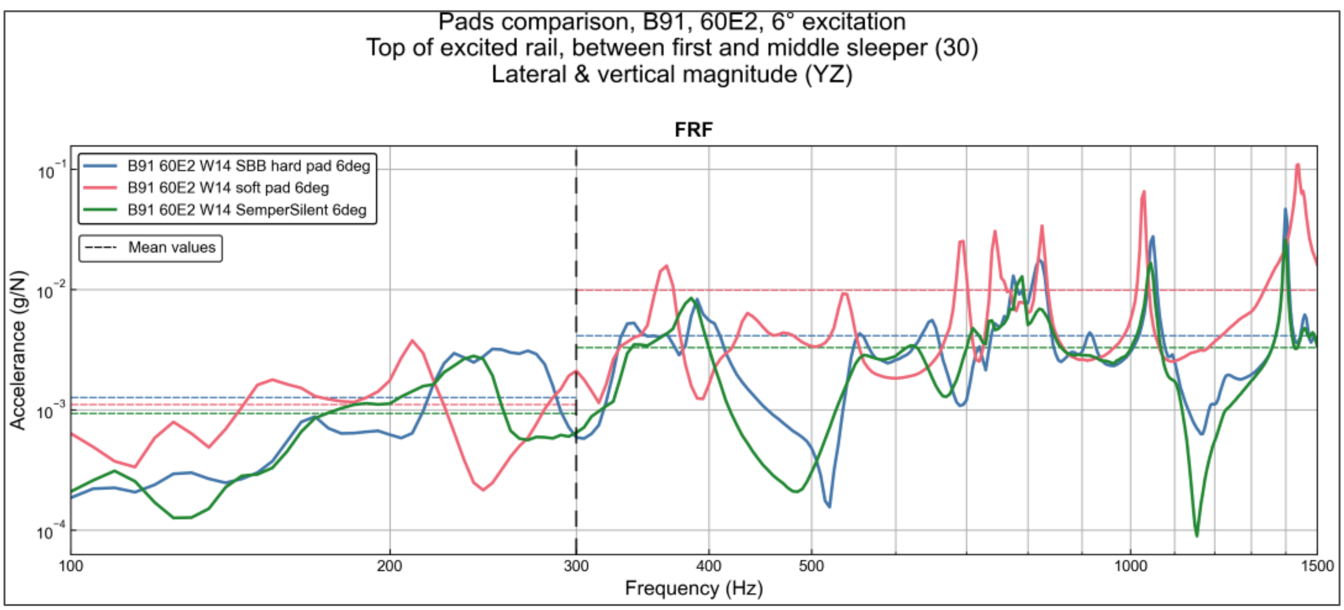

Figure 26 – Sample of FRF plot. The mean values of the LF and HF ranges are superimposed on the plot as horizonal dotted lines.

The FRF of the nodes 10, 31, and 31, as illustrated in Figure 25, are used to evaluate the vibrations of the rail and the sleeper, as they are representative of the behavior of those components. The node 10 likely captures all the modes of the sleeper since it is located at the end of the sleeper. On the rail, two nodes are used in order to capture as many modes as possible.

There are two frequency ranges of interest: the low frequency (LF) range from 100 Hz to 300 Hz, and the high frequency (HF) range from 300 Hz to 1500 Hz. The LF range relates to the vibrations of the sleeper and the ballast, whereas the HF range relates to the vibrations of the rail. In addition to the spectrums, numerical indicators are needed to quantify the vibration levels. For each of the three nodes of interest, the mean values of the FRF are computed over the LF range and the HF range. For the rail, the mean values are averaged between the nodes 30 and 31.

There are therefore **four vibration indicators** in total:

– mean *LF* accelerance of the sleeper, node 10, vertical (Z) magnitude
– mean *HF* accelerance of the sleeper, node 10, vertical (Z) magnitude
– mean *LF* accelerance of the rail, nodes 30 & 31, vertical and lateral (YZ) magnitude
– mean *HF* accelerance of the rail, nodes 30 & 31, vertical and lateral (YZ) magnitude

1.11.4 Numerical indicators, ranking and rating

As stated above, numerical indicators are used to compare the different systems with each other. There are 5 of those indicators:

1. L_W acoustic power 300-1500 Hz
2. mean *LF* accelerance of the sleeper
3. mean *HF* accelerance of the sleeper
4. mean *LF* accelerance of the rail
5. mean *HF* accelerance of the rail

For all indicators, the lower the better. From these, a ranking of the systems (sorting the systems from best to worst) could be made, but the rank does not tell the full picture. For this reason, a normalised rating has been introduced. The rating is comprised between 0 and 1, with 1 being the best. The rating maps the values of a given indicator over the range of all the measured values for that indicator. It is calculated with equation (1):

$$Rating_{indicator-system} = \frac{Value_{indicator-MAX} - Value_{indicator-system}}{Value_{indicator-MAX} - Value_{indicator-MIN}} \qquad (1)$$

The rating is a normalised number that gives insight into how far or how close the systems are to each other in terms of performance (Figure 27).

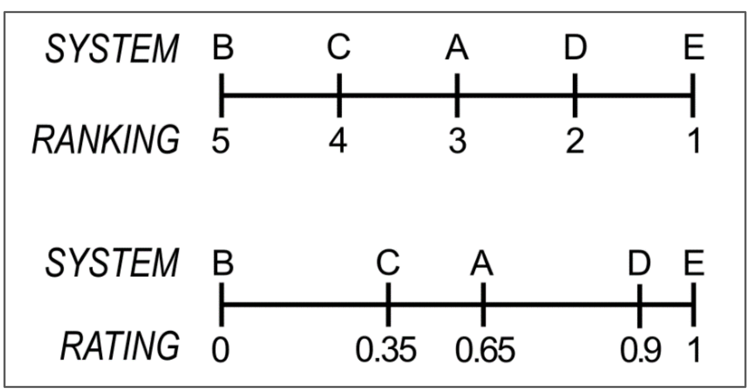

Figure 27 – Visual representation of the differences between the ranking and the rating. A, B, C, D, and E designate hypothetical systems. A ranking and a rating can be calculated for each indicator.

A normalized rating can be derived from each indicator and for two types of loading conditions (45° = curves, 6° = straight lines). The four vibration ratings can also be averaged to obtain only one ”composite” vibration rating. In the end, depending on the point of view of the comparison, the individual ratings can be combined (by mean-averaging) to obtain different comparisons tables as illustrated in Figure 28 below. Finally, a global rankings can derived from these ratings by sorting the systems from the best to worst.

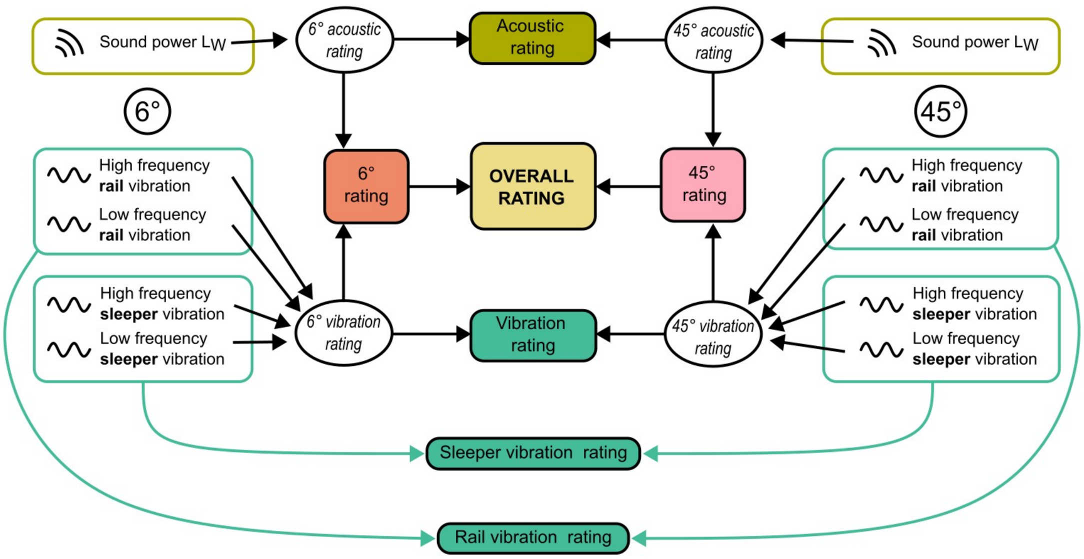

Figure 28 – Relationship and combination between the different ratings. Two arrows pointing at a frame represent a mean-average.

1.11.5 Selected combination of components and naming convention

Different kinds of rail pads, rails, sleepers, and fastener have been selected to be evaluated in different combinations. A specific combination of components is referred to as a system. The 10 different systems that have been tested are listed in the table below. The name *SemperSilent* is a tradename of a high damping pad developed and produced by Semperit Technische Produkte GmbH, Austria. Each system has been tested both with 45° and 6° excitation, and both the acoustic and vibratory measurements have been done. Systems are referred to as the combination of their components in the order *sleeper – rail– fastener – pad*. The soft pad is a foamed PU pad with a static stiffness of 130-140 kN/mm.

For example: *B91 60E2 W14 SBB hard pad*.

Sleeper	Rail	Fastener	Pad	Colour-code
B91 (concrete)	60E2	W14	SBB hard pad	
			Soft pad	
			SemperSilent	
B91 USP (concrete)	60E2	W14	SBB hard pad	
			Soft pad	
			SemperSilent	
B91 (concrete)	54E2	W14	SBB hard pad	
			Soft pad	
Rp-IV (wood)	54E2	SKL-12 (Ke)	SBB hard pad	
		Kpo-3 (K)	None	

Table 6 – List of the systems that have been measured, with the related components.

1.12 Task 3.3: Experimental ranking of the most dominant components and related properties

1.12.1 Rankings and colour-and-texture legend

The sections that follow discuss the ranking of the systems regarding various perspectives and indicators. The various rankings are:

- Acoustic ranking
- Vibration ranking
- 45° ranking
- 6° ranking
- Overall ranking

In the coming ranking bar graphs and tables, a colour-and-texture code has been used for quick identification of the different systems. The four colours designate the four types of pads, and the four textures designate the four types of sleepers / USP combination. The rail type is implied by the sleeper type. The colour-and-texture legend is described in Figure 29 below.

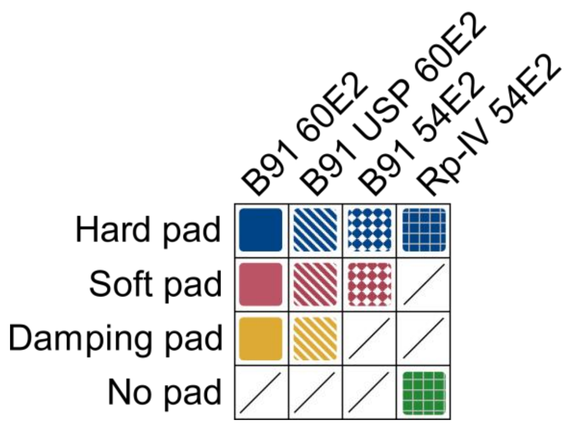

Figure 29 – Colour-and-texture legend for the various bar graphs and ranking tables.

1.12.2 Acoustic ranking

When looking at the acoustic performances of the various systems on Figure 30, we can clearly see that the systems with high damping pads have significantly better acoustic performances than all other systems, with an advantage of ~2-3 dB, whereas the remaining systems are comprised in a range of ~2 dB. This is observable with both 6° and 45° excitation angles.

In straight lines (6° excitation), systems with soft pads appear slightly quieter than systems with hard pads, which is contrary to evaluation on real tracks. This discrepancy can in part be related to the fact that the three sleeper setup cannot replicate the TDR effect and thus underestimates the noise radiation for softer pads. However, if we look at the normalized sound power spectrum in Figure 31, we can see that soft pad systems have a strong modal behaviour characterized by tall and sharp peaks, which are ~5 dB above the other curves. Such high amplitude peaks are known to be particularly annoying, and the human ear tends to be mostly sensitive to dominant harmonic contents. Thus it can be inferred that despite having a relatively low average sound intensity in this measurement setup, soft pads would generate highly noticeable harmonic noise in a real track.

Another visible clearly visible effect in the 6° acoustic ranking in Figure 30, is that wooden sleepers are at least 2 dB louder than all other systems. However, this does not appear under a 45° loading.

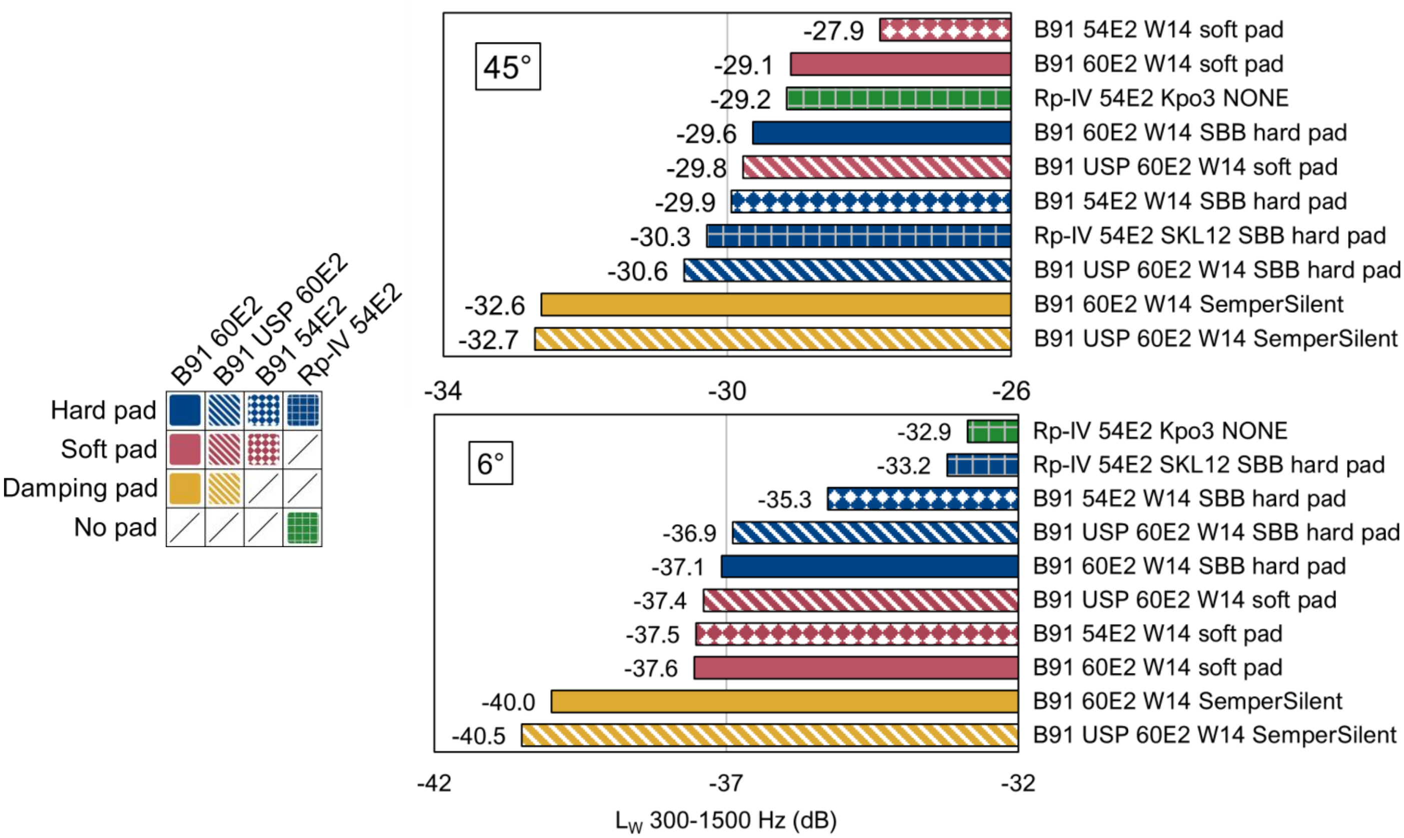

Figure 30 – Acoustic ranking of the different systems, for 45° (top) and 6° (bottom) excitation, with their associated normalised acoustic power levels Lower is better. (L_W)

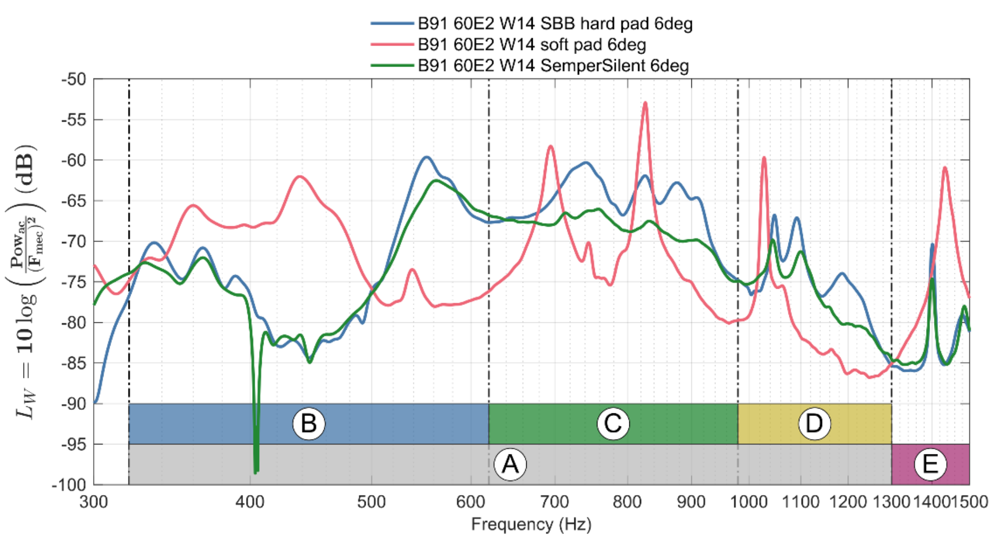

Figure 31 – Normalised sound power spectrum of three systems differentiated by their pads. The strong modal behaviour of the system with a soft pad is clearly discernible.

1.12.3 Vibration ranking

Figure 32 show the rail vibration rankings. In both in straight lines (6°) and curves (45°), the systems with damping pads are among the top three systems. After damping pads, systems with a high rail-sleeper coupling (hard pads or no pads) also show good performance when it comes to HF rail vibration. In curves (45°), systems with damping pads or wooden sleepers show the least LF rail vibration. In straight line (6°), systems with damping pads, and systems with USPs and hard or damping pads, show the least LF rail vibration.

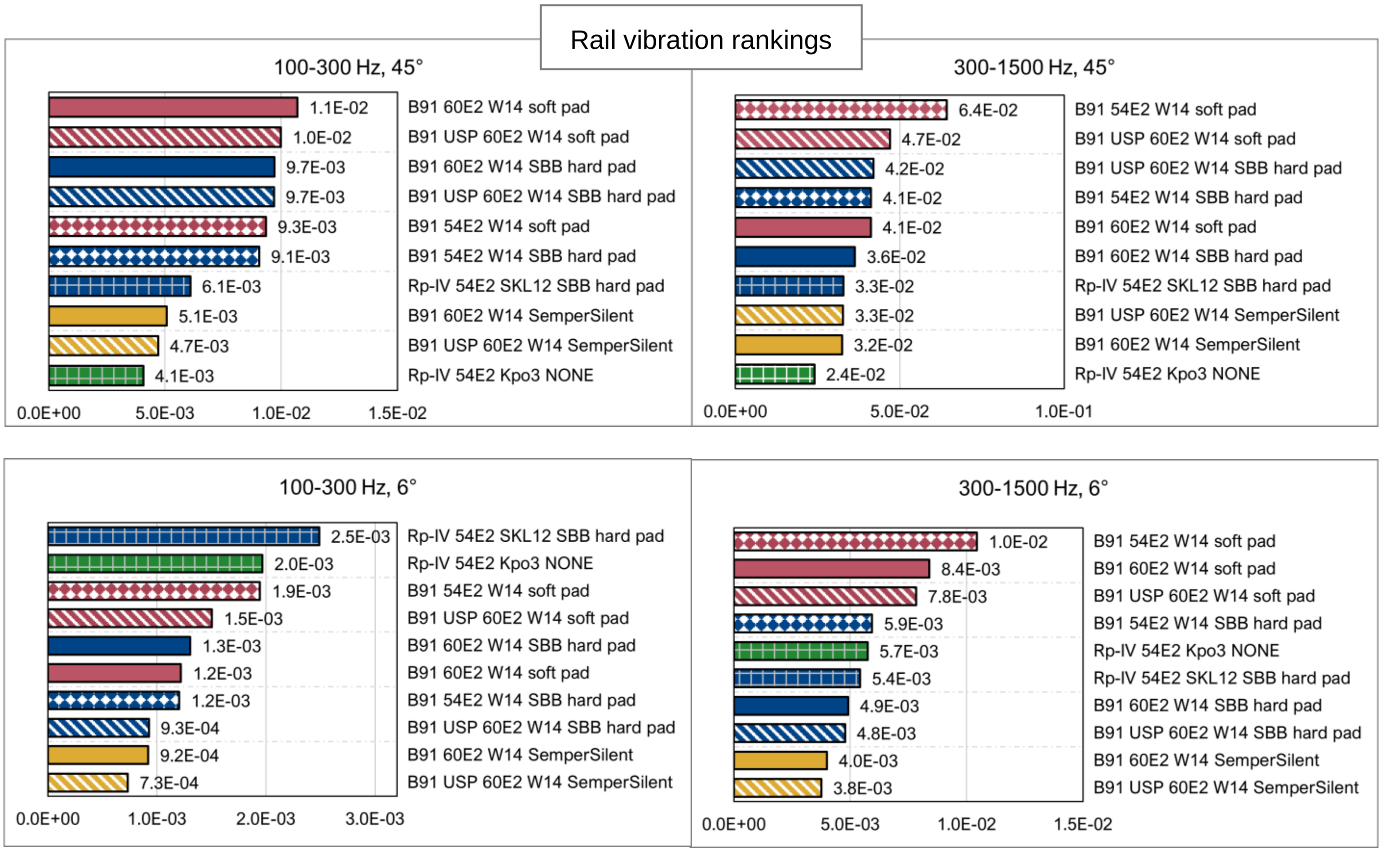

Figure 32 – **Rail** vibration rankings, for the LF and HF ranges, 45° and 6°. The values refer to the mean lateral & vertical (YZ) accelerance in g/N, measured on node 30 & 31 (mean

Sleeper vibration rankings are shown in Figure 33. Hard EVA pads or no pads in the case of the wooden sleeper are the worst conditions in terms of transfer of vibrations to the sleeper and thus the ballast too. HF sleeper vibrations are lowest when systems with soft pads (low rail-sleeper coupling) or damping pads are used. In curves (45°), system with damping pads, and systems with USPs and hard pads are the best at reducing LF sleeper vibration. Overall, systems with 54E2 rails and/or wooden sleepers show the most LF & HF sleeper vibration, except if soft pads are also used. This may be due to the reduced mass, and therefore inertia, compared to other systems.

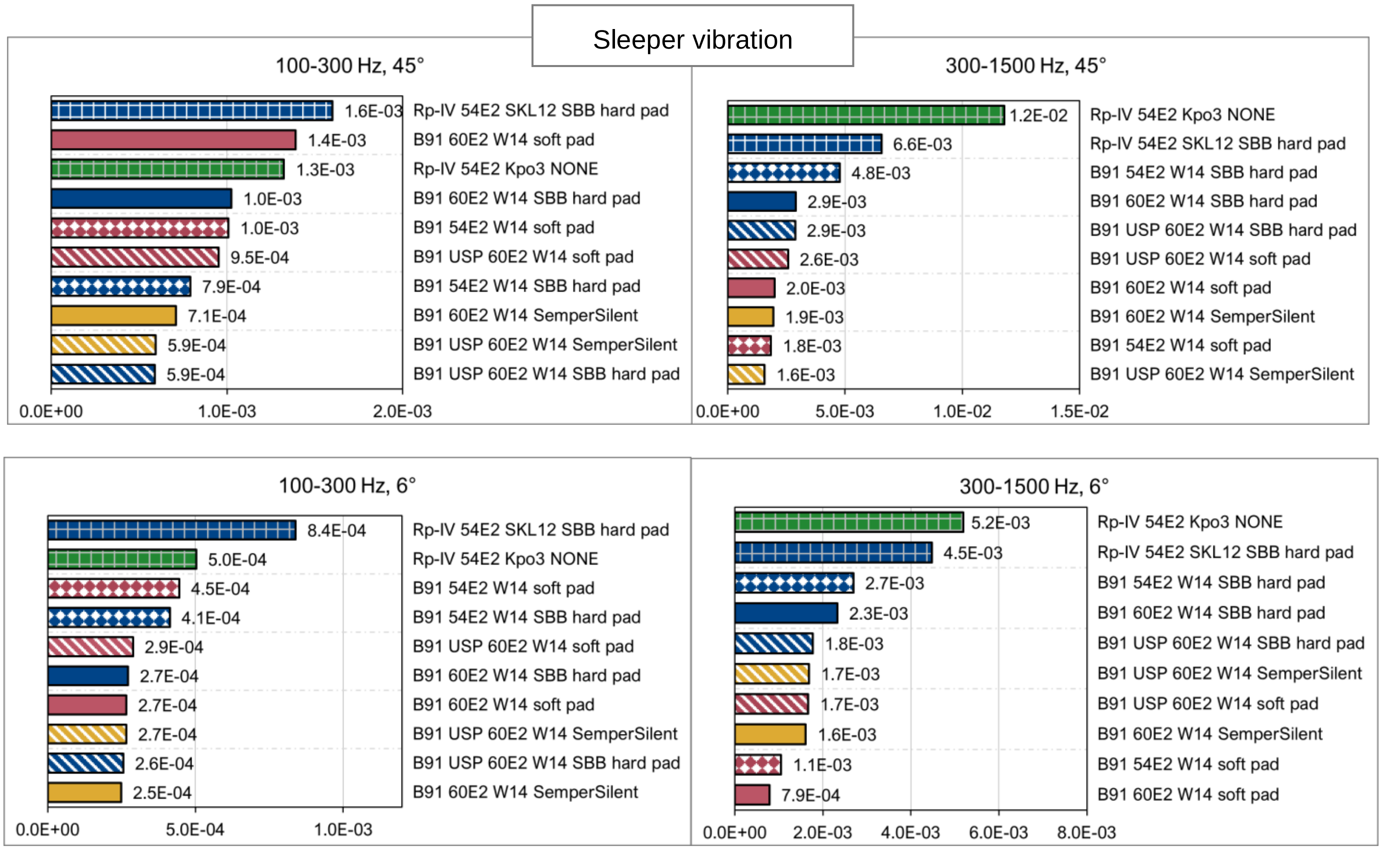

Figure 33 – **Sleeper** vibration rankings, for the LF and HF ranges, 45° and 6°. The values refer to the mean vertical (Z) acceleration in g/N, measured on node 10 of

1.12.4 45° ranking (curved track conditions)

Table 7 shows a recap of the 45° data contained in Figure 30, Figure 32 and Figure 33 in addition to the ranking and ratings for each indicator. The overall 45° ratings show a clear advantage for systems with damping pads. They are

Rating 0.0 … 1.0 best→
Rank 10 … 1 best→

		ACOUSTICS			VIBRATION													
					SLEEPER NODE 10 (Z)						RAIL NODES 30-31 MEAN (YZ)							
		300-1500 Hz			100-300 Hz			300-1500 Hz			100-300 Hz			300-1500 Hz				
		dB (W/N²)	(-)	(-)	(g/N)	(-)	(-)	(g/N)	(-)	(-)	(g/N)	(-)	(-)	(g/N)	(-)	(-)	(-)	
SYSTEM		Lw	Rating	Rank	LF mean acceleration	Rating	Rank	HF mean acceleration	Rating	Rank	LF mean acceleration	Rating	Rank	HF mean acceleration	Rating	Rank	Mean vibration rating	45° normalised rating
B91 USP 60E2 W14 SemperSilent		-32.7	1.00	1	5.9E-04	0.99	2	1.6E-03	1.00	1	4.7E-03	0.90	2	3.3E-02	0.78	3	0.92	0.96
B91 60E2 W14 SemperSilent		-32.6	0.98	2	7.1E-04	0.88	3	1.9E-03	0.96	3	5.1E-03	0.85	3	3.2E-02	0.79	2	0.87	0.93
B91 USP 60E2 W14 SBB hard pad		-30.6	0.57	3	5.9E-04	1.00	1	2.9E-03	0.87	6	9.7E-03	0.15	7	4.2E-02	0.55	8	0.64	0.61
B91 54E2 W14 SBB hard pad		-29.9	0.43	5	7.9E-04	0.80	4	4.8E-03	0.69	8	9.1E-03	0.25	5	4.1E-02	0.57	7	0.58	0.50
Rp-IV 54E2 SKL12 SBB hard pad		-30.3	0.50	4	1.6E-03	0.00	10	6.6E-03	0.51	9	6.1E-03	0.69	4	3.3E-02	0.78	4	0.50	0.50
B91 60E2 W14 SBB hard pad		-29.6	0.37	7	1.0E-03	0.57	7	2.9E-03	0.87	7	9.7E-03	0.15	8	3.6E-02	0.69	5	0.57	0.47
B91 USP 60E2 W14 soft pad		-29.8	0.40	6	9.5E-04	0.64	5	2.6E-03	0.90	5	1.0E-02	0.11	9	4.7E-02	0.43	9	0.52	0.46
Rp-IV 54E2 Kpo3 NONE		-29.2	0.27	8	1.3E-03	0.27	8	1.2E-02	0.00	10	4.1E-03	1.00	1	2.4E-02	1.00	1	0.57	0.42
B91 60E2 W14 soft pad		-29.1	0.26	9	1.4E-03	0.21	9	2.0E-03	0.96	4	1.1E-02	0.00	10	4.1E-02	0.57	6	0.43	0.35
B91 54E2 W14 soft pad		-27.9	0.00	10	1.0E-03	0.59	6	1.8E-03	0.97	2	9.3E-03	0.20	6	6.4E-02	0.00	10	0.44	0.22

Table 7 – Recap of performances for a 45° excitation. For each indicator, their measured value, their rating and their rank are given. Systems are sorted according to their overall 45° rank.

followed by systems with hard pads and finally systems with soft pads, although the contrast between these systems is less strong than the one with damping-pad-systems. Systems with USP's seem to perform a bit better than their non-USP counterparts.

1.12.5 6° ranking (straight line conditions)

Table 8 shows a recap of the 6° data contained in Figure 30, Figure 32 and Figure 33 in addition to the ranking and ratings for each indicator.The systems with damping pads are the best here as well, with a significantly better 6° rating than other systems. The B91 systems, with and without USP's, are next, with no clear trends among them and very similar ratings. At last, the systems with 54E2 rail, and especially those with wooden sleepers, have the clearly lowest ratings.

Rating 0.0 … 1.0 best→
Rank 10 … 1 best→

	ACOUSTICS 300-1500 Hz			VIBRATION: SLEEPER NODE 10 (Z) 100-300 Hz			SLEEPER NODE 10 (Z) 300-1500 Hz			RAIL NODES 30-31 MEAN (YZ) 100-300 Hz			RAIL NODES 30-31 MEAN (YZ) 300-1500 Hz				
	dB (W/N²)	(-)	(-)	(g/N)	(-)	(-)	(g/N)	(-)	(-)	(g/N)	(-)	(-)	(g/N)	(-)	(-)	(-)	
SYSTEM	L_W	Rating	Rank	LF mean acceleration	Rating	Rank	HF mean acceleration	Rating	Rank	LF mean acceleration	Rating	Rank	HF mean acceleration	Rating	Rank	Mean vibration rating	6° normalised rating
B91 USP 60E2 W14 SemperSilent	-40.5	1.00	1	2.7E-04	0.97	3	1.7E-03	0.80	5	7.3E-04	1.00	1	3.8E-03	1.00	1	0.94	0.97
B91 60E2 W14 SemperSilent	-40.0	0.93	2	2.5E-04	1.00	1	1.6E-03	0.81	3	9.2E-04	0.89	2	4.0E-03	0.96	2	0.92	0.93
B91 USP 60E2 W14 SBB hard pad	-36.9	0.53	7	2.6E-04	0.99	2	1.8E-03	0.78	6	9.3E-04	0.89	3	4.8E-03	0.85	3	0.88	0.70
B91 60E2 W14 soft pad	-37.6	0.61	3	2.7E-04	0.97	4	7.9E-04	1.00	1	1.2E-03	0.72	5	8.4E-03	0.30	9	0.75	0.68
B91 60E2 W14 SBB hard pad	-37.1	0.55	6	2.7E-04	0.96	5	2.3E-03	0.65	7	1.3E-03	0.67	6	4.9E-03	0.83	4	0.78	0.66
B91 USP 60E2 W14 soft pad	-37.4	0.59	5	2.9E-04	0.93	6	1.7E-03	0.80	4	1.5E-03	0.56	7	7.8E-03	0.39	8	0.67	0.63
B91 54E2 W14 soft pad	-37.5	0.61	4	4.5E-04	0.67	8	1.1E-03	0.94	2	1.9E-03	0.31	8	1.0E-02	0.00	10	0.48	0.54
B91 54E2 W14 SBB hard pad	-35.3	0.31	8	4.1E-04	0.72	7	2.7E-03	0.57	8	1.2E-03	0.73	4	5.9E-03	0.67	7	0.67	0.49
Rp-IV 54E2 Kpo3 NONE	-32.9	0.00	10	5.0E-04	0.57	9	5.2E-03	0.00	10	2.0E-03	0.30	9	5.7E-03	0.70	6	0.39	0.20
Rp-IV 54E2 SKL12 SBB hard pad	-33.2	0.05	9	8.4E-04	0.00	10	4.5E-03	0.16	9	2.5E-03	0.00	10	5.4E-03	0.75	5	0.23	0.14

Table 8 – Recap of performances for a 6° excitation. For each indicator, their measured value, their rating and their rank are given. Systems are sorted according to their overall 6° rank.

1.12.6 Overall ranking

The Table 9 shows the overall ranking and ratings of the ten evaluated systems. The previous 45° ratings and 6° ratings are also present, as well as an overall acoustic rating and an overall vibration rating. The two latter are found by mean-averaging the corresponding 6° and 45° ratings.

The acoustic rating shows a significant advantage for systems with damping pads compared to other systems. This is also the case with the vibration rating. Unsurprisingly, this is also true in the overall rating, where they have far greater ratings than all the other systems.

Table 9 – Overall ranking of the systems with their associated overall rating. Other ranking and rating that give insight in other perspectives are also given. Ranking and ratings are explained in Section 1.11.4 Numerical indicators, ranking and rating, p.26

Rating 0.0 → 1.0 (best→); Rank 10 → 1 (best→)

OVERALL			45° curves		6° straight lines		ACOUSTICS		VIBRATION: SLEEPER + RAIL		VIBRATION: SLEEPER		VIBRATION: RAIL	
Rank	Rating	SYSTEM	Rank	Rating	Rank	Rating	Rank	Rating	Rank	Rating	Rank	Rating	Rank	Rating
1	0.97	B91 USP 60E2 W14 SemperSilent	1	0.96	1	0.97	1	1.00	1	0.93	1	0.94	1	0.92
2	0.93	B91 60E2 W14 SemperSilent	2	0.93	2	0.93	2	0.96	2	0.89	2	0.91	2	0.87
3	0.65	B91 USP 60E2 W14 SBB hard pad	3	0.61	3	0.70	3	0.55	3	0.76	3	0.91	4	0.61
4	0.57	B91 60E2 W14 SBB hard pad	6	0.47	5	0.66	5	0.46	4	0.67	7	0.76	5	0.59
5	0.55	B91 USP 60E2 W14 soft pad	7	0.46	6	0.63	4	0.49	6	0.60	4	0.82	9	0.37
6	0.51	B91 60E2 W14 soft pad	9	0.35	4	0.68	6	0.44	7	0.59	6	0.78	8	0.40
7	0.50	B91 54E2 W14 SBB hard pad	4	0.50	8	0.49	7	0.37	5	0.62	8	0.69	7	0.56
8	0.38	B91 54E2 W14 soft pad	10	0.22	7	0.54	8	0.30	9	0.46	5	0.79	10	0.13
9	0.32	Rp-IV 54E2 SKL12 SBB hard pad	5	0.50	10	0.14	9	0.27	10	0.36	10	0.17	6	0.56
10	0.31	Rp-IV 54E2 Kpo3 NONE	8	0.42	9	0.20	10	0.13	8	0.48	9	0.21	3	0.75

Also, different patterns emerge from the overall ranking:

- From best to worst, sleepers and rail are ranked as *B91 60E2→ B91 54E2→ Rp-IV 54E2.*
- Within those sleeper types, pads are ranked as *damping → hard → soft*. This is also true for *Rp-IV 54E2* sleepers, where hard pads happen to be more damping than no pad at all.
- Among *B91 60E2* sleepers, systems with USPs are ranked just above their non-USP counterpart.

It is though important to note that the ratings of some systems are close to each other. Given that there is some level of uncertainty in the measurement, it may be possible that some of the patterns mentioned above result from a coincidence. However, the observations that:

- systems with damping pads have the best performance,
- systems with 54E2 rail and especially with wooden sleepers, have the least good performance,
- remaining systems fall somewhere in between,

are clear and evident. This is also true for the acoustic ranking which is almost identical to the overall ranking, except for two systems of which ranks are swapped.

1.13 Influence of the individual parameters on the measured three-sleeper cell performance indicators

For each of the following parameters, one or more comparisons have been done between two systems which are differentiated by a change of said parameter. In this manner, the influence of a change to that parameter on acoustic and vibratory indicators can be studied. Each comparison is done with both 6° and 45° excitation. To keep the main part of the document concise, the details of this analysis can be found in the appendix, section 2.2.

– Influence of pad static stiffness §2.2.1

– Influence of pad damping §2.2.2

– Influence of Under-Sleeper Pads (USP) §2.2.3

– Influence of rail profile §2.2.4

- Influence of sleeper material §2.2.5

– Influence of clamping on wooden sleepers §2.2.6

1.14 Key takeaways from the component analysis in the three-sleeper cell measurements

Considering the data that has been presented in Section 1.12 and 2.2, the main observation is that pad damping is the property that has the strongest beneficial influence on noise, as well as on vibrations. The acoustic and vibration ratings show damping pads systems surpass all the others in terms of overall performance. Also, they offer the advantage of not compromising on the different performance indicators, as they provide increased performance of both acoustics and vibration, and both in curves (45°) and straight lines (6°).

Another aspect that appears to be beneficial in noise reduction is the mass and inertia of the components. 60E2 rail and concrete sleepers show reduced noise emissions in comparison to, respectively, 54E2 rail and wooden sleepers, and more so in straight lines (6°). Obviously, as the performance indicators are all normalized by force, the more massive the components, the less acceleration will ensue and thus a decreased level of sound radiation is to be expected outside of resonances. However, added mass on sleepers also change their own resonances. For example sound of concrete sleeper systems tended to display a slightly more modal sound behaviour, probably due to the reduced damping properties of concrete compared to wood.

USP systems did not have a significant influence on noise in these measurements, but they tend to decrease LF sleeper vibrations, especially in curves / 45° loading. In conjunctions with damping pads, HF sleeper vibration is also decreased, whereas it is increased if used with soft pads.

Pads with a higher static stiffness can improve noise and rail vibration performance, while increasing HF sleeper vibration. In curves (45°), they decrease LF sleepers vibrations, and even more if used with USPs.

WP4: Numerical design space exploration to identify optimal component properties

1.15 Task 4.1: Sensitivity analysis of the different performance criteria with respect to component properties to identify the dominant parameters

1.15.1 Parameters

The sensitivity analysis aims at understanding the impact of a set of parameters on performance criteria related to noise radiation and ballast protection. It allows focusing on the most relevant parameters for the parametric studies carried out in Task 4.3. The numerical models used are the multi-sleeper model (MSM) and the impulse model. The parameters, presented in Table 10, are varied individually around the reference configuration consisting of the following components:

- 60E2 rail profile
- SBB hard pad (EVA)
- B91 concrete sleeper without USP
- Vossloh W14 clamps
- Gravel ballast

Table 10 - Parameters summary of the sensitivity analysis

Parameter	Model(s)	Simu name	Reference value	Deviation	Comment
Rail geometry	MSM, Impulse	P1_rail	60E2	54E2	Sleeper switches from B91VI to B91IV
Sleeper stiffness	MSM, Impulse	P2_slpStiff	E1=46 GPa, E2=E3=20 GPa	15 GPa, 7 GPa	Close to properties of wood ; Shear moduli scaled accordingly
Sleeper density	MSM	P3_slpRho	2436 kg/m3	800 kg/m3	Close to density of wood ; No densities in Impulse because quasi-static
Sleeper spacing	MSM, Impulse	P4_slpSpa	600 mm	900 mm	
Clamp stiffness	MSM, Impulse	P5_clampStiff	W14: 0.75 kN/mm	7.5 kN/mm	
Pad stiffness	MSM, Impulse	P6_padStiff	E (EVA)	E (EVA) x 0.1	
Pad damping	MSM, Impulse	P7_padDamp	tanD (EVA)	tanD (EVA) x 2	
USP	MSM, Impulse	P8_USP	No USP	Include USP	Properties estimation: E=6 MPa, tanD=0.25
Ballast stiffness	MSM, Impulse	P9_balStiff	Empa properties / 350 MPa*	x 0.33	*For impulse model: static value (Thesis Paderno, EPFL)
Ballast damping	MSM	P10_balDamp	Empa properties	x 0.33	In Impulse model, damping not implemented for ballast
Sleeper damping	MSM	P11_slpDamp	0.016	0.04	From concrete to wood ; no sleeper damping in Impulse model
Train velocity	Impulse	P12_trainVel	160 km/h	80 km/h	Time scale of the load profile doubled

The parameters are varied such that the parameter changes make a physical sense, i.e by representing the change from the reference configuration to one possible alternative feasible choice. For example, the properties of the sleepers are chosen such that it changes from concrete to wood, approximately. Concerning frequency-dependent properties such as the pads and the ballast, they are attributed a constant factor along the spectrum in order to keep the number of parameters involved to a manageable level.

1.15.2 Performance criteria

The simulation setups are described in Figure 34. For the multi-sleeper analysis, the track is 400 sleepers long, such that its dynamics at the locations of interest have converged towards an infinitely long track. The excitation is a harmonic force of 1N acting on one rail from 300Hz to 1500Hz, and oriented at 5.7° outwards of the track. The impulse response model correspond to a three sleeper section where the axel loading is approximated by load history with two peaks, separated in time by the interval between two axels of a bogie at the velocity to be modeled.

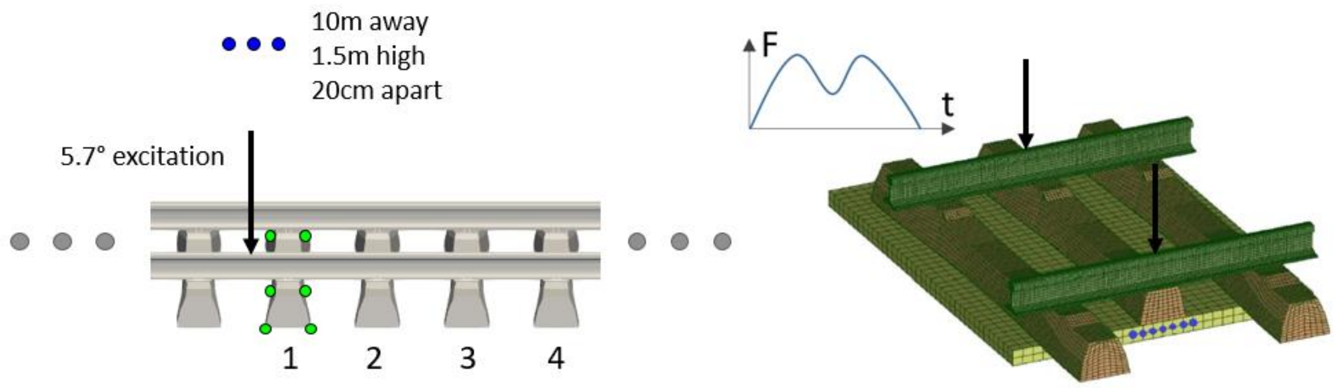

Figure 34 - Multi-sleeper and impulse models

Three performance criteria are considered, all considered the lower the better:

1. Radiated acoustic pressure: to model the loudest noise a microphone would capture during a pass-by, the acoustic pressure is computed at the three blue points located 10m away from the track, 1.5m high and 20cm apart, the middle point being aligned with the excitation force. With a single point, the resulting value would be too sensitive on its location due to additive and substractive interferences. The spatial and spectral average is then computed to define a scalar indicator.
2. Ballast dynamic loading: the vertical acceleration of the sleeper, which is the closest to the excitation, is taken at 14 points and averaged in space and frequency as well. This sleeper is selected because it is the one undergoing the largest accelerations, hence participating the most to the ballast settlement. Obviously, as the sleeper is in contact with the ballast, the sleeper acceleration corresponds to the local acceleration of the contacting layer of ballast and thus serves as an indicator of the forces for the dynamic settlement of the ballast (micro motion due to wear and temporary loss of friction).
3. Ballast static loading: this indicator is calculated with the impulse model, taking the average of the vertical stress in the ballast at the purple dots. The largest stress encountered in time gives the ballast static loading indicator. Due to ballast degradation by wear and fracture, the higher the ballast stress, the faster the track geometry will degrade. This indicator thus indirectly represents the potential effect on track tamping interval and thus maintenance costs.

These indicators being defined, the values of interest in this section are actually their sensitivity to a nominal change in the parameters. The sensitivity is defined as the relative change of an output y normalized by the relative change of an input parameter p and can be visualized as a sensitivity matrix, whose dimensionless components are

$$S_{ij} = \frac{\frac{y_i - y_{ref}}{y_{ref}}}{\frac{p_j - p_{ref}}{p_{ref}}} \quad i = 1, \ \dots, 3\,; j = 1, \ \dots, 12.$$

Thus for example, a sensitivity Sij of 10% means that for a doubling of the input parameter (+100% change), the performance indicator only changes by +10%. Thus the magnitude of the sensitivity represents the “amplification factor” of that system to a given input *i* with respect to the output *j* . The sign of the sensitivity also informs about the positive or negative effect of the parameter on the output. A positive sign means that if the input increases, the output increases as well, while a negative value represents and opposite trend.

1.15.3 Results

The sensitivity values are shown in the graphs below. Note that for parameters P1_rail and P8_USP, there is no normalization by the parameter relative increase because of their boolean nature: the rail switches from 60E2 to 54E2 in the first case, and the USP is included in the second.

These graphs can be interpreted as the amplification factor of the system between a change of input (component property) to a change of output (performance indicator). It is therefore interesting to see that all indicator changes are bounded between -1 and +1 meaning that all performance indicators scale in a less than proportional (<1x amplification factor) for any parameter.

The parameter, which has the largest influence on these indicators is the sleeper spacing: the first graph shows that increasing the sleeper spacing would increase significantly the radiated noise as one could intuitively expect. If the system was simply linear, it could be considered in the opposite way, meaning that reducing the sleeper spacing could reduce noise. However, decreasing sleeper spacing would create many challenges in terms of maintenance and additional costs & material use for the construction. it would also highly increase the sleeper acceleration (from 300Hz to 1500Hz), and the stress in the ballast.

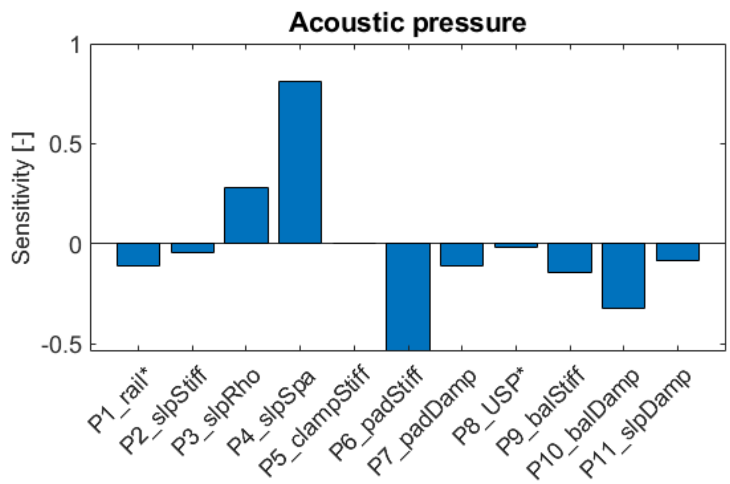

Figure 35 - Sensitivity of acoustic pressure to the parameters

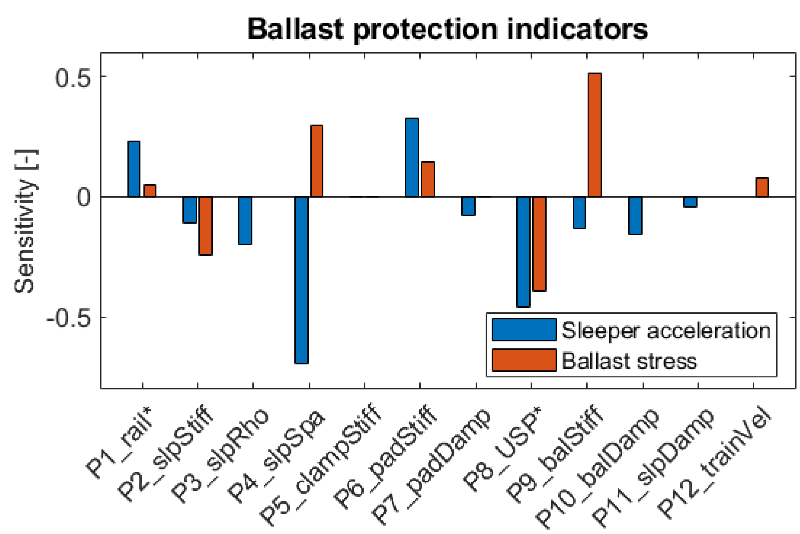

Figure 36 - Sensitivity of ballast protection indicators to the parameters

The pad stiffness has a large impact on the radiated noise as well: increasing the stiffness decreases noise because the rail is more coupled to the sleepers and the ballast. However, for the same reasons, it increases the vertical acceleration of the sleepers and tend to increase the peak stress in the ballast during impulse loading. Concerning the noise indicator, the next most influent parameters are the ballast and sleeper properties. Ballast damping obviously reduces noise and sleeper acceleration, but it is difficult to control. Ballast stiffness tends to decrease noise as it provides a stronger coupling of the sleeper – rails to the ground, but it increases a lot the static stress concentrations in the ballast. Whether this is a critical increase depends on the actual strength of the “ballast” bed.

The inclusion of USP has very little impact on noise in the model, but has an important impact on ballast protection. The results show that with USP, the sleeper vertical acceleration and the vertical stress in the ballast are reduced by about 40%. Without any bad impact on noise, it appears very beneficial to use USP.

1.16 Task 4.2: Evaluation of performance indicators based on application scenarios

1.16.1 Parameters

In this section, various possible configurations will be compared in terms of noise and ballast protection. The reference remains exactly as described in 1.15, and five “derived” configurations, summarized in Figure 37, have been simulated. Each configuration differs from the reference as it is indicated, either by changing the sleeper, the rail pad, or by including a soft or a hard USP. Thus this parametric study corresponds to the analysis of potential realistic component changes in the track construction.

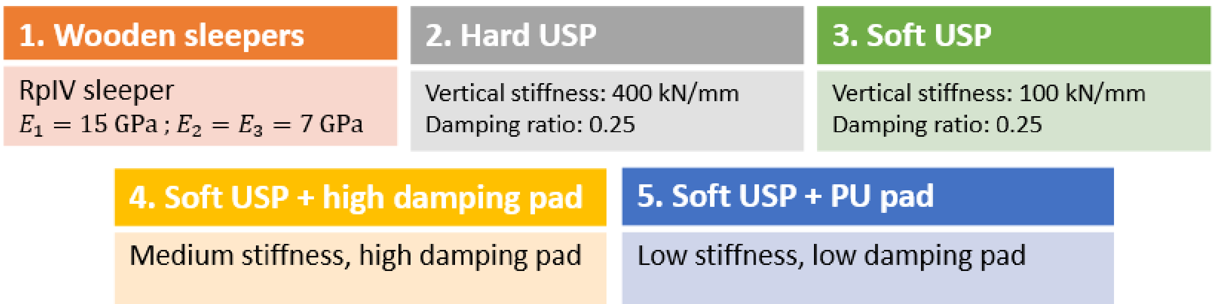

Figure 37 - Derived configurations evaluated wrt to the reference configuration (60E2/hard EVA pad/B91/no USP)

The performance criteria are very similar to those presented in 1.15, except that more points were used for the acoustic calculations. The group of three points shown previously provides an acoustic indicator for a location in front of the excitation point, and two additional sets of points, 10m and 20m further along the track, allow computing two more acoustic indicators that allow evaluating how quickly the noise radiation decreases with distance (TDR effect).

Also, the dynamic ballast protection criterion, based on the vertical acceleration of sleepers, was observed on other sleepers: on sleepers number 1, 2, 3, 21, 22 and 23 from the excitation force, to have a broader overview of the tracks dynamics.

1.16.2 Noise results

In Figure 38 are shown the SPL differences obtained with each configuration, with respect to the reference configuration from 300Hz to 1500Hz. The figure also shows SPL differences in dB(A), meaning that an A-weighting filter has been applied to take into account the sensitivity of the human ear to different frequencies.

The configuration with wooden sleepers reduces the SPL in front of the excitation, but it increases it further: almost +4dB 20m away. This effect can be expected to be related to a reduced track decay rate (TDR) which make a longer part of the track vibrate.

With USP, whether they are hard (400kN/mm) or soft (100kN/mm), the differences are very small. Track noise is slightly increased below 1kHz and decreased above, which somehow compensates the effect on SPL once integrated. However, in the dBA scale, it makes a larger difference: SPL are reduced by up to 2dBA, and this effect is the same with both of the USPs used. Thus the effect of USP on noise is potentially more pronounced at higher frequencies in the model where A weighting is the strongest. This trend has not been observed in real measurement to our knowledge but it could be related to the assumed damping properties of the USPs which where roughly estimated due to a lack of detailed material properties of the USP.

Combining soft USP and a high-damping pad decreases significantly the radiated noise SPL at the three observed points: -2dB to -5dB depending on the observation point. In the dBA scale, the noise reduction is more pronounced too and reaches -4dBA to -7dBA.

For soft USP with PU pads, it is the opposite. There is a very large SPL increase is predicted by the model, which can be explained by the reduction of the coupling of the rail from the sleepers and ground, and thus allow the rail to vibrate more freely. Moreover, the low damping of those two components lead to FRF peaks that are very high and narrow, making a more modal sound, which is usually more annoying than broad band noise.

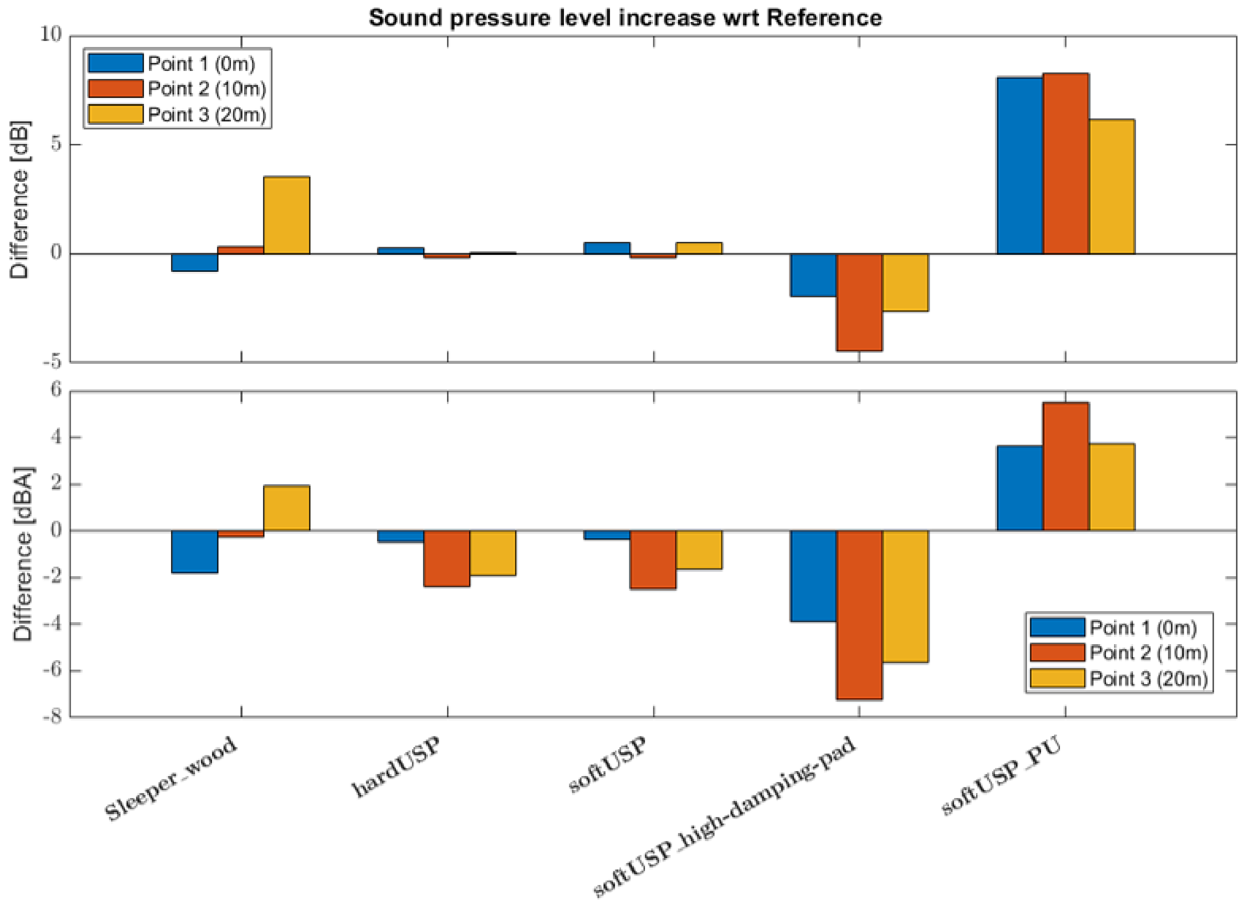

Figure 38 – SPL in dB & dB(A) increase at three locations, compared to the reference configuration

1.16.3 Ballast protection results

The largest stresses in the ballast, computed as explained in 1.15.2, are presented in Figure 40 with their variations with respect to the reference configuration. It is clear that the sleeper type and the USP stiffness have a larger influence on this criterion than the pad properties. With soft USP, the stress is decreased by more than 50%, and by about 40% with hard USP. The role of the USP is to spread the load more evenly from the sleeper to the ballast, and also to reduce the peak forces by deforming and spreading them in time like a shock absorber. Furthermore, USP redistribute the load to the surrounding sleepers more efficiently. This can be observed on Figure 39, where the stresses on the ballast are compared from one system to another.

On the other hand, the RpIV wooden sleeper turns out to locally increase the stress. Its compliance could suggest that the forces will be attenuated the same way they are with USP, but since they bend much more under the load, the stress distribution is far from homogeneous. Figure 39 clearly shows large concentrations under the load application. Therefore, regarding this criterion, the best solution appears to be a combination of stiff sleepers and soft USPs.

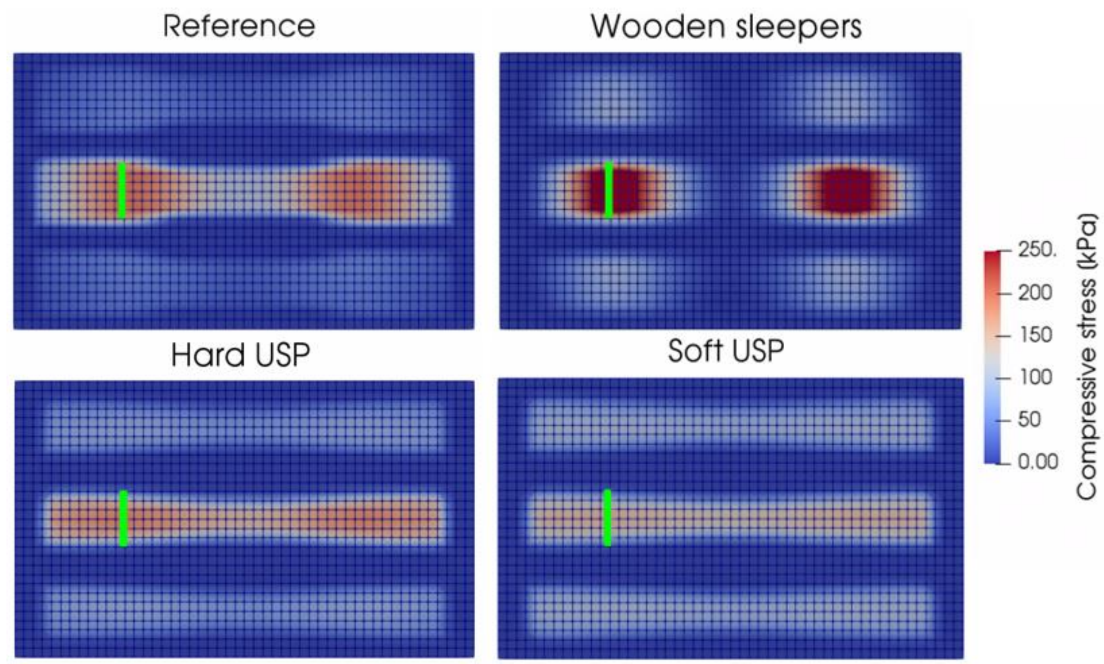

Figure 39 - Vertical stress distribution in the ballast during pass-by

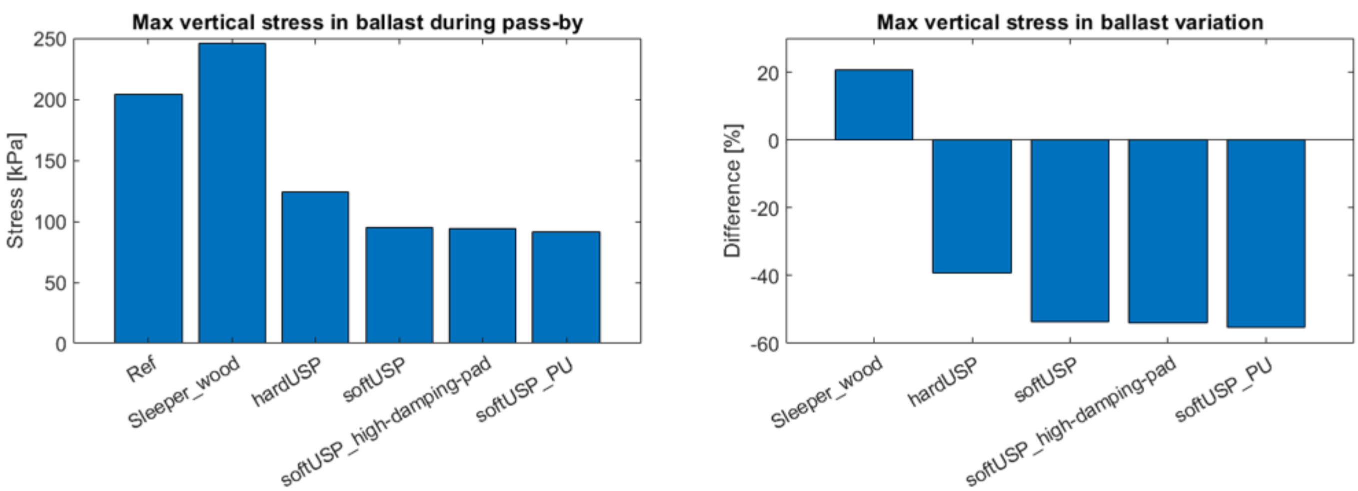

Figure 40 - Maximum stress in the ballast during pass-by

The second ballast protection criterion, based on sleeper vertical acceleration, is presented in Figure 41. For each configuration, the mean vertical acceleration was calculated from 300Hz to 1500Hz, and compared to the reference configuration. Firstly, wooden sleepers vibrate much more than concrete ones because they are lighter and thus easier to excite for a unit applied force. The larger mass of B91 sleepers acts as an inertial cantilever in this part of the spectrum.

USPs tend to damp vibrations, especially close to excitation (sleepers 1-3), but they do not make a large difference further (sleepers 21-23). Harder USPs seem to be reduce vibrations a bit more efficiently.

The effect of pad stiffness and damping is strong too. With a high-damping pad, the vertical acceleration on the sleepers decrease a lot, for all sleepers that have been observed. Indeed, the larger damping attenuates vibrations in the whole spectrum, along the whole track. With PU pads, the sleepers 21 to 23 vibrate much more while the closer ones (1-3) vibrate less. It reflects again the fact that the TDR is lower with these pads.

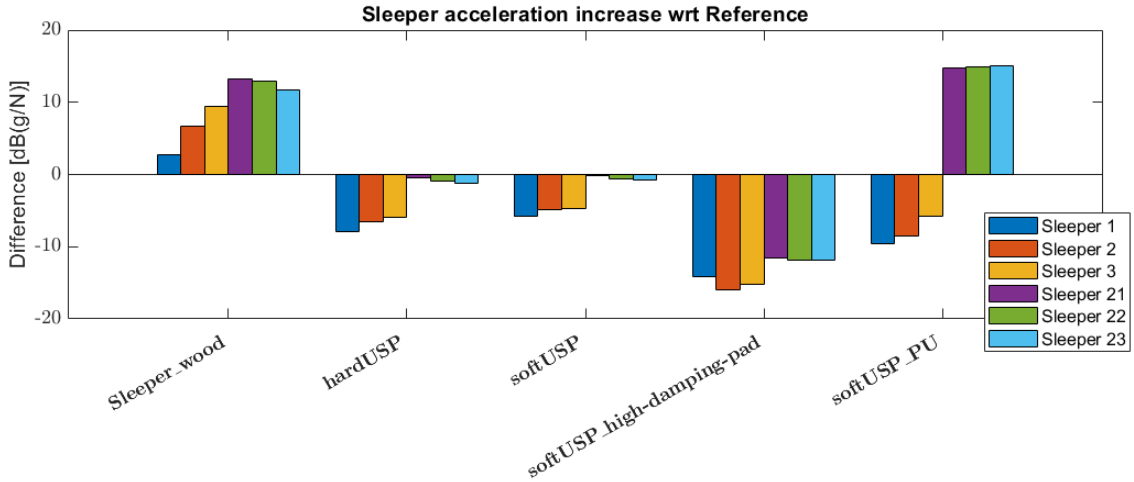

Figure 41 - Sleepers vertical acceleration compared to reference configuration (300-1500Hz)

To conclude, taking into account all aspects of this scenario analysis, the best configuration would be to keep B91 concrete sleepers for their stiffness, mass and stability. To enhance ballast protection, the use of soft USPs turns out to be efficient for the static criterion as well as for the dynamic one. As for rail pads, a medium stiffness with a high damping is the best option among the considered cases.

1.17 Task 4.3: Design space exploration to highlight the optimal component properties

1.17.1 Parametric study 1

Parameters

In this first parametric study, the design space is explored by choosing relevant component parameters and varying them independently around a reference from very low to very high values, thus allowing to identify potential non-linearities or threshold effects in the system's response. Based on the results of the sensitivity analysis detailed in 1.15 and on discussions with SBB representatives, the chosen set of parameters and values is shown in Table 11.

The reference configuration here, which corresponds to bolded values, is similar to the reference described in the previous sections (SBB pads, B91 sleepers, 60E2 rail profile), but for simplicity all values are constant in the frequency range, therefore it does not exactly correspond to physical components. The sleeper geometry parameter was added to simulate the fact that sleepers could hypothetically be made thinner or larger. To avoid modifying their mass with this purely geometric parameter, the product of the stretches in the X (horizontal) et Y (vertical) directions is equal to 1. The sleeper spacing was keep constant however as it would require more radical changes to the whole operation / maintenance of the railway network.

Table 11 - Parametric study parameters

		Val1	Val2	Val3	Val4	Val5	Val6	Units	Comments
Sleeper	Density	800	1500	**2500**	4500	8000	None	kg/m3	From wood to steel
	Modulus	10	20	**50**	120	200	None	GPa	" & transverse modulus halved
	Geometry (scale X,Y)	1.5, 0.66	1.25, 0.8	**1, 1**	0.8, 1.25	0.66, 1.5	None	-	Volume remains constant
Pad	Stiffness	30	120	400	**1100**	2000	4500	kN/mm	Controlled by E with Poisson=0 ; Frequency-independent
	Damping ratio	0.01	**0.15**	0.35	1	2.5	None	-	Frequency-independent
USP	Stiffness	90	150	250	**420**	700	None	kN/mm	Controlled by E with Poisson=0 ; Freq-independent ; tanD=0.2
	Damping ratio	0.01	**0.2**	0.35	1	2.5	None	-	Frequency-independent
Ballast	Stiffness	100	200	**1000**	8000	40000	None	kN/mm	From a soft ballast layer to a 300mm thick concrete slab ; tanD=1

The indicators considered, computed with the multi-sleeper model, are similar to those explained earlier:

- Mean and max acoustic pressure in front of the excitation force (from 300Hz to 1500Hz), see Figure 34.

- Mean and max vertical acceleration of the first sleeper (from 300Hz to 1500Hz); the ballast protection criterion is computed with the multi-sleeper model because it would have taken too much time to simulate all these cases with the impulse model, which is much less automated.

Results

The results in terms of acoustic pressure radiated at the point of observation are presented in Figure 42. To reduce the radiated noise SPL, some parameters are much more efficient than others. The most noticeable ones are:

- Rail pad damping ratio: increasing it decreases the SPL drastically in the total range of simulated values.
- Pad dynamic stiffness: below 400kN/mm, it has very little effect on the noise indicator, but there is a threshold around 400kN/mm, above which the noise clearly decreases. In the second parametric study (1.17.2), it will be shown that this behavior happens with a pad damping ratio under about 0.2.
- Ballast stiffness: there is also an interesting threshold at 1000kN/mm, above which the radiated noise tends to decrease. It should be noted that this threshold values is roughly equal to the rail pad stiffness in this case.
- Sleeper density: the SPL constantly increases with the sleeper density. It may be due to the fact that the increasing mass of the sleeper makes it vibrate less, hence transmitting less vibrations to the ballast and by conservation of energy, concentrating most of the vibrations into the rails. However, thanks to the scenarios evaluation presented in 1.16, it is observed that the SPL reduction is not as significant along the whole track (as sleeper mass also affects TDR), and that lighter sleepers (which are generally more compliant too) such as the RpIV have a negative effect regarding the ballast protection criteria.

The influence of the other parameters is quite low compared to the ones highlighted above.

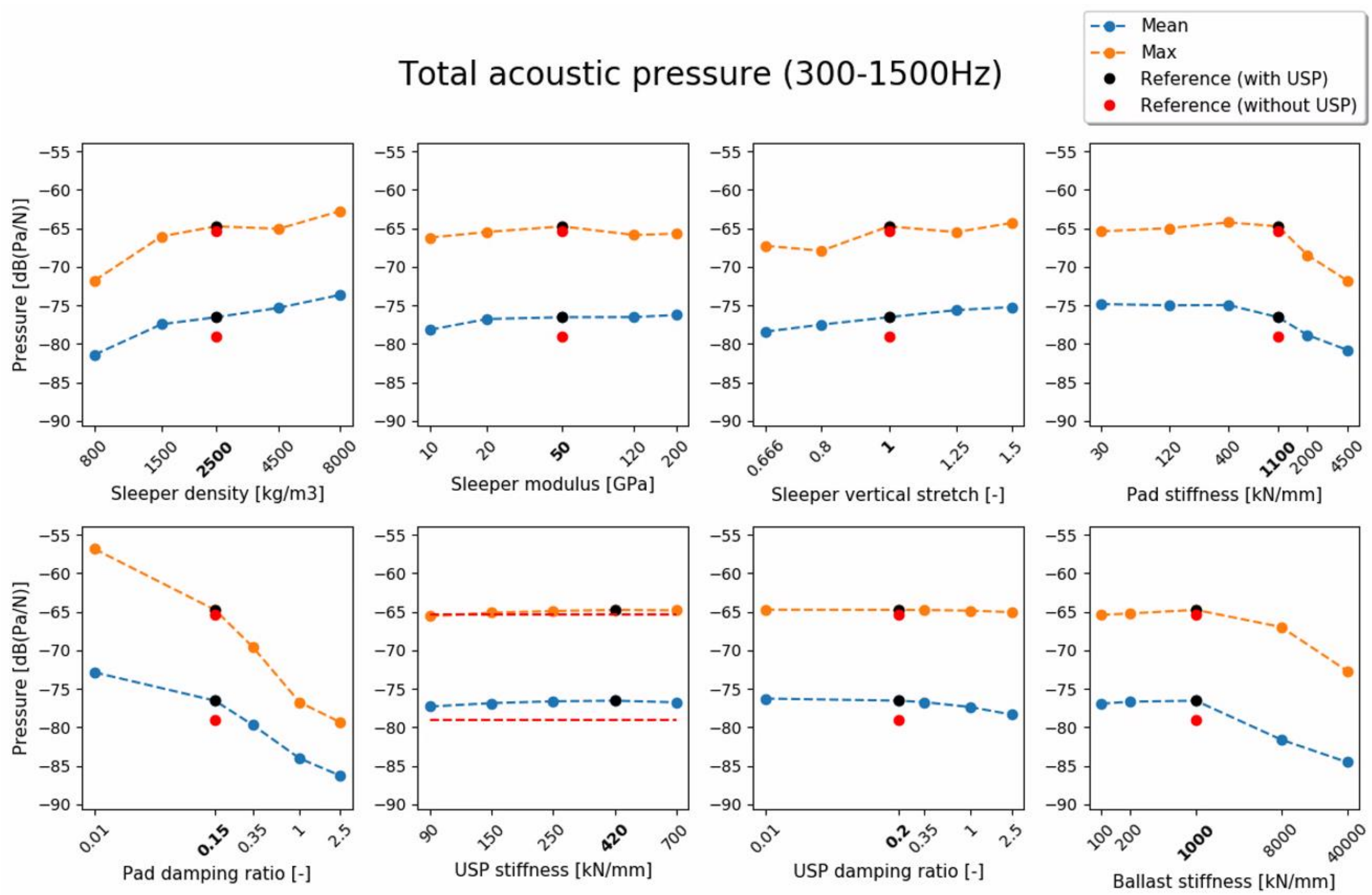

Figure 42 - Acoustic pressure in front of the excitation force, 10m away

The ballast protection indicator results are shown in Figure 43.

- It is interesting to notice that ballast protection indicators all improve in the presence of USPs, for all simulated value of these parameters.

- Pad stiffness highly increases sleeper acceleration. Unfortunately, its effect on this indicator is totally opposed to the noise indicator. Thus changing only the pad stiffness requires to find a compromise between noise and ballast loading. So it is more interesting to adjust simultaneously multiple properties of the track components to bypass this tradeoff situation . For example, if the pad stiffness is increased to improve the noise indicator, the decay in dynamic ballast protection could be compensated by including USPs.
- The ballast stiffness of 1000kN/mm turns out to be a local minimum for sleeper acceleration. It is in particular the peaks around 1kHz, corresponding to pin-pin rail modes, that are responsible for that.
- As explained previously, heavier sleepers vibrate less, which is beneficial for the ballast. However, this effect is opposed to the effect on noise and it is therefore a trade-off as well
- The only parameters, that can be tuned to improve both indicators for noise and ballast, or to improve one indicator without ruining the other are the pad damping ratio and the USP stiffness.

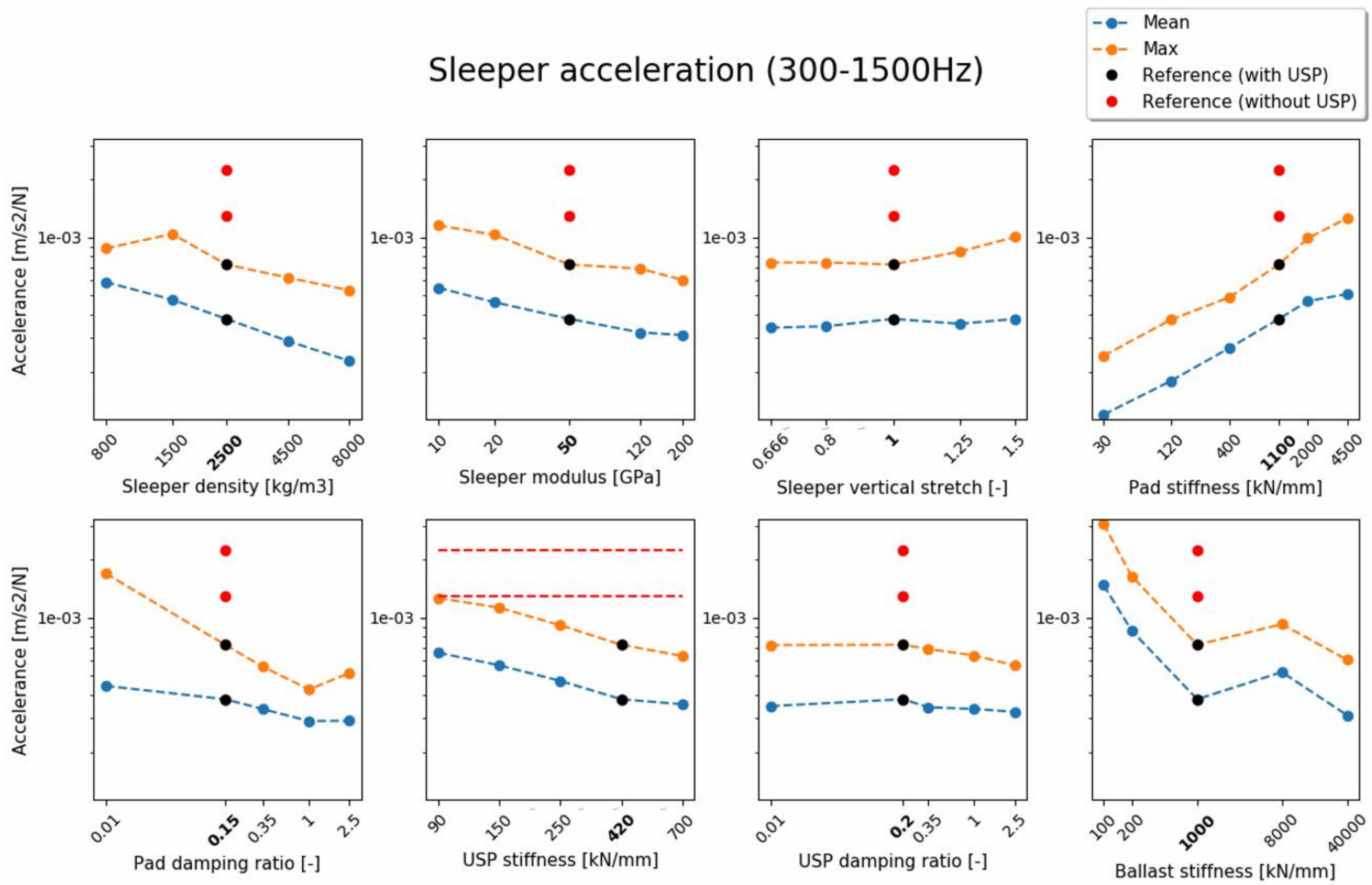

Figure 43 - Vertical sleeper acceleration

1.17.2 Parametric study 2.1

Parameters

Now that all selected parameters have been varied independently throughout a large range of values, the goal is to couple some of them to deeper explore interesting and achievable regions of the component property design space. However, coupling parameters can quickly lead to a lot of simulations, so careful choices are required. As changes on rail pads have been shown to be both very influential and provide unique advantages on the different indicators, this second parametric study focuses on the rail pads properties: stiffness and damping. Firstly, without USP, and then with USP (1.17.3). Rail pads and USP properties are indeed the easiest most realistic parameters that can be tuned, from a financial and practical point of view.

Table 12 - Parametric study 2.1 parameters

	1	2	3	4	5	Units
Pad stiffness at 1kHz	50	300	1000	4000	8000	[kN/mm]
Pad damping (const)	0.01	0.4	0.8	1.5	2.5	[-]

In this study, the fixed parameters still correspond to the reference configuration:

- 60E2 rail profile
- B91 concrete sleeper with Vossloh W14 clamps
- No USP
- Gravel ballast (properties detailed in 2.1.3)

The varied parameters are the pad dynamic stiffness at 1kHz, and the pad damping. Their values are shown in Table 12. The pad damping is assumed constant over the frequency range of interest, but it is also assumed to have an effect on the dynamic stiffness variation in the frequency domain as observed in the Novel Railpad project. Referring to known materials, the dynamic stiffness is assumed to vary linearly with frequency and with damping. For a given dynamic stiffness at 1kHz K_{1kHz} and a given damping ratio $\tan\delta$, the slope of the dynamic stiffness is estimated as $S = 4.1 \cdot 10^{-4} \cdot \tan\delta \cdot K_{1kHz}$ based on the available data obtained in previous projects. As an example, Figure 44 shows the stiffness curves obtained for $K_{1kHz} = 1000\ \mathrm{kN/mm}$ and all possible damping ratios.

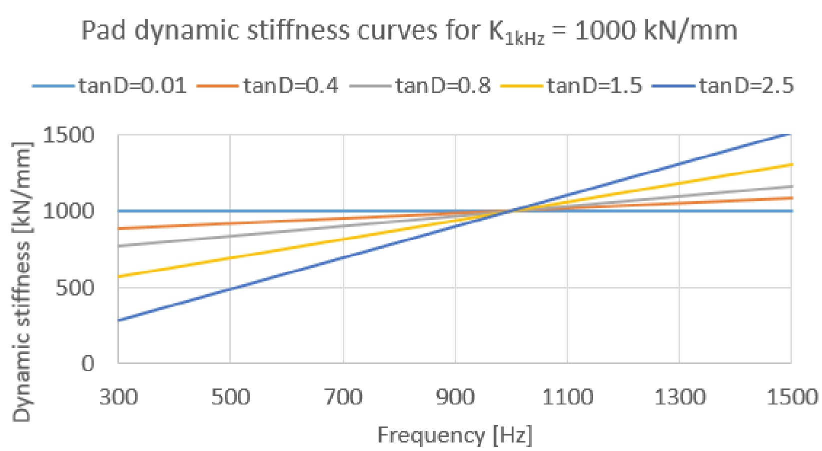

Figure 44 - Pad dynamic stiffness modelling

In a second step, the impulse model is used to compute the quasi-static ballast protection indicator. The cases considered are the six properties combinations described in Table 13. A smaller region of the design space is explored because the impulse model is less automated and much more time consuming than the multi-sleeper model, so planning a large number of simulations takes more time.

Table 13 - Pad static stiffness and damping simulated with the impulse model

K_stat [kN/mm]	Damping [-]
200	0.15
500	0.6
1500	

As for the performance indicators, as explained previously, they consist in the following

- Ballast protection indicator 1: mean vertical acceleration of the first sleeper between 300Hz and 1500Hz (multi-sleeper model)
- Ballast protection indicator 2: largest stress in the ballast under the loading force during pass-by (impulse model)

- Noise indicator: the SPL (300Hz to 1500Hz) at three locations (0m, 10m, 20m from the excitation force) are integrated in space to obtain the area under the curve schematized in Figure 45. This provides a single indicator, that is sensitive to the radiated acoustic noise along the track. It is defined as

$$\text{Track noise} = 20\log_{10}\left(\int_{-20}^{20} p_{acoustic}(x)\cdot \mathrm{d}x\right)$$

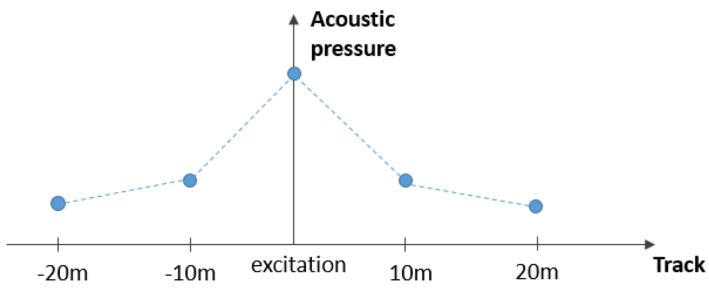

Figure 45 - Track noise definition

Results

The results for each indicator can be visualized as a response surface, whose height is represented by a color map (Figure 46). Note that the rail pads, which have been designed and studied during the Railpad project, are approximately located in the region defined by the three annotated pads.

One interesting point to observe is the direction of the gradients to get better performances. For track noise, the gradient does not point in the same direction everywhere. For example, with a soft pad with low damping, increasing damping has more effect than varying the stiffness. In the region described above, the direction to aim at is clearly towards more damping and more stiffness. Increasing damping is beneficial up to a certain point, beyond which the dynamic stiffness factor has more influence on track noise.

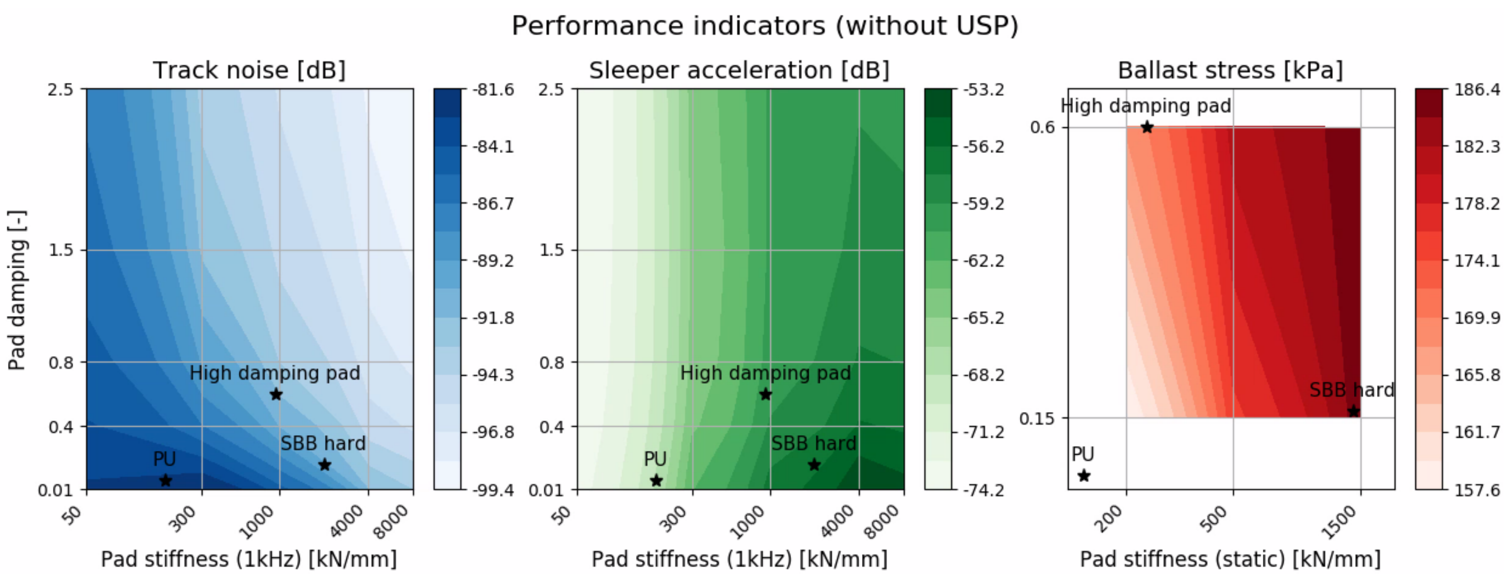

Figure 46 - Performance indicators (without USP)

As for the ballast protection indicators, the influence of the pad properties is similar in the region of the three annotated pads: softer pads improve ballast protection dynamically (green) as well as statically (red) and the pad damping does not have a very strong effect. Its influence becomes more important for the dynamic indicator, for pads with a rather large dynamic stiffness.

In order to reduce track noise without worsen ballast protection, the pad damping should be increased as much as possible, while minimally increasing the pad stiffness. According to these results, the dynamic ballast protection indicator would even be improved, while the static one would be slightly declined.

1.17.3 Parametric study 2.2

This parametric study is identical to the previous one (1.17.2), except that 400kN/mm USPs with a damping ratio of 0.2 are included. The surface responses are presented in Figure 47. The noise indicator does not change much compared to the one without USP: the gradient directions are almost identical and the surface is embedded by roughly the same bounds.

As for the two ballast protection indicators, their response surfaces show the same trends as the ones without USP. The gradients are also aligned to the same directions as in the previous study, but both surfaces are much lower (about 5 to 10dB for sleeper acceleration and 40 to 60kPa for ballast stress). This simply means that the effect of pad stiffness and damping is approximately the same with or without USP, but with USP the ballast is much better protected dynamically and statically, while not changing track noise significantly.

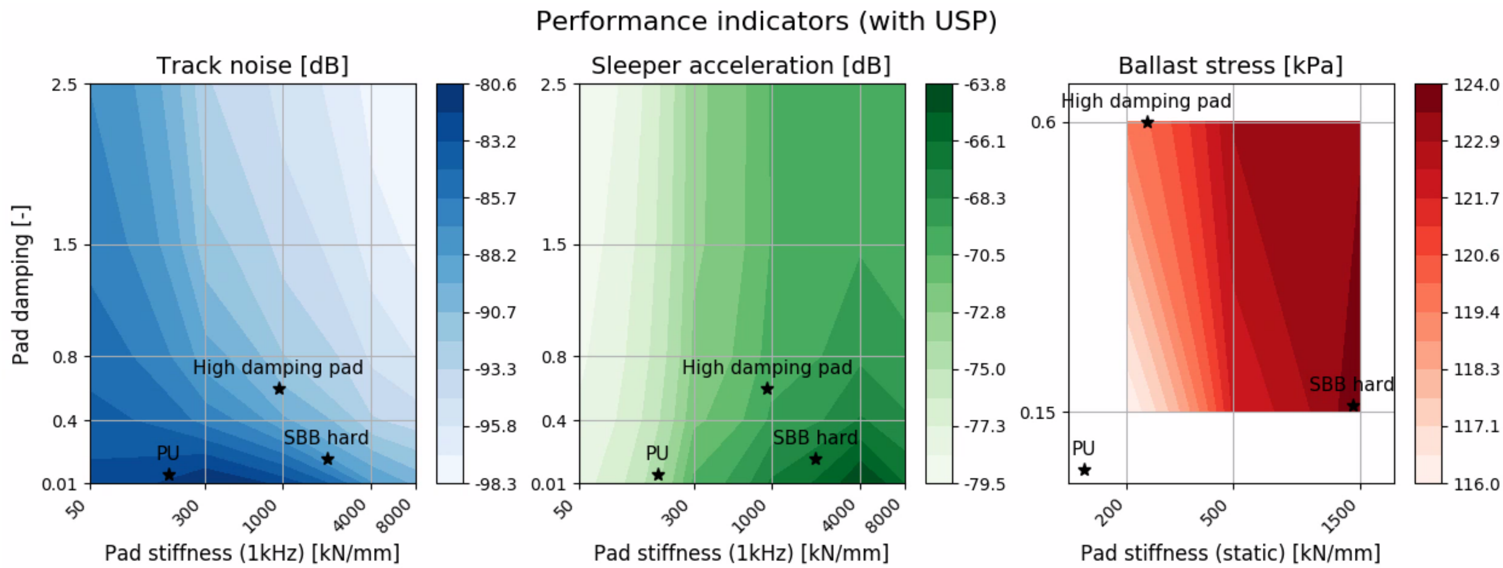

Figure 47 - Performance indicators (with USP)

1.17.4 Parametric study 3

In this third parametric study, the parameters that are varied are the dynamic stiffness and the damping ratio of the USP. The rail pad used is the high-damping pad and is fixed. All other parameters and components correspond to the reference configuration described previously. The properties of the USP are shown in Table 14: each property can take five values, which makes a total of 25 simulations with the multi-sleeper model. Since the USP materials properties have not been measured, the hypothesis of constant dynamic stiffness and damping coefficient is made. The performance indicators observed are exactly as described in 1.17.2.

Table 14 - Materials properties of the USP

	1	2	3	4	5	Units
USP stiffness	80	150	275	500	900	[kN/mm]
USP damping	0.05	0.25	0.6	1	1.5	[-]

The response surfaces are shown in Figure 48. Since the viscoelastic properties of USP were not measured, they have not been implemented in the impulse model, so only the influence of USP stiffness on the ballast stress is studied. For noise reduction, the gradients directions are similar to those of rail pad properties: more stiffness and more damping is the optimal combination to reduce noise. But the response surface is relatively flat, with a difference of only 2.4dB between the highest and the lowest simulated points. So as observed in 1.17.1, the properties of the USP have a relatively low impact on noise.

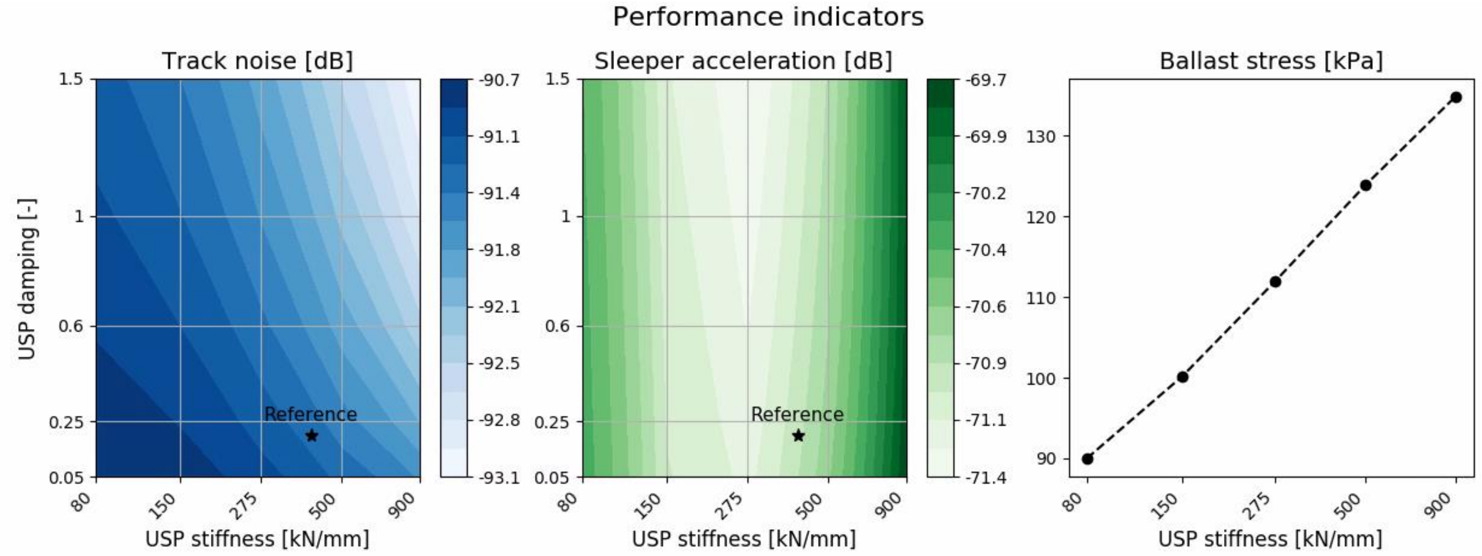

Figure 48 - Performance indicators vs. USP properties

The sleeper acceleration indicator is nearly independent on USP damping and has a very clear minimum at a dynamic stiffness of about 275kN/mm. However, the response surface is relatively flat compared to those obtained when varying the rail pad properties. The highest and lowest point are only 1.7dB apart. So the fact that USPs are included or not has a much larger impact on the sleeper vertical acceleration than whether USPs are soft or hard, and whether their damping is low or high.

On the other hand, the USP stiffness has a much larger influence on the static ballast protection indicator, which is the largest vertical stress in the ballast during a pass-by. The third graph in Figure 48 shows a logarithmic evolution of the latter with respect to USP stiffness (note the logarithmic scale of the x-axis and the linear scale of the y-axis). Given these results, since the main role of the USP is to protect the ballast, the optimal solution would be to use relatively soft USP with as much damping as possible.

1.18 Key takeaways from the numerical parametric study & component optimization

Sleeper spacing has a very strong influence on the considered indicators but in terms of infrastructure cost, maintenance and use of material resources (concrete and steel), it is a parameter that is difficult to change in practice.

In general, the best way to reduce noise is to increase pad stiffness and damping. Above a damping of about 0.8, the noise indicator is mostly sensitive to stiffness; the stiffer the better. With a pad damping below 0.2, pad stiffness has almost no effect on track noise below a dynamic stiffness of 400kN/mm.

Pad damping has a small influence on ballast protection. Soft pads protect the ballast much better than hard pads. Improving ballast protection and noise is a trade-off when it comes to tuning rail pads properties only. One way to improve noise without ruining ballast protection is to focus on increasing pad damping.

USPs, whether they are soft or hard, have a rather small impact on noise. But according to the presented criteria, they improve ballast protection very significantly. Soft USPs reduce further the stress in the ballast at low frequency, while hard USPs perform better regarding the 300 to 1500Hz sleeper vertical acceleration.

Wooden sleepers do not have a significant impact on SPL directly in front of the excitation source in the current model, but show a large noise radiation with distance linked to a probable reduction of the TDR. Their softness makes them bend more and locally transmit more stress to the ballast during a pass-by. As for soft, low damping PU pad, it increases SPL by several dB. Moreover, it makes a more modal, hence annoying sound, due to the high and narrow peaks of the SPL FRFs.

Among the components that have been studied, the best configuration would be to use a rail pad with medium stiffness (~1000 kN/mm at 1Khz, ~300 kN/mm static stiffness) and high damping (as high as possible, at least tan δ ~= 0.5 – 0.7) which reduces track noise by 2 to 5dB (4 to 7dBA), according to these simulations. Such pads combined with the B91 concrete sleepers (which seem appropriate compromise in terms of their stiffness, mass and stability) and soft USPs (around 200-300kN/mm), both noise reduction and significant ballast protection could be achieved simultaneously.

Discussion / conclusions

Development of experimental methods / simulation tools

This project lead to the successful development of several experimental methods to determine the dynamic properties of rail pads and sleeper components from simple dynamic testing / modal analysis data.

The open source Rail track modelling toolbox has been extended as planned to provide more flexibility in the modeling of different track components such as different sleeper (geometry, material and spacing) and clamping systems, as well as the possibility to carry out batch analysis for parametric study using simple parameter description files. The code has been published on GitHub in a new branch name "track evaluation" here : https://github.com/jcugnoni-heig/RailTrackModellingToolbox/tree/track_evaluation .

The predictions achieved with the rail track modelling toolbox models (semi-analytical and multi-sleeper numerical model) have been further compared and validated against experimental data.

Nevertheless, it should be noted that the noise radiation predictions remain only comparative as the noise radiation model used does not properly account for ground effects, occlusion, reflection and occlusion. Also, the results obtained only represent the noise radiated by a track subjected to a unit excitation force, and thus does not represent the wheel or vehicle noise radiation neither the effect of combined roughness. Further development in these directions and validation against noise measurement data obtained from field tests could further improve the prediction capability of the modeling toolbox.

Parametric analysis of track component properties and optimization

Both parametric studies using the three sleeper cell experimental setup and the multi-sleeper / impulse simulation models lead to the same overall conclusions:

1. The dominant parameter for the noise reduction is the use of a high damping pad, which also provide the best performances in terms of reduced rail and sleeper vibrations both in 45° loading conditions (curves) and 6° (straight lines). The best combination overall to combine a high damping pad with USPs. In terms of economic and fossile resource usage, just changing from hard EVA to high damping pads seem an advantageous option.
2. USPs do not seem to affect significantly the noise radiation but are effective at reducing ballast loading (both static and dynamic). Thus USPs can be used relatively independently of the choice of the pads to provide ballast additional protection.
3. The worst conditions in terms for noise are overall with soft pads with low damping, 54E2 rails or wooden sleepers.
4. The current SBB reference configuration of 60E2 rail with hard EVA pads and B91 sleepers without USPs is in the upper half of the combinations tested, but can be improved at least in terms of reducing ballast vibrations by adding USPs. However, switching to high damping pads seem more beneficial overall both in terms of noise radiation and ballast protection.
5. As a final result, the following sweet spot for the track component properties have been identified as: 60E2 rails with B91 sleepers with a rail pad of medium stiffness (~1000 kN/mm at 1Khz, ~300 kN/mm static stiffness) and high damping (as high as possible, at least tan δ ~= 0.5) combined with soft USPs (around 200-300kN/mm).

References

[1] *DIN EN 15461:2011-01 Bahnanwendungen - Schallemission - Charakterisierung der dynamischen Eigenschaften von Gleisabschnitten für Vorbeifahrtgeräuschmessungen.*

[2] HEIG-VD, Empa, EPFL, SBB, "Novel Rail Pads for Improved Noise Reduction and Reduced Track Maintenance," 2022.

[3] HEIG-VD, "Study of rail clamps preload influence on," 2021.

[4] *EN ISO 9614-1:2009 Acoustics. Determination of sound power levels of noise sources using sound intensity Measurement at discrete points.*

[5] Brüel & Kjaer, “Sound Intensity: Theory and Measurements,” [Online]. Available: https://www.bksv.com/en/knowledge/blog/sound/sound-intensity.

[6] C. Paderno, "Comportement du ballast sous l'action du bourrage et du trafic ferroviaire," EPFL, 2010.

[7] T. X. Wu and D. J. Thompson, "The influence of random sleeper spacing and ballast stiffness on the vibration behaviour of railway track," *Acta Acustica united with Acustica,* vol. 86, pp. 313-321, 2000.

List of figures

2.1 Materials properties

2.1.1 EVA

The frequency-domain mechanical properties come from DMA measurement done at EPFL during the Railpad project. The data used in the models is based on a linear fitting from 300Hz to 1500Hz. The Poisson's ratio used is 0.484.

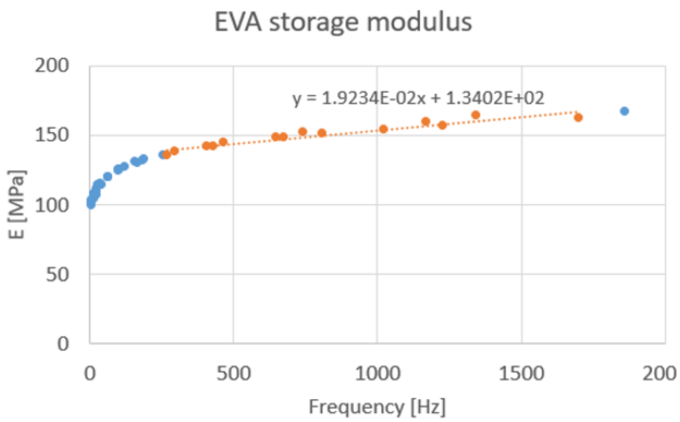

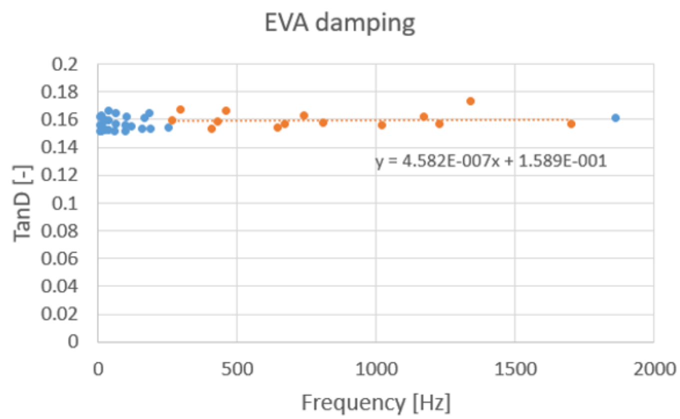

2.1.2 PU

PU properties were extrapolated from DMA measurements done on softer PU, based on their compression stiffness. The Poisson's ratio used is 0.3.

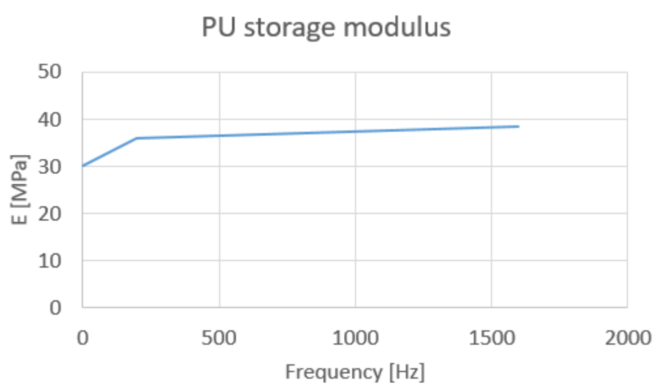

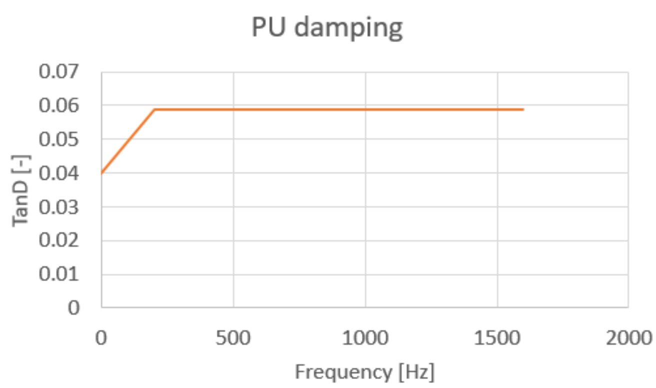

2.1.3 Ballast

The ballast properties used come from measurements done at Empa during the Railpad project. Note that the ballast height is usually set to 0.3m, and the effective area is assumed to be 1.5 times the sleeper bottom surface area. In the impulse model, which is much closer to static conditions, the value of 350MPa was found in the literature [6], and scaled such that the vertical stiffness of the ballast is correct in the model.

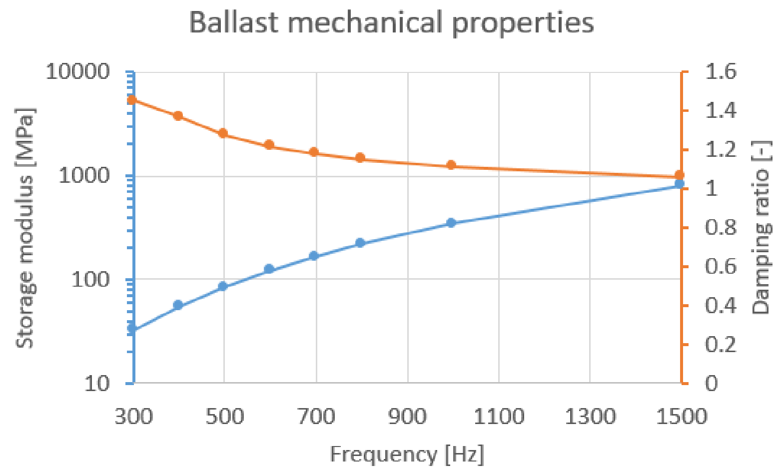

2.2 Influence of the individual parameters on the measured three-sleeper cell performance indicators

2.2.1 Influence of pad static stiffness

Figure 49 shows the effects of an increase in pad static stiffness on the performance indicators for three different systems. We can see that stiffer pads reduce noise in curves (45°), this is less apparent in straight lines (6°). But as stated in Section *1.12.2 Acoustic ranking*, although soft pads have lower L_W values, they produce a sound spectrum that is very modal, with tall and sharp peaks (see Figure 31, p.29).Also, we can see that stiffer pads significantly decrease HF rail vibration in both straight lines and curves, and HF rail vibration is usually correlated with noise emissions. Reduced HF rail vibration is a result of increased rail-sleeper coupling, which is also the reason for the increase of HF sleeper vibration. HF sleeper vibration increase is however mitigated by the use of USP. The effects of increased pad static stiffness on HF vibration and noise are stronger on a 54E2 rail system. Increased pad static stiffness decreases LF sleeper vibration in curves (45°).

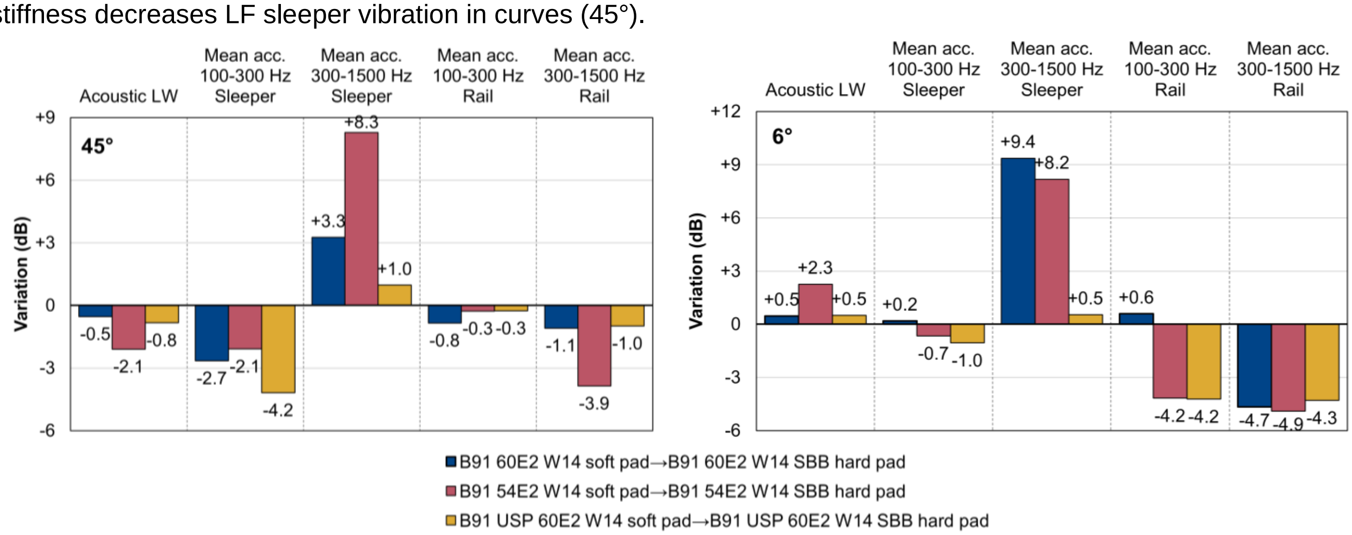

Figure 49 – Influence of pad static stiffness increase under a 45° (left) and a 6° (right) loading.

2.2.2 Influence of pad damping

The effects of an increase of the pad damping are shown in Figure 50. We can see that increased pad damping leads to a significant reduction in noise levels of 2 to 3.5 dB. It also leads to significantly decreased vibration of both the sleeper and of the rail. This is also very apparent in the noise and rail vibration spectrums in Figure 51 & Figure 52, where peaks are significantly attenuated and dampened by the use of damping pads, thus diminishing the modal aspect of sound and vibration.

Damping has less effect on sleeper vibration if USPs are used, but USP already significantly reduce sleeper vibrations. Using damping pads in conjunction with USP is even more beneficial for noise in straight lines (6°), but not as much in curves (45°).

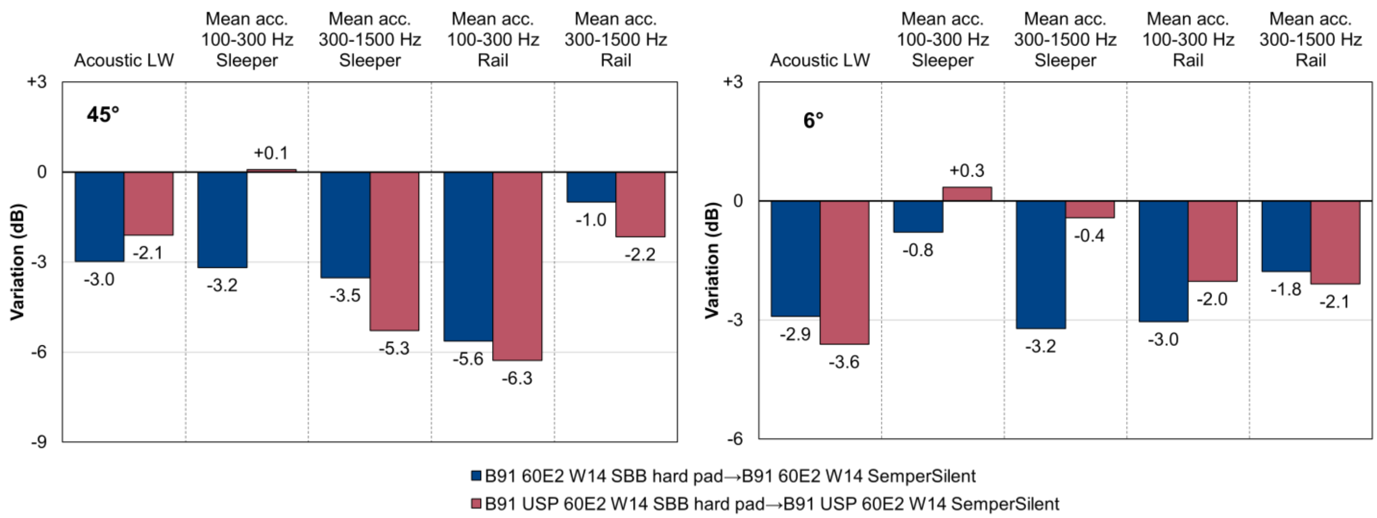

Figure 50 – Influence of pad damping increase under a 45° (left) and a 6° (right) loading.

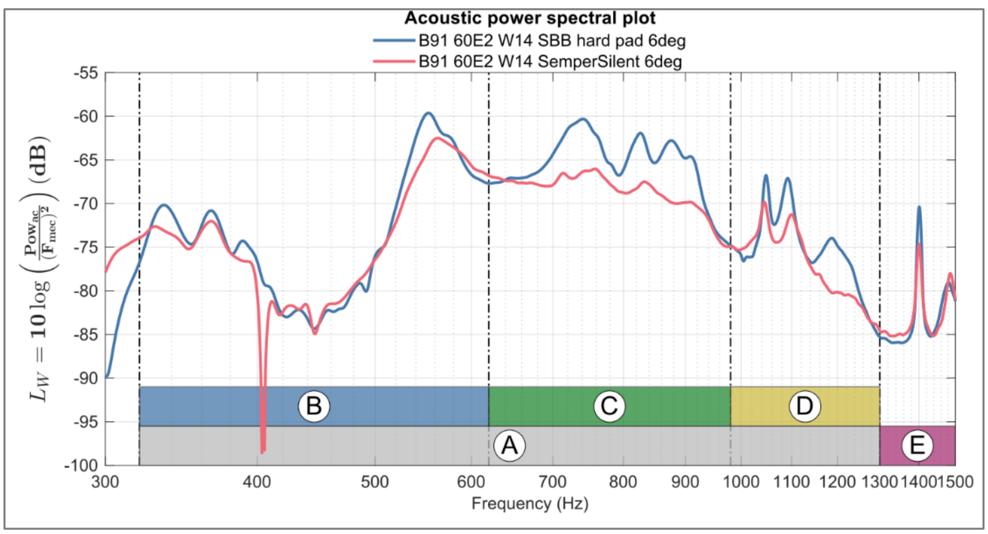

Figure 51 – Noise emission spectrum comparison between a hard pad and a damping pad system under 6° excitation.

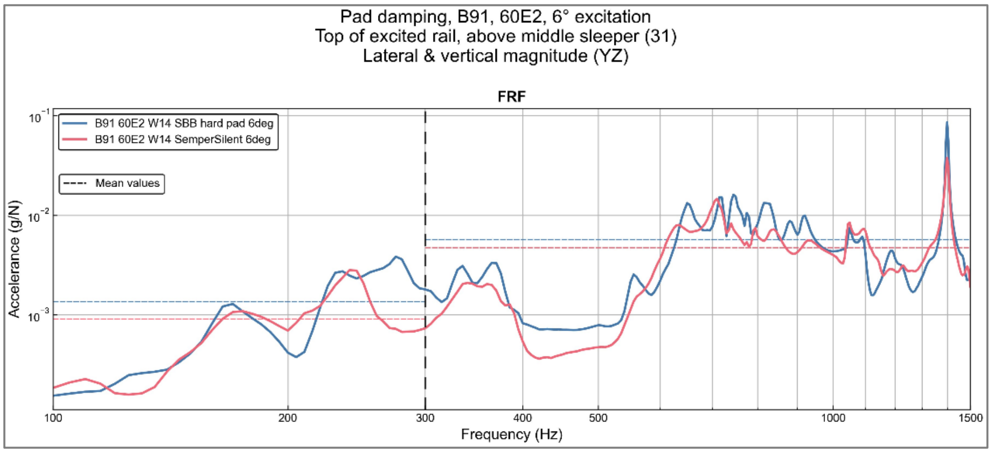

Figure 52 – Rail vibration spectrum comparison between a hard pad and a damping pad system under 6° excitation.

2.2.3 Influence of Under-Sleeper Pads (USP)

Figure 53 shows the effects of adding USP to three different systems. Based on the L_W values, USPs have no significant influence on noise. However, the sound and rail vibration spectrums in Figure 54 and Figure 55 show that adding USPs to a soft pad system seem to reduce the amplitude of the peaks, thus slightly decreasing the modal character, even if this is not captured by the indicators. This could be due to the already poor performance of soft pads, which can easily be improved.

Apart from this, USPs seem to have no significant influence on rail vibration, although in curves (45°), it may slightly increase HF rail vibration, except if used in conjunction with damping pads. In curves (45°), adding USPs greatly decrease LF sleeper vibrations and, if used in conjunction with damping pads, also HF sleeper vibration.

Adding USP to a soft pad system increases HF sleeper vibration both in curves (45°) and straight lines (6°).

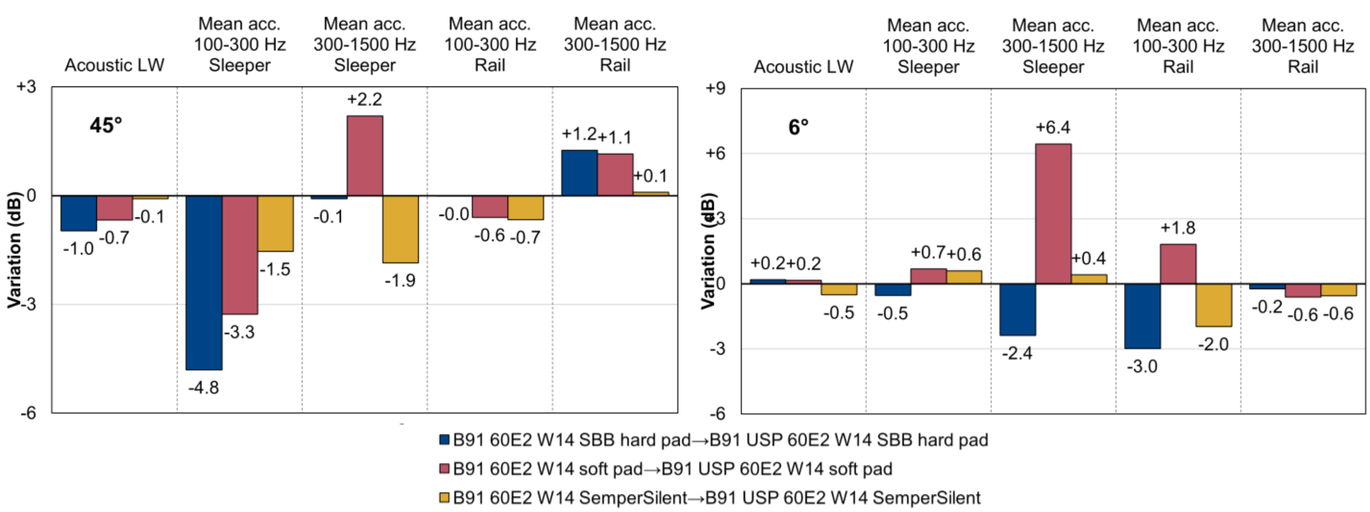

Figure 53 – Influence of USPs under a 45° (left) and a 6° (right) loading.

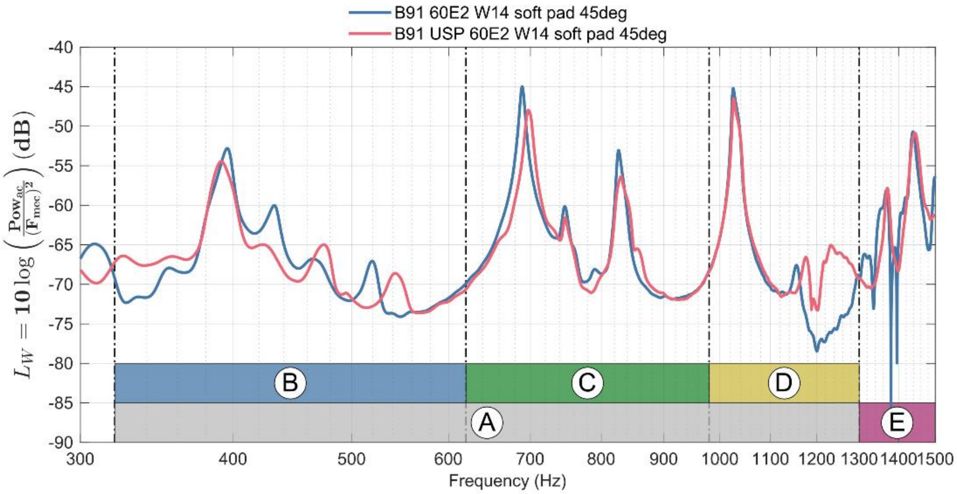

Figure 54 – Influence on noise spectrum (6°) of adding USPs to a soft pad system. The slight decrease of peaks amplitude is visible.

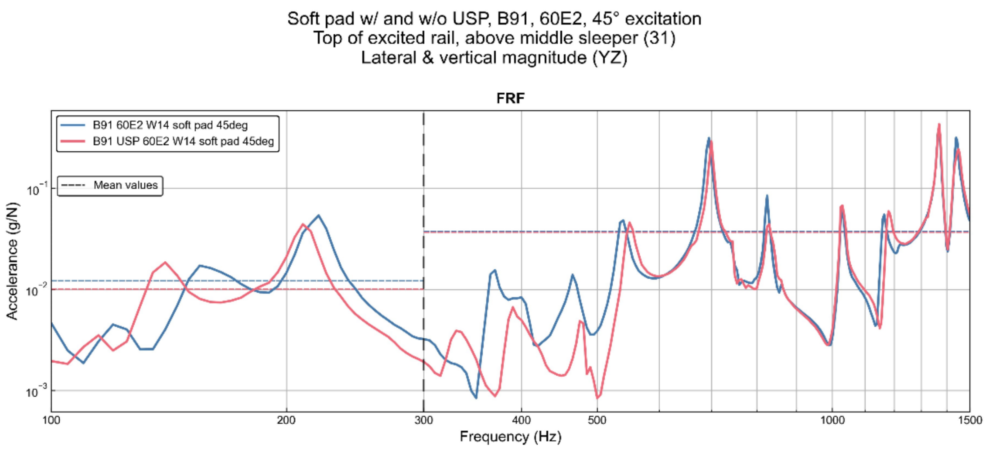

Figure 55 – Influence on rail vibration spectrum (45°) of adding USPs to a soft pad system. The slight decrease of peaks amplitude is visible.

2.2.4 Influence of rail profile

The influence of switching from a 54E2 rail profile to a 60E2 rail profile is represented in Figure 56.

54E2 rail profile emits more noise than 60E2 if used with soft pads in curves (45°) or with hard pads in straight line (6°). In straight lines (6°), both rail and sleeper vibration are increased by using 54E2.

In curves (45°), using 54E2 reduces LF sleeper vibration. If used with hard pads, HF sleeper vibration increases; If used with soft pads, it is HF rail vibration that increases. Due to its reduced section and thus reduced moment of inertia, the 54E2 vibrates more than 60E2, especially if the excitation has a strong lateral component, as it is the case under a 45° loading. With hard pads and high coupling, this vibration increase is captured on the sleeper, whereas it is captured on the rail when soft pads with low coupling are in play.

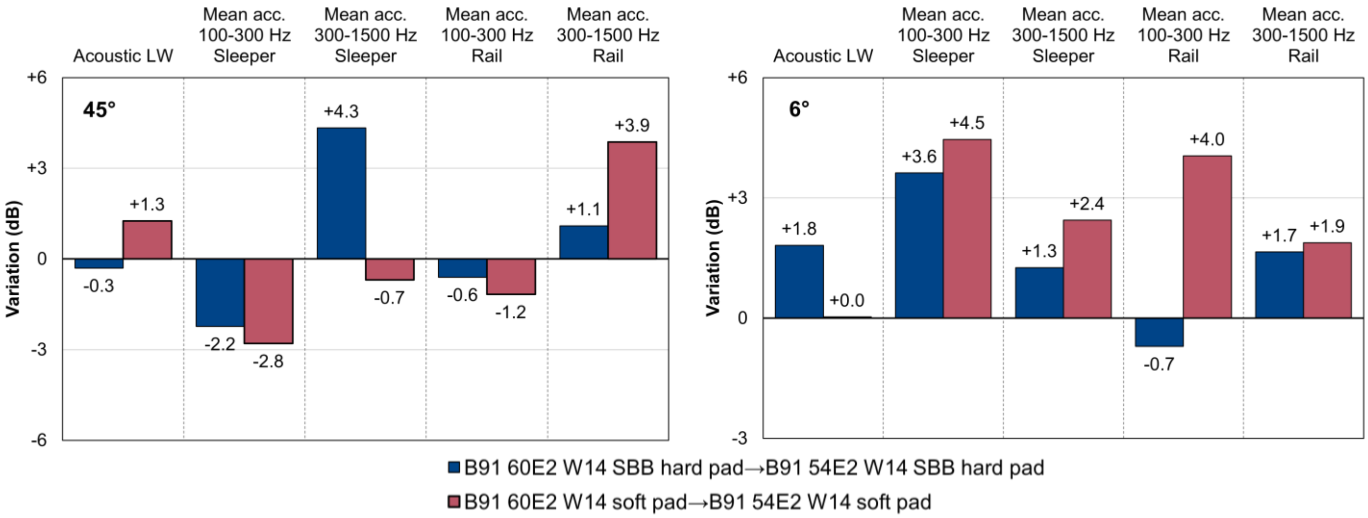

Figure 56 – Influence of rail profile change (section decrease) under a 45° (left) and a 6° (right) loading.

2.2.5 Influence of sleeper material

Figure 57 shows the influence of switching from wooden Rp-IV sleepers to concrete B91 sleepers, in a system with hard pads and 54E2 rail.

Concrete sleepers appear quieter than wooden sleepers in straight lines (6°). In curves (45°), there seem to be no significant influence on noise. However, noise and rail HF vibration spectra of concrete sleepers (Figure 58 and Figure 59) display a more modal behaviour and show that some peak amplitudes are increased. This is captured by indicators at 45°, but less at 6°. This could be due to the poor damping properties of concrete compared to wood, as wood could contribute to dampen noise and HF rail vibration and make them less modal. At the same time, this effect is countered by the increased mass and inertia of the concrete sleepers system, which contributes to lower overall vibrations, as shown by sleeper vibrations which are significantly reduced when concrete sleepers are used.

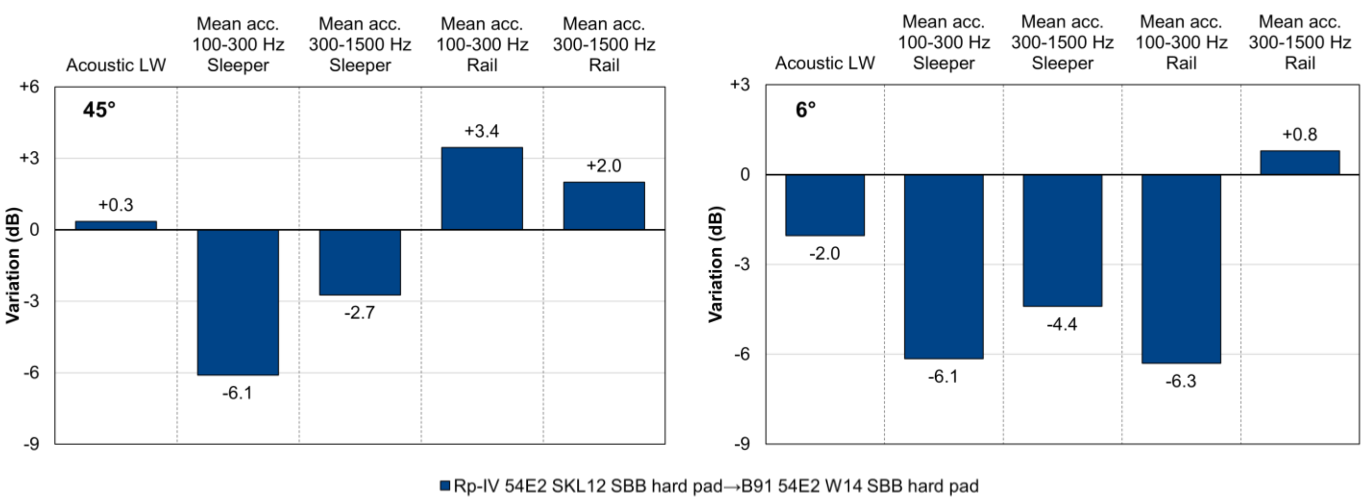

Figure 57 – Influence of sleeper material under a 45° (left) and a 6° (right) loading.

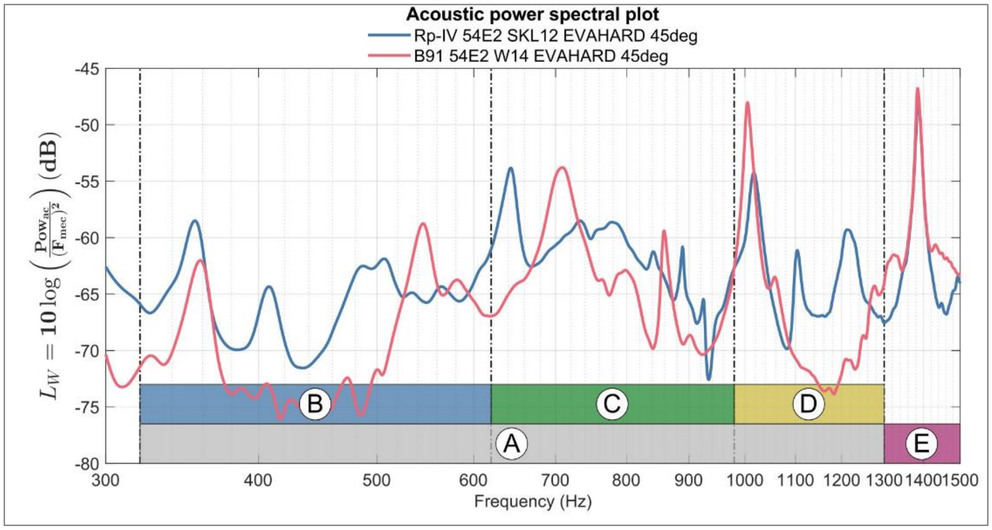

Figure 58 – Sound spectrum comparison between a wooden sleeper and a concrete sleeper system under 45° excitation.

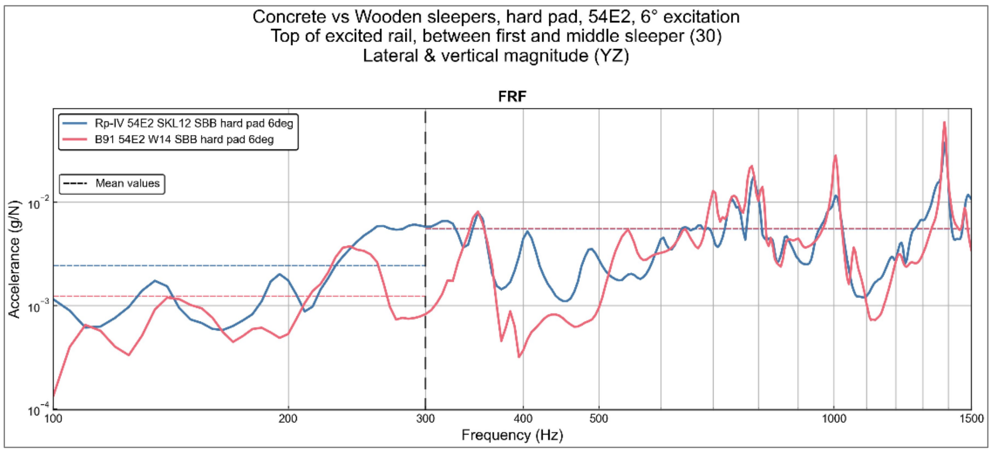

Figure 59 – Rail vibration spectrum comparison between a wooden sleeper and a concrete sleeper system under 6° excitation.

2.2.6 Influence of clamping on wooden sleepers

Figure 60 shows the influence of switching from rigid Kpo3 (“K”) clamping to an elastic SKL12 + hard pad (“Ke”) clamping on wooden Rp-IV 54E2 sleepers.

In curves (45°), elastic clamping reduces noise by about 1 dB. In straight lines (6°), no significant effect on noise can be observed.

In curves (45°), there appears to be an increase of HF rail vibrations with elastic clamping- However, the spectra in Figure 61 and Figure 62 show that this increase is largely driven by the peak at 1400 Hz, and that the rest of the HF spectrum rather appears decreased, or at least not as much increased. This peak is mainly present on the three-sleeper cell and is marginally relevant to continuous tracks. LF rail vibration is increased in both curves and straight lines.

LF sleeper vibration is increased by elastic clamping, especially in straight lines (6°). HF vibration is however decreased, especially in curves (6°).

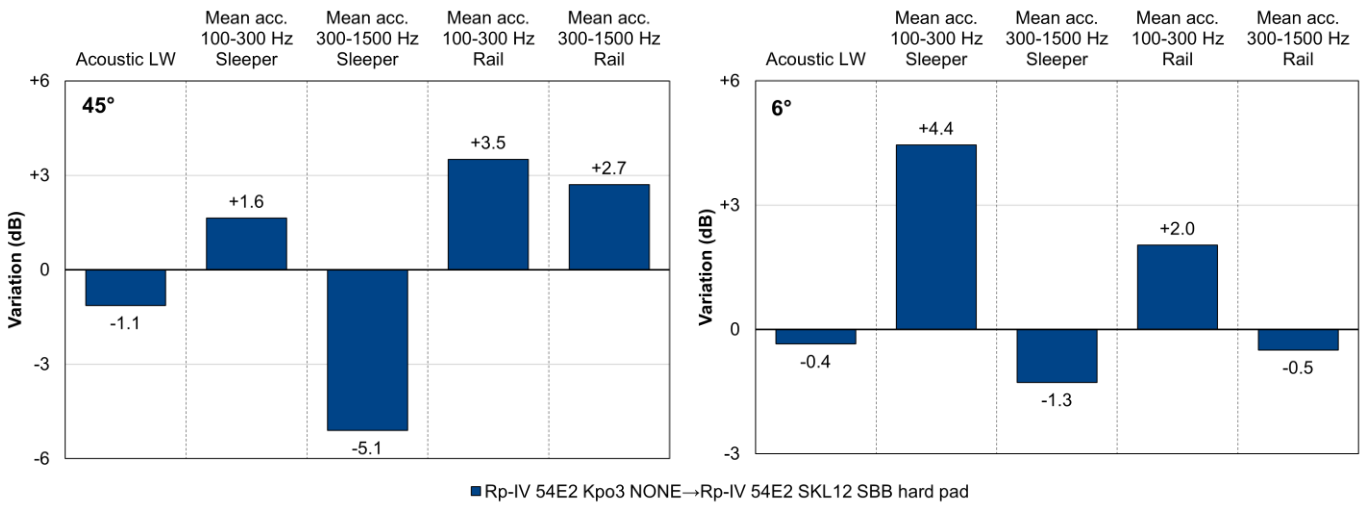

Figure 60 – Influence of clamping on wooden sleepers under a 45° (left) and a 6° (right) loading.

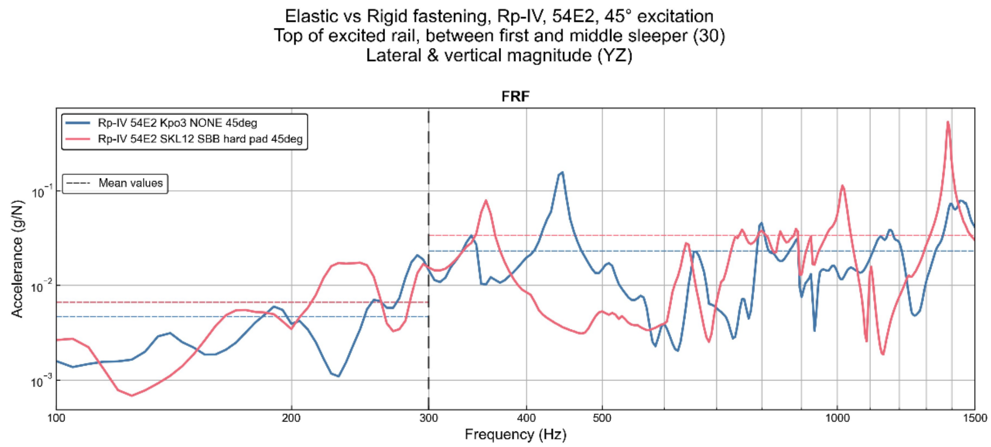

Figure 61 – Rail (between sleepers) vibration spectrum comparison between rigid and elastic clamping on a wooden sleeper system under 45° excitation.

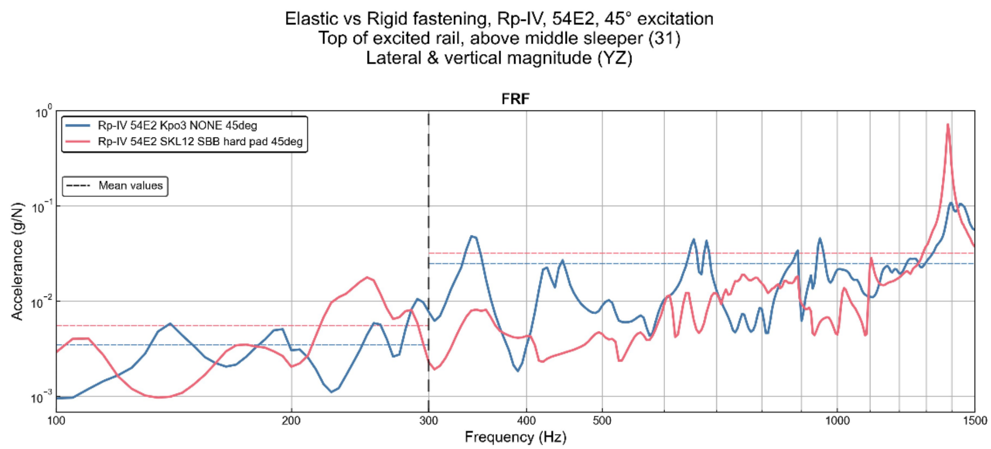

Figure 62 – Rail (above middle sleeper) vibration spectrum comparison between rigid and elastic clamping on a wooden sleeper system under 45° excitation.

2.2.7 Influence of clamping and sleeper material

The SBB manifested interest in the contrast between a system with wooden sleepers and rigid clamping, and a system with concrete sleepers and elastic clamping. The difference between those two systems is illustrated in Figure 63. Basically, it amounts to the cumulation of the effects described in the two previous sections (2.2.5 & 2.2.6).

Concrete sleepers with elastic fastening significantly reduce noise in straight lines (6°), but not in curves (45°). This could be linked to the increased rail vibration at 45°, whereas in straight lines (6°), LF rail vibration is significantly decreased, and HF rail vibration remains unchanged.

In both curves and straight lines, sleeper vibration is significantly reduced.

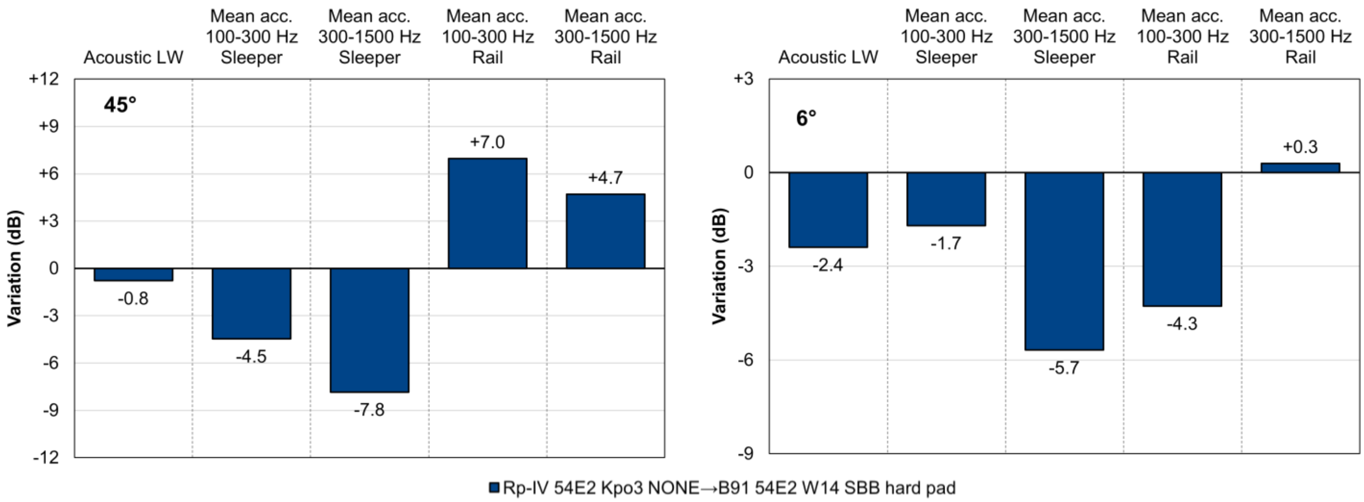

Figure 63 – Influence of sleeper material and clamping change under a 45° (left) and a 6° (right) loading.